



Attenuation of Petroleum Generation Characteristics by the Sulfurization of Organic Matter in Westphalian Carboniferous Lacustrine Source Rocks (A Geochemical Study of Potential Marine Incursions)

FINAL REPORT

Start Date: October 15th 2017

End Date: 15th May 2019

Research Grant Number: 171010

G. TODD VENTURA AND ANDREW MACRAE

Department of Geology

Saint Mary's University

SUBMISSION

June 28th, 2019

EXECUTIVE SUMMARY

This study marks an initial step in the development of geochemical techniques to 1) detect marine influences in pre-rift Paleozoic source rocks and to 2) evaluate the degree to which sulfurization of organic matter (SOM) has affected the preservation and generation characteristics of organic matter in these rocks. SOM primarily occurs when seawater sulfate is reduced in marine sediments to form sulfides that can further bind to organic matter during early diagenesis. This process is a mechanism of kerogen formation that changes the petroleum generation characteristics of source rocks.

The potential influence of SOM on age equivalent and younger sections of the Scotian margin has yet to be studied. To begin to remedy this, the following investigation focused on the Joggins Formation locality of Nova Scotia. The Joggins Fm consists of a series of parasequences that transition from clastic mudrocks/marls to root-bioturbated under-layers of the coal seam, the coal seam itself, and the transition zone to a more carbonate-rich cap rock that marks the maximum flooding surface. Of the fifteen well-characterized, cyclothems, seven were targeted for this chemostratigraphic survey. For this study, 42 samples were selected for Rock-Eval pyrolysis and molecular biomarker analyses. An additional 47 samples were measured for carbon and nitrogen isotope analyses as well as a range of elemental concentrations (including sulfur and most transition metals) using portable x-ray fluorescence (pXRF). As such, this project provides the first comprehensive chemostratigraphic study of the Joggins Fm.

The Joggins Fm source rocks were subdivided by lithology into shales, paleosols, limestones, coaly mudstones, and coals. Several trends are present in their source rock properties, which are diagnostic of paleoenvironmental conditions during sediment deposition. These attributes have effected the quality, quantity, and maturity of the organic matter.

Description of organic matter:

- With the exception of one limestone sample, the limestones, coals and coaly mudstones contain Type II/III organic matter. The generative potentials for the limestones is very good to excellent for oil and gas. However, the coals and coaly mudstone are inert. The outlier limestone samples contains Type I kerogen sourced from lacustrine environments and has excellent potential for generating oil. The shales and paleosols have Type III and IV kerogens capable of generating gas or are completely inert.
- The limestones have organic matter compositions that are distinctly different from that of the other lithofacies based on bulk and molecular geochemical proxies. In this respect, the organic matter was primary and not inherited or migrated from closely associated organic-rich coal and coaly mudstone units.
- The determination of organic matter maturity was based on bulk pyrolysis and molecular biomarker analyses that produced similar results. Despite its age, the organic matter of the Joggins Fm is thermally immature to early mature indicating a shallow burial for these rocks.
- The biomarker and trace metal data (V/Ni, Ni/Co, and V/Cr ratios) for all sample lithofacies indicates a predominant pattern of sediment deposition in an oxic water column and/or near surface sediments.

Evidence of SOM and marine transgression:

- Geochemical evidence of marine incursions is thus far less compelling. Some of the limestone units have Type II kerogens that can be sourced from marine organic matter or a mix of lacustrine and terrestrial organic matter.
- The low relative abundance of C_{27} steranes in most shales and limestones points to terrestrial and lacustrine conditions for the Joggins Fm. A notable exception are the limestone samples JF-73.8m, which is stratigraphically close to previously reported putative echinoderm fossils (Grey et al., 2011)

and JF-547.25m that is also near to the ~550m limestone units containing agglutinated forams (Archer et al., 1995).

- Organosulfur compounds such as benzothiophene and dibenzothiophenes, which would likely arise from SOM are of low abundance in the extracted bitumens. However, alkylated moieties are more abundant and the difference in these may be a function of low maturity.
- The coals and coaly mudstones typically have higher sulfur concentrations compared to the other documented lithologies. This presents the possibility that stratigraphically similar lithologies may have inherited their sulfur through leaching. As such, the sulfur concentrations of many shales and limestones may not reflect microbial sulfate reduction.
- The coals and coaly mudstones have low T_{max} values and high sulfur concentrations. Many of these are stratigraphically adjacent to shales and limestone units of higher maturity. The discontinuity in maturities is likely the result of increased cracking from matrix affects relating to low organic matter contents, the lower chemical bond strength associated with carbon-sulfur and sulfur-sulfur linkages, and the elevated presence of free sulfur radicals that can cleave carbon-carbon bonds in the kerogen.
- Nonetheless, total sulfur measures were used to calculate the initial, pre-SRB degraded TOC values. These results indicate a stratigraphic pattern whereby greater heterotrophic activity appears to have occurred at the base of the section than in other parts of the formation.
- This, in addition to elevated Sr/Ba value for limestones, as well as low Mn/Ca ratios for shale units is also consistent with brackish or more marine conditions.

These results provide evidence that some level of SOM likely occurred within the Joggins Fm source rocks. However, its effects appear to be limited to maturation of the organic matter with no additional impact being observed in the quality or quantity of the organic matter that had been preserved. Consistent evidence between bulk organic, molecular, and inorganic proxies indicate oxic conditions prevailed within the water column and much of the surface sediments. The geochemical data is in many cases consistent with brackish to marine conditions being present during the initial basin fill marking portions of the lower limestone and shale intervals within the section. Additionally, geochemical evidence also points to an additional transgressive events at 447.55 – 550m and near the top of the Joggins Fm at 872.3m. However, little evidence was obtained that these events significantly effected the petroleum generative potentials of the Joggins source rocks. Together, these data provide a clearer picture of the geochemical conditions occurring in this section.

TABLE OF CONTENTS

1. INTRODUCTION	7
2. GEOLOGICAL SETTING	12
3. PREVIOUS GEOCHEMICAL ANALYSES	13
4. METHODS	13
4.1. Sample Collection and Preparation	13
4.2. Bulk Pyrolysis	14
4.3. Biomarker Analysis	14
4.4. Carbon Isotope Analysis	14
4.5. Portable X-ray Diffractometer (pXRF)	15
5. RESULTS	15
5.1. Bulk Rock Geochemistry	15
5.2. Carbon and Nitrogen Stable Isotopes	18
5.3. Petroleum Biomarkers	21
5.3.1. Normal alkanes and acyclic isoprenoids	22
5.3.2. Tricyclic terpanes (chielanthanes)	24
5.3.3. Steroidal biomarkers	24
5.3.4. Hopanoid biomarkers	24
5.4. Organic Matter Thermal Maturity Based on Molecular Parameters	27
5.5. Elemental Geochemistry	28
6. DISCUSSION	28
6.1. Caveats About Marine Microscopic Bioclast Indicators in the Joggins Formation	28
6.2. Sulfurization of Organic Matter	29
6.3. Marine Incursions and Paleoredox	29
6.3.1. Biomarker evidence of marine and paleoredox conditions	29
6.3.2. Elemental concentrations and salinity and redox conditions	33
6.3.3. Elemental ratios for redox conditions and salinity	35
7. SUMMARY AND CONCLUSIONS	38
7.1. Significance to Hydrocarbon Exploration and Development	39
7.2. Future Work Possibilities	39
Acknowledgements	40
References	40
APPENDIX I: EXAMPLES OF SAMPLES COLLECTED FOR STUDY	47
APPENDIX II: SAMPLE ANALYSES	48
APPENDIX III: BULK PYROLYSIS MEASUREMENTS	50

APPENDIX IV: BIOMARKER AND STABLE ISOTOPE MEASUREMENTS52

APPENDIX V: PORTABLE-XRF ELEMENTAL RATIOS.....68

APPENDIX VI: PXRF ELEMENTAL CONCENTRATION DATA (PPM).....70

TABLE OF FIGURES

Figure 1. Map of the Maritimes Basin indicating the location of Joggins Fossil Cliffs locality (top). Map of the Cumberland Basin with accompanying stratigraphic section (bottom) indicating the stratigraphic target of the study (after Davies et al., 2005).	8
Figure 2. Photos of the Joggins fossil cliffs. Photo on the left provides an example of the dipping bedding visible in the rock outcrop exposed as ~20m high cliffs. The photo on the right is an outcrop photo from Cycle 3 showing the location of samples collected for this study.	9
Figure 3. Paleogeographic reconstruction of Pangaea during the Carboniferous. Red square indicates the location of the Joggins Formation. During lowstands the depocenter was approximately 2,500km from the paleoshoreline (artwork by Ron Blakey based on plate reconstructions by Scotese and McKerrow, 1990). Larger scale blow-up map represents the possible open-water connection to the Paleo-Tethys Ocean during sealevel highstands (Gibling et al., 1992; Carpenter et al., 2015).	10
Figure 4. Bivalve-bearing limestone units of the Joggins Formation (“clam coals”) can be organic-rich, laminated and contain abundant bivalves, ostracods, fish bones and teeth, and coprolites.	11
Figure 5. The Sr marine isotope curve for the Permian and Carboniferous periods (McArthur et al., 2001). Overlaid on the curve are the Brand (1994) Joggins aragonitic bivalve fossil measurements, which fall outside the Carboniferous trend.	12
Figure 6. Summary stratigraphic profile and base level changes of the Joggins Formation modified from Davies et al. (2005) to reflect the change in Joggins/Springhill Mines contact proposed by Rygel et al. (2014) (left). Numbers in the column labeled “Cycle” are the 15 recognized cyclothems. Samples collected for this study are marked by sideways triangles. Stars represent stratigraphic level of echinoderm ossicles reported by Grey et al. (2011) and Carpenter et al. (2015). Enlargement of the lower section of the Joggins Formation in the interval suspected to have been effected by marine incursions (modified from Davies et al., 2005) (right). Samples collected for this study are indicated by colored circles.....	16
Figure 7. Bulk pyrolysis of the Joggins Fm samples. Low S2 values have caused some T_{max} maturity measures to be inaccurate (light green fields). However, this has likely not resulted in spurious HI measures for equivalent TOC lean samples. Comparisons of S1 versus TOC indicates the Joggins Formation organic matter is likely syngeneic.....	17
Figure 8. Cross-plots of HI, TOC, OI, PI, T_{max} , and S2 depicting kerogen quality, quantity, type, maturity, and generative potential. The Joggins Formation rocks have variable kerogen types that are lithologically controlled. The remaining petroleum generative potential for the Joggins Formation source rocks are at best very good to excellent for oil and gas formation. Coal samples (figure inset) are excellent for gas or inert (Peters and Cassa, 1994).	18
Figure 9. Stratigraphic trends in TOC and HI for the Joggins Formation samples. Blue bars indicate the stratigraphic position of agglutinated forams (Archer et al., 1995) and echinoid ossicles (Grey et al., 2011), which are strong indicators of marine conditions in the depositional environment.....	19
Figure 10. Cross-plot of carbon and nitrogen stable isotope values for the Joggins Formation samples.	20
Figure 11. Cross-plots of carbon and nitrogen isotope versus the bulk pyrolysis parameters of TOC and HI.	20
Figure 12. GC×GC-FID chromatogram of a limestone apolar extract from JF-547.25m (dotted lines indicate the elution direction for various compound classes used in the biomarker analyses). From bottom to top the elution of <i>n</i> -alkanes and acyclic isoprenoids (I), cycloalkanes (II), tricyclic terpanes and alkylbenzenes (III), indenes (IV), naphthalenes (V), steranes (VI), and hopanes (VII), triaromatic steranes (VIII).....	21
Figure 13. Concentration profiles for <i>n</i> -alkane and the acyclic isoprenoids pristane (Pr) and phytane (Ph; See Appendix IV) for the Joggins Formation lithologic groups.....	23

Figure 14. Cross-plots of CPI versus Pr/Ph and Pr/n-C ₁₇ versus Ph/n-C ₁₈ ratios indicating the Joggins Formation samples have inputs of terrestrial sources higher plant waxes and were likely deposited under suboxic to oxic conditions.	24
Figure 15. Ternary diagram indicating the relative abundance of C ₂₇ , C ₂₈ , and C ₂₉ regular steranes.	25
Figure 16. Cross-plots of various triterpenoid biomarkers relating to bacterial inputs of organic matter. Gammacerane index is a measure of water column stratification. The 3β- and 2α-methylhopane indices do not have diagnostic trends of either photosynthesis and methylotrophy or lacustrine conditions. The sterane/hopane ratio measures the relative proportion of bacterial to eukaryotic (predominately algal input).	26
Figure 17. Cross-plot of four sterane and hopane thermal maturity parameters.	27
Figure 18. Stratigraphic trends in TOC, TOC _{initial} , and HI for the Joggins Formation samples. Blue bars indicate the stratigraphic position of agglutinated forams (Archer et al., 1995) and echinoid ossicles (Grey et al., 2011), which are strong indicators of marine conditions in the depositional environment.	30
Figure 19. Cross-plots of bulk rock pyrolysis richness, quantity, and maturity parameters versus total sulfur measurements.	31
Figure 20. Cross-plot of the Pr/Ph and dibenzothiophene/phenanthrene (DBTs/Ps) ratio indicating potential paleoenvironmental conditions of the depositional environment.	32
Figure 21. Cross-plot of the average sample abundance of C ₃₁ to C ₃₅ homohopanes.	32
Figure 22. Hierarchical cluster analysis of the Joggins Formation limestone (“clam coal”) samples of common elements found in seawater and marine sediments (Left; S, Cl, V, Sr, K, Ti, Mn, Ba, Cr). Dendrogram for all elements excluding Si and S (Right).	33
Figure 23. Hierarchical cluster analysis of the Joggins Formation shales and paleosol samples of common elements found in seawater and marine sediments (left; S, Cl, V, Sr, K, Ti, Mn, Ba, Cr). Dendrogram for all (middle). Dendrogram for all elements excluding Si and S (right).	34
Figure 24. Dendrograms produced by hierarchical cluster analyses of the Joggins Formation coals and coaly mudstones. A) Elements included are S, Cl, K, Ca, Ti, V, Ni, Cr, Mn, Fe, Zn, Cu, Sr, Mo, Ba, Pb, Th, U and B, the same selection without S, Fe, and Mo.	34
Figure 25. Cross-plots of Sr/Ca, Mn/Ca, V/Cr, Ni/Co, Sr/Br, and V/Ni derived from pXRF analyses of rock powders. Similar to the Pr/Ph ratios (Figure 9), the elemental ratios of V/Cr, Ni/Co, and V/Ni indicate deposition under predominately oxic conditions. Elevated salinity for some Joggins Formation source rocks is indicated for several of the limestone samples.	36
Figure 26. Stratigraphic profile of pXRF determined elemental ratios.	37

ATTENUATION OF PETROLEUM GENERATION CHARACTERISTICS BY THE SULFURIZATION OF ORGANIC MATTER IN WESTPHALIAN CARBONIFEROUS LACUSTRINE SOURCE ROCKS (A GEOCHEMICAL STUDY OF POTENTIAL MARINE INCURSIONS)

FINAL REPORT

1. Introduction

Pre-Atlantic-rift (prior to Triassic-Jurassic) marine incursions from the Tethys paleo-ocean into the largely fluvial/deltaic and lacustrine interior of the Maritimes Basin are well known from the Visean (Early Carboniferous) carbonates and evaporites of the Windsor Group (Calder, 1998; Gibling et al., 2008), but are otherwise equivocal and much debated in the literature in other parts of the Maritimes Basin fill (Gibling and Wightman, 1994; Tibert and Scott, 1999; Naylor et al., 1998; Whiteman et al., 1994; Calder, 1998). One such occurrence is the Carboniferous, Langsettian-aged (Westphalian A) fluvial-lacustrine clastics, calcareous source rocks, and coal seams of the Joggins type section (Davies et al., 2005). The Joggins Fm dramatically outcrops as a continuous sea cliff at Joggins, Nova Scotia, Canada (Figure 1 and 2). The site is a UNESCO World Heritage Site famous for its Pennsylvanian coal measures and associated tropical biota (Falcon-Lang and Calder, 2004; Falcon-Lang et al., 2010). The region, initially made famous by Sir William Dawson, Sir Charles Lyell, Sir William Logan, and Walter Bell, still draws considerable interest and new discoveries. Since then, the region has continued to be of scientific interest.

More recently, there has been considerable debate on if, or to what degree, there was connectivity between sediment depocenters and the Paleo-Tethys Ocean in the Carboniferous Period (Figure 3). This debate spanning nearly fifty years focuses on sedimentological, paleontological, and geochemical lines of evidence. Duff and Walton (1973) interpreted organic-rich, bivalve-bearing, calcareous shales (“clam coals”; Figure 4) as being marginal marine deposits emplaced during aborted marine transgression events. This interpretation was later found inconsistent with the common occurrence of coeval freshwater ostracods (Brand, 1994); which is more in line with Gibling et al. (1992), who inferred the Joggins fossil cliffs to have been deposited within an ecosystem primarily of continental affinity based on comparisons with other faunas in peat-forming settings. The clam coals were later interpreted to be the product of lacustrine or interdistributary bay environments at Joggins and other Maritimes Basin sites (Gibling and Kalkreuth, 1991). Additionally, Brand (1994) reported high enrichment factors for Mn and Fe in aragonitic bivalves at Joggins. These signatures likely derive from slightly dysaerobic water conditions during shell secretion. The analyzed bivalves have much higher $^{87}\text{Sr}/^{86}\text{Sr}$ ratios (>0.7093) than time-equivalent marine brachiopod and mollusc Sr-isotopes values based on data compiled since Brand's work (McArthur et al., 2001). This unambiguously indicates non-marine conditions existed in the mid- to upper-sections of the formation from which Brand's samples were sampled (Figure 5). Nonetheless, more recent reports indicate the possibility of shorter-duration marine-influenced events, particularly early in the deposition of the Joggins Fm. Archer et al. (1995) identified agglutinated forams at ~550m in the Joggins Fm. These microfossils are strong indicators of brackish-water conditions. Similarly, Tibert and Dewey (2006) identified the *Velatomorpha* and *Curvirimula* ostracodes, which are diagnostic indicators of marginal marine conditions. Grey et al. (2011) discovered putative echinoderm and brachiopod fragments in the lower formation that would require some connectivity between the Joggins

paleoshoreline and open waters of the Paleo-Tethys Ocean (Figure 3), although there may be alternative explanations for these occurrences (see section 5. Discussion). Our investigation attempts to further complement these studies by producing an organic and inorganic chemostratigraphic study of the Joggins Fm. with the emphasis on identifying geochemical indicators of marine transgression especially within the “clam coals”.

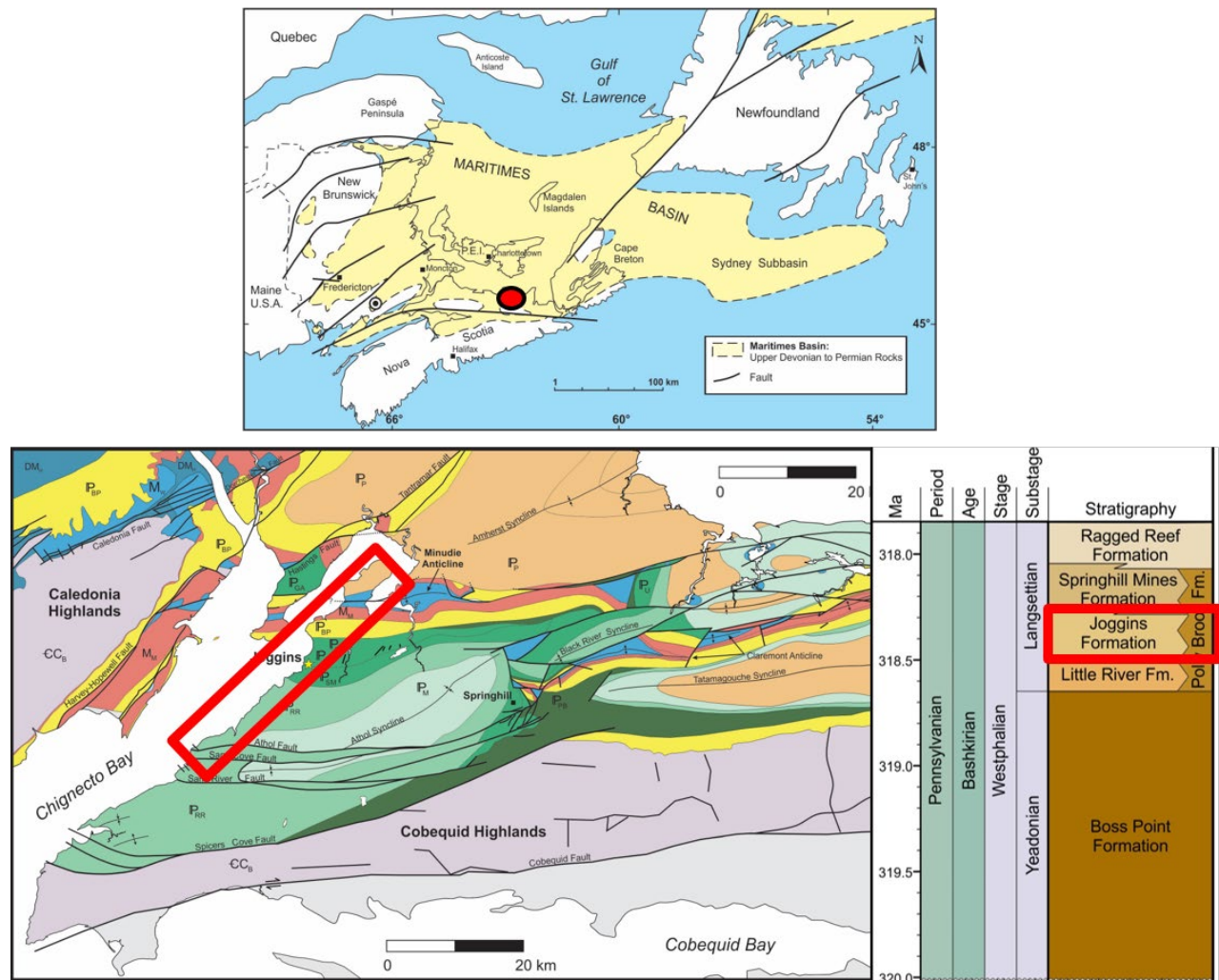


Figure 1. Map of the Maritimes Basin indicating the location of Joggins Fossil Cliffs locality (top). Map of the Cumberland Basin with accompanying stratigraphic section (bottom) indicating the stratigraphic target of the study (after Davies et al., 2005).



Figure 2. Photos of the Joggins fossil cliffs. Photo on the left provides an example of the dipping bedding visible in the rock outcrop exposed as ~20m high cliffs. The photo on the right is an outcrop photo from Cycle 3 showing the location of samples collected for this study.

A fundamental question from the Play Fairway Analysis on the Scotian Margin (OETRA, 2011) was the prediction of Early Jurassic and potentially Late Triassic aged source rocks that may have contributed petroleum hydrocarbons to reservoirs in the southeastern Scotian Margin. These hypothetical source rocks would represent pre-rift accumulations from lacustrine or marine pre- to post-salt intervals. Even older Paleozoic pre-rift basins such as the Maritimes and Sydney basins are known to have experienced marine phases (e.g., the Windsor Group). Other intervals are proposed to have experienced marine incursions from the Paleo-Tethys Ocean (Gibling et al., 2008; Wightman et al., 1994; Archer et al., 1995, Tibert and Scott, 1999, Wightman et al., 1994). Unpenetrated Paleozoic sediments are suspected beneath some of the Scotian Margin. Two examples are the Georges Bank (Wade, 1990) and the LaHave Platform (Deptuck and Altheim, 2018). Paleozoic sediments are also expected to be present within the easternmost Scotian Basin on the southern Grand Banks (Bell and Howie, 1990). If so, mobilized hydrocarbons in younger Mesozoic sequences could be composed of a mix of oil and gas-prone, marine and terrestrial Type I and II kerogen, derived from both Paleozoic and Mesozoic sources.

If such older rocks were deposited in marine conditions, their organic matter may be affected by sulfization. The SOM is an early diagenetic process that leads to the selective preservation of hydrogen-rich labile organic matter such as carbohydrates (Sinninghe Damsté et al., 1998) and thus affects the quality and to a lesser degree the quantity of organic matter preserved in marine source rocks. Furthermore, SOM leads to petroleum generation at shallower burial depths because lower temperatures are required to break the less stable sulfur-carbon bonds, which further releases sulfur radicals that act as catalysts for hydrocarbon cracking (i.e. Lewan, 1998; Hines et al., 2019). These processes are an important kerogen formation pathway in Oxfordian and Kimmeridge clay units of other regions (i.e. Sinninghe Damsté et al., 1998). However, the influence of SOM on age-equivalent and younger Scotian Margin sections is still to be examined. A site with known abundant sulfur present in coals, such as Joggins, can assist with calibration of lab techniques to monitor SOM occurrence in other intervals.

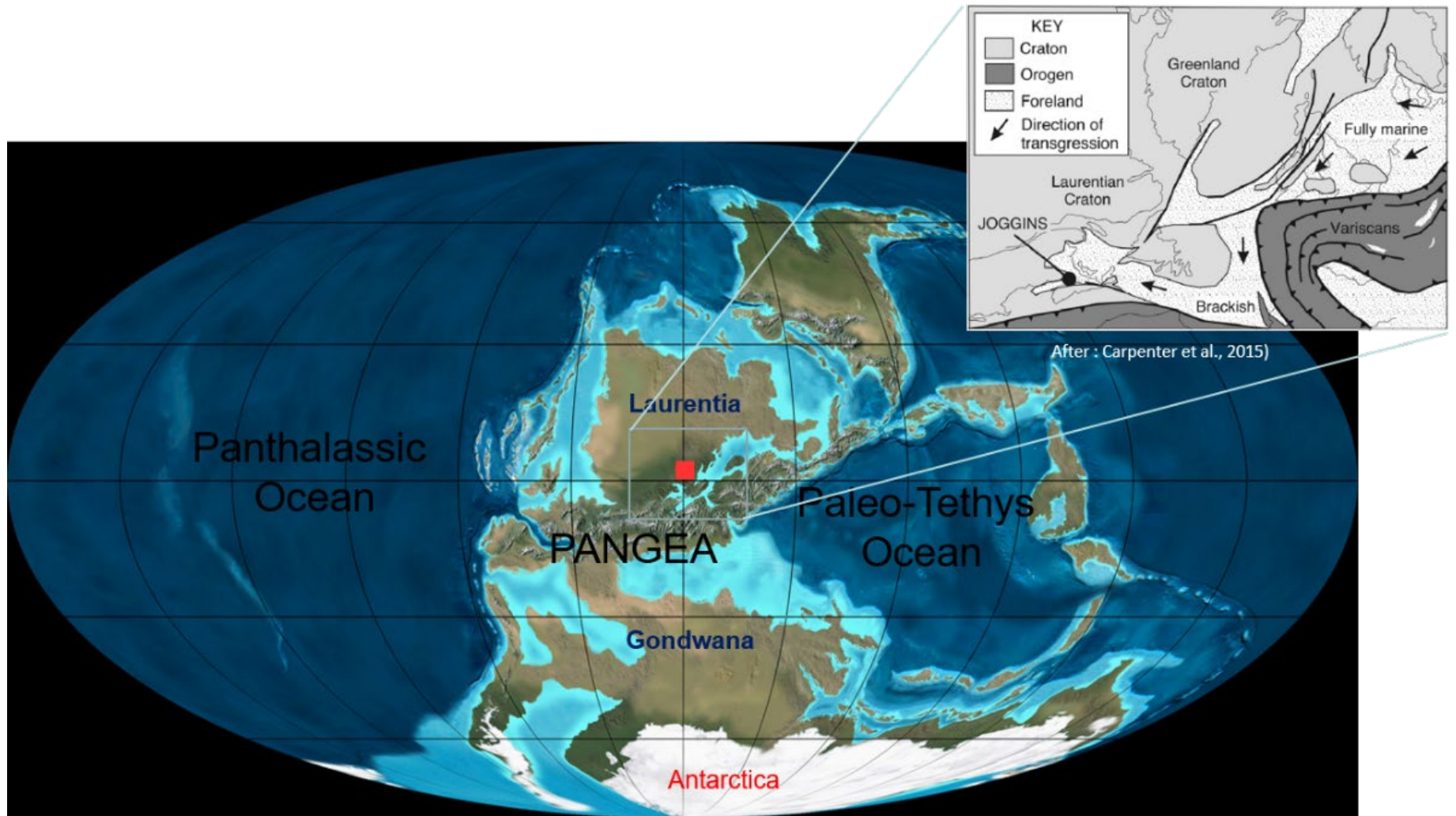


Figure 3. Paleogeographic reconstruction of Pangaea during the Carboniferous. Red square indicates the location of the Joggins Formation. During lowstands the depocenter was approximately 2,500km from the paleoshoreline (artwork by Ron Blakey based on plate reconstructions by Scotese and McKerrow, 1990). Larger scale blow-up map represents the possible open-water connection to the Paleo-Tethys Ocean during sealevel highstands (Gibling et al. 1992; Carpenter et al., 2015).

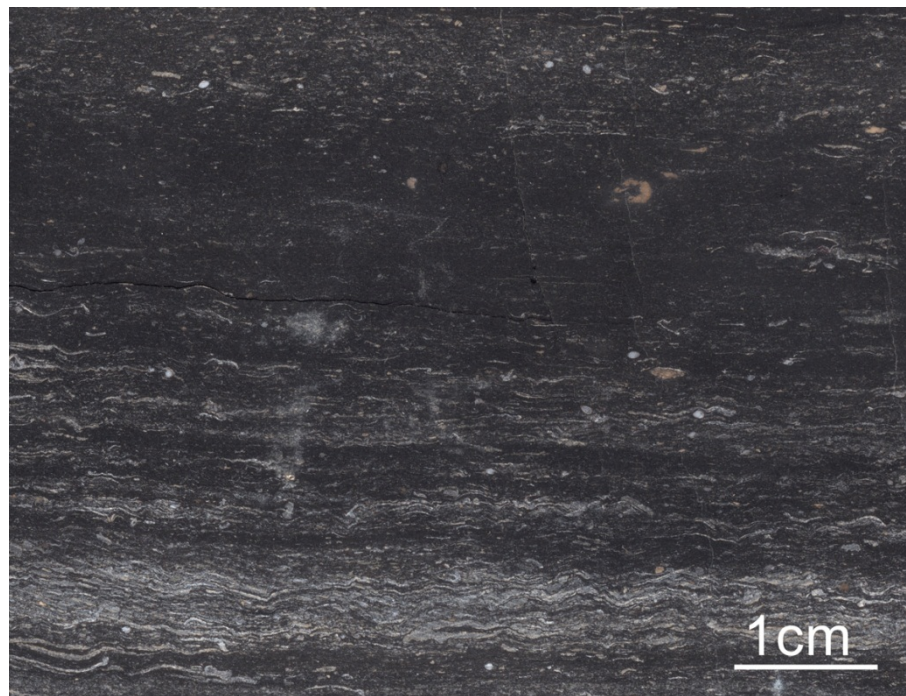
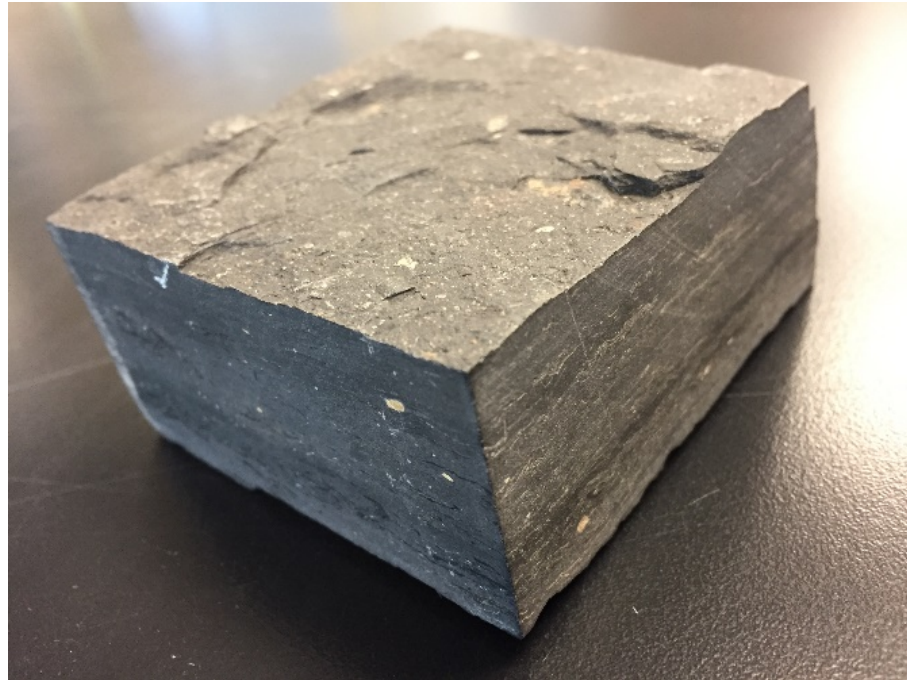


Figure 4. Bivalve-bearing limestone units of the Joggins Formation (“clam coals”) can be organic-rich, laminated and contain abundant bivalves, ostracods, fish bones and teeth, and coprolites.

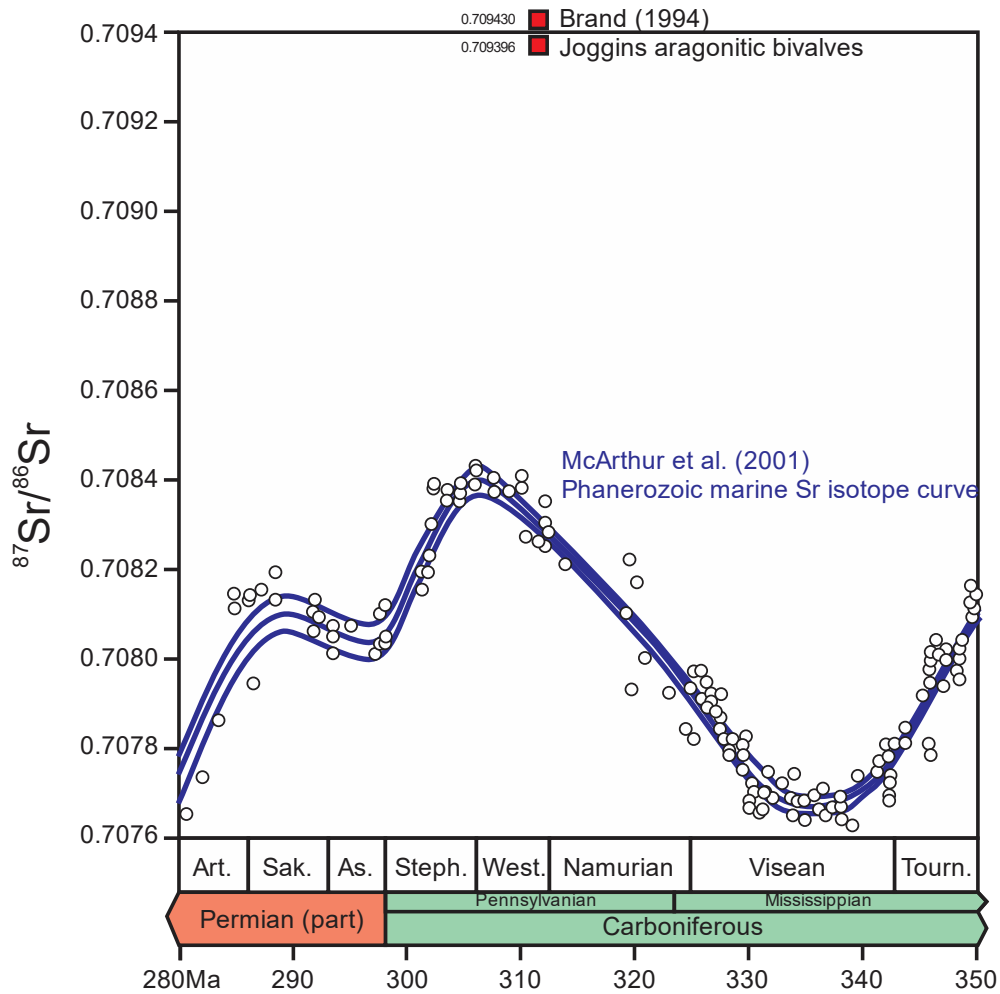


Figure 5. The Sr marine isotope curve for the Permian and Carboniferous periods (McArthur et al., 2001). Overlaid on the curve are the Brand (1994) Joggins aragonitic bivalve fossil measurements, which clearly fall outside the Carboniferous trend.

2. Geological Setting

The Maritimes Basin of Nova Scotia, New Brunswick, Newfoundland, and Quebec provides a nearly complete stratigraphic record from Middle Devonian through Lower Permian in an ~12km thick sequence that is spectacularly exposed along continually eroding coastal sections across the region (Gibling et al., 2008, Figure 1 and 2). The basin was born from the Acadian-Caledonian orogeny that first witnessed the suture of the Iapetus in the Devonian and thereafter was shaped by the closing of Gondwanaland and Laurasia. During the Carboniferous, Nova Scotia lay at the heart of paleo-equatorial Euramerica in a broadly intermontane paleo-equatorial setting. The Joggins formation is located in the Cumberland Sub-basin, which is a component depocenter of the composite Maritimes Basin (Figure 1). The Joggins section is located between Lower Cove and the old Joggins Wharf (latitude 45°42' N; longitude 64°26' W) on Chignecto Bay, Bay of Fundy, Nova

Scotia, Canada. The formation is stratigraphically underlain by the Little River Formation and overlain by the Springhill Mines Formation (Davies et al., 2005; Rygel et al., 2014). Deposition of the 932.4m thick section occurred in less than one Myr beginning at ~318.5 Ma within the Langsettian (Westphalian A) as a result of subsidence related in part to salt tectonics (Waldron et al. 2013).

Lithostratigraphic changes across the Joggins Fm have been carefully mapped (Davies and Gibling, 2003; Davies et al., 2005; Falcon-Lang et al., 2006) as a series of 15 sedimentary cycles based on major flooding surfaces resulting from base level changes in the basin. The section is further subdivided based on a paleoenvironmental classification. This includes well-drained floodplain facies association (WDFa) representing floodplain aggradation above base level as well as progradational, poorly-drained floodplain facies association (pPDFa) that are marked by bay-fill deposits formed by wetland deltas. Open-water facies association (OWFA) and retrogradational, poorly-drained floodplain facies association (rPDFa) represent basin-wide flooding by a 'brackish sea'.

3. Previous Geochemical Analyses

Given the geological significance, surprisingly little geochemical work has been conducted on the Joggins Fm. Mukhopadhyay (1991a,b) provided selected RockEval analyses in petroleum prospectivity open file report. The Queens Seam coal generative potentials were determined based on hydrous pyrolysis experiments. Stankiwicz et al. (1998) exemplified the molecular taphonomy of Carboniferous arthropods in the Joggins Fm using pyrolysis-gas chromatography/mass spectrometry. The pyrolysates included homologous series of alkanes and alkenes as well as phenolic and other aromatic constituents. Hower et al. (2000) examined five metalliferous high-vitrinite coals from the Joggins Fm. These coals were humic and mixinitic (rich in pitinitic) and contained abundant telocollinite and geloliptinite with resinite and sporinite as the main liptinitic macerals. The coals were high in total and pyritic sulfur, but also had high concentrations of chalcophile elements. Zinc, ranging up to 15,000 ppm (ash basis), was bound as sphalerite in fusain lumens. Arsenic and lead each exceeded 6000 ppm (ash basis) in separate lithotypes of the Kimberly coals. Together these data are consistent with elevated pH in planar mires. The source of the elemental enrichment in this presumed continental section is enigmatic. Although this prior work has examined selected samples for their organic and inorganic geochemical signatures, these studies are largely comparative – aiming to survey various Carboniferous sections across the Maritimes.

4. Methods

4.1. Sample Collection and Preparation

Forty-seven rock samples were collected from the Joggins Fossil Cliffs (Figure 1; Appendix I) under permit from the Joggins Fossil Center and the Nova Scotia Museum. Sampled rock units were selected to establish representative coverage of the overall stratigraphic interval of the Joggins Formation as well as to maximize efforts to capture lithologic changes associated with base level changes within multiple cyclothems. Within this context, the basal units of the Joggins Fm was more heavily surveyed in areas that have previously been identified as having marine-sourced fossil signatures (Grey et al., 2011, Figure 4). In total 7 of the 15 documented cyclothems were surveyed. Example photographs of the rock samples collected for each of the major lithologies (shale, limestone, coal and coaly mudstones) are provided in Appendix II. Rock samples were powdered and homogenized by hand with mortar and pestle, and separated into sample splits that were

used for bulk rock pyrolysis, pXRF, solvent extraction for biomarker studies, and for carbon and nitrogen isotope measurements. The summary of analyses completed for each sample is provided in Appendix II.

4.2. Bulk Pyrolysis

A 2g split of the rock powders from 41 of the 47 samples was sent to APT Ltd. Norway for bulk pyrolysis measurements. Total organic carbon was measured using a Leco instrument. Hydrogen and oxygen indices, as well as T_{\max} values were measured using a HAWK source rock pyrolyzer from Wildcat using industry-specific external standards. Bulk pyrolysis data are provided in Appendix III.

4.3. Biomarker Analysis

Rock powders were solvent extracted three times using a CEM MARS 6 microwave extraction system. For each sample 30g of sediment was extracted three times with 60ml of DCM:MeOH (7.5:1) with an oven ramp of up to 200°C for 15 min at 1500 V. Replicates of each sample extract were combined and rotary evaporated to 2ml before being filtered using a .45µm GF filter cartridge. The resulting total lipid extracts (TLE) was transferred to pre-weighed sample vials. An aliquot of TLE was further separated into apolar and polar fractions by flash chromatography using activated silica gel (60-200 mesh) as the stationary phase in Pasteur pipette column. DCM:Hexane (9:1) was used to collect the apolar fraction followed by DCM:MeOH (1:1) to obtain the polar fraction. The apolar fractions were then cleaned of elemental sulfur by passing the sample through a column containing activated Cu (HCl 6N) with hexane as the eluent.

The resulting apolar fractions were analyzed by comprehensive two-dimensional gas chromatography (GC×GC) using an Agilent 7890B gas chromatograph equipped with a Zoex Corp. ZX1 cryogenic modulator and flame ionization detector (GC×GC-FID) also interfaced to an Agilent 7200B quadrupole mass spectrometer (GC×GC-qToFMS). The 1st dimension separation was performed on a nonpolar 5% phenyl polydimethylsiloxane phase (Agilent, DB-5ms, 20.0-m; 0.25-mm ID; 0.25-µm film thickness) and temperature programmed from 80 (held for 20 min) and ramped to 320 °C at 2 °C min⁻¹. The modulation column was a deactivated silica (1.0-m, 0.10-mm ID). The hot jet temperature programmed began at 200 °C (held for 20 min) and then ramped to 400 °C at 2 °C min⁻¹. The 2nd dimension separation was performed using a polar 50% phenyl equivalent polysiloxane (BPX-50, SGE, 1.5-m; 0.10-mm ID; 0.1-µm film thickness) column. A 1.0-m length 0.10-mm ID deactivated silica column was used to join the 2nd dimension column via the capillary flow splitter into the ToF detector transfer line held constant at 230 °C. Hydrogen was used as the carrier gas in constant flow mode (1.2 mL/min). The GC×GC modulator period was 10 s. The qToFMS collected 50 spectra/s at 4 GHz. A detector voltage of 1800 V was used with a solvent delay of 12 min. The similar column array used for GC×GC-FID provided equivalent compound separation. Quantitation of all biomarkers was performed using GC-Image software. The biomarker concentration and ratio data are provided in Appendix IV.

4.4. Carbon Isotope Analysis

For carbon isotope analyses, 3g of the rock powder was further decarbonated with 30ml of 6N hydrochloric acid (Argos reagent grade HCl) using a CEM MARS 6 microwave (work in progress). The decarbonated sediments were transferred to centrifuge tubes and then returned to neutral pH by rinsing the decanted sediments with ultrapure (18.2 MΩ.cm at 25°C) water vortex mixed, centrifugation of the tube at 1400 rpm for 10 min, followed by decanted the supernatant. This process was repeated until the supernatant reached neutral pH. The isotope values for the samples were then measured using an elemental analyzer at Memorial

University in St. John's, Newfoundland to obtain carbon and nitrogen isotope compositions. The pXRF data are provided in Appendix IV.

4.5. Portable X-ray Diffractometer (pXRF)

A Niton™ field x-ray lab pXRF s with a 10–40 kV(10–50 μ A) Rh X-ray tube and a high-count rate detector. sourced from the Nova Scotia Geoscience and Mines Branch, Halifax, was used to measure total sulfur, transition metal, and rare Earth element concentrations on non-extracted sample powders. Elemental concentrations were measured in triplicate and calibrated to in-house external standards. To limit this uncertainty, but still maximise throughput, the total analysis time was set to 60 seconds (30 seconds per beam). Analytical uncertainties were typically $\leq 3\%$ as reported by the pXRF unit. To check for contamination, SiO₂ blanks were analysed periodically. The pXRF data are provided in Appendix V and VI. Due to limitations of the instrument Al values and standard oxides were not measured. Efforts to find another instrument to include these data were unsuccessful. For this reason shale enrichment factors were not tabulated.

5. Results

5.1. Bulk Rock Geochemistry

The Joggins Fm rocks were grouped by lithology into mudrocks, paleosols, limestones, coals, and coaly mudstones. Bulk pyrolysis measurements were in some cases hampered by low organic matter contents, which can produce spurious HI and T_{max} values (Figure 7). Therefore, all samples with S2 values less than 0.5mgHC/gTOC should be carefully screened. For this study, several T_{max} values from TOC lean samples gave false indications. The HI values, however, appeared to be largely reliable, even with extremely lean samples (Figure 7). Furthermore, a comparison of the volatile organic matter related to S1 parameter in comparison to sample TOC indicates the Joggins Fm rocks contain primary organic matter that has not been affected by, or over printed with, secondary sources of organic matter.

The TOC of the shale and paleosols ranges from 0.25 to 6.99 wt.% with values over 3 wt.% incorporating carbonized plant debris. The TOC of the limestones range from 0.6 to 5.98 wt.%. Coals and coaly mudstones have TOC values that span 29.3 to 70.4 wt.%. No stratigraphic trends were apparent in organic matter enrichment within the formation. The oxygen index ($OI=S3*100/TOC$) for the Joggins Fm rocks range from 2 to 60 mg CO₂/g TOC. As with T_{max}, the OI values for samples having <0.5 wt.% TOC may also be meaningless (Espitalie et al., 1982; Jarvie and Tobey, 1999).

The hydrogen index ($HI=S2*100/TOC$) of the Joggins Fm rocks ranges from 20 to 520 mg HC/gTOC (Figure 7 and 8). Higher HI values are associated with the limestone, coals, and coaly mudstones. A general stratigraphic trend of increasing organic matter quality in the limestone unit up the section is observed (Figure 9). Following the classification scheme of Peters and Cassa (1994), Type II kerogens have HI values ranging from 300 to 500 mg HC/g TOC). Type III kerogens have HI values between 50–200 mg HC/g TOC) and Type IV kerogens have HI values <50 mg HC/g TOC. Based on T_{max} measures the Joggins Fm source rocks are largely immature to early mature and composed of Type II (one limestone sample), a mix of Type II-III (majority of all other limestones), or Type III (coals, coaly mudstones, and shales) kerogens (Figure 8). The remaining petroleum generative potential of the limestones samples range from very good to excellent for oil and gas generation with one sample being very good for oil generation. All of the shales and paleosols are fair to excellent for gas or are inert. The coals and coaly mudstones are all inert. The kerogens contain immature to mature organic matter with T_{max} values ranging from 415–450°C, based on Peters and Cassa (1994), with one spurious outlier of 512°C that is due to analytical error from the very low TOC in the sample (Figure 7; Appendix III). The production index ($PI=S1/(S1+S2)$) can also be used to estimate source rock maturity. PI

values are low and range from 0 to 0.29 indicating that these Joggins kerogens are mature (Figure 8; Appendix III).

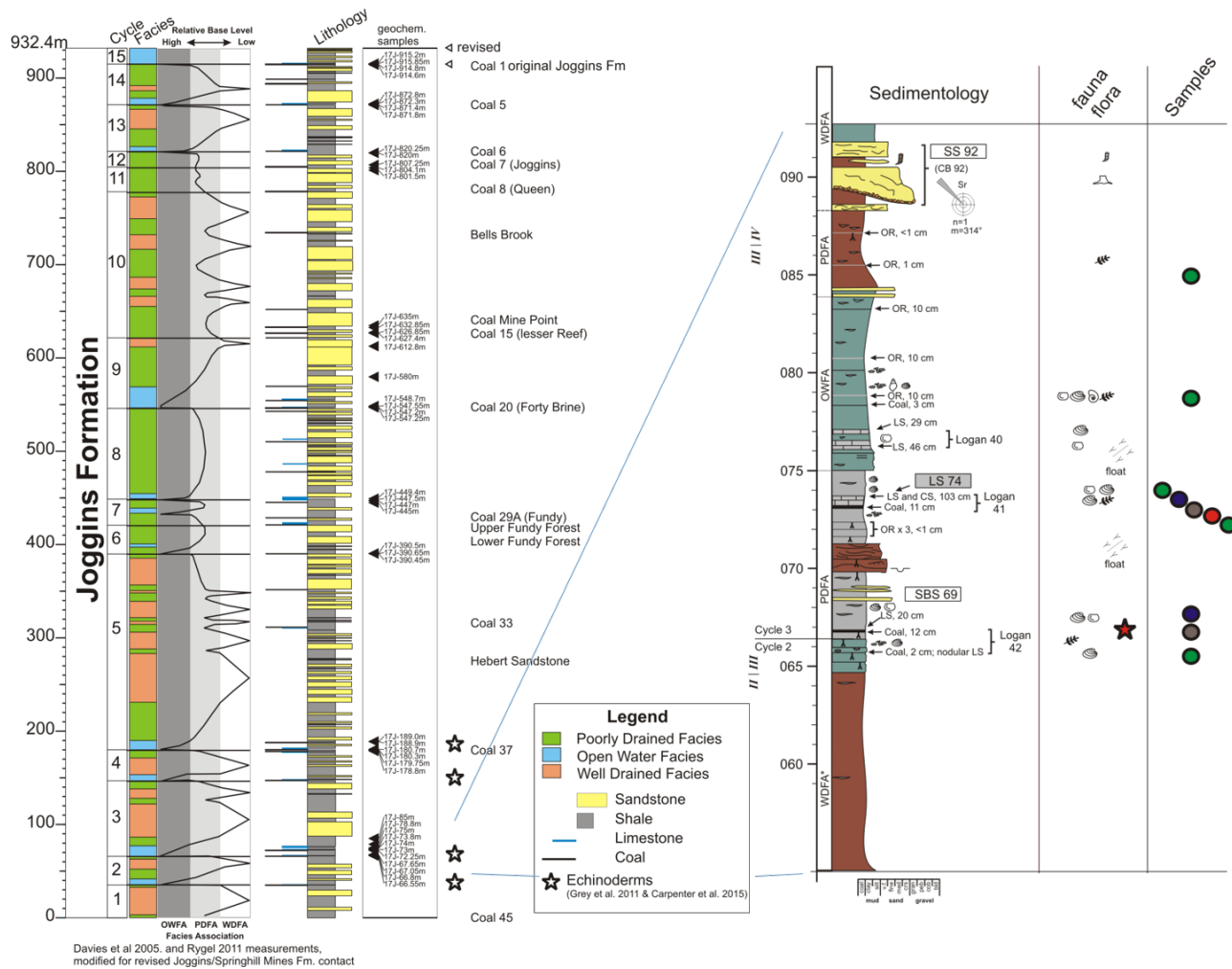


Figure 6. Summary stratigraphic profile and base level changes of the Joggins Formation modified from Davies et al., 2005 to reflect the change in Joggins/Springhill Mines contact proposed by Rygel et al. (2014) (left). Numbers in the column labeled “Cycle” are the 15 recognized cyclothems. Samples collected for this study are marked by sideways triangles. Stars represent stratigraphic level of echinoderm ossicles reported by Grey et al. (2011) and Carpenter et al. (2015). Enlargement of the lower section of the Joggins Formation in the interval suspected to have been effected by marine incursions (modified from Davies et al., 2005) (right). Samples collected for this study are indicated by colored circles.

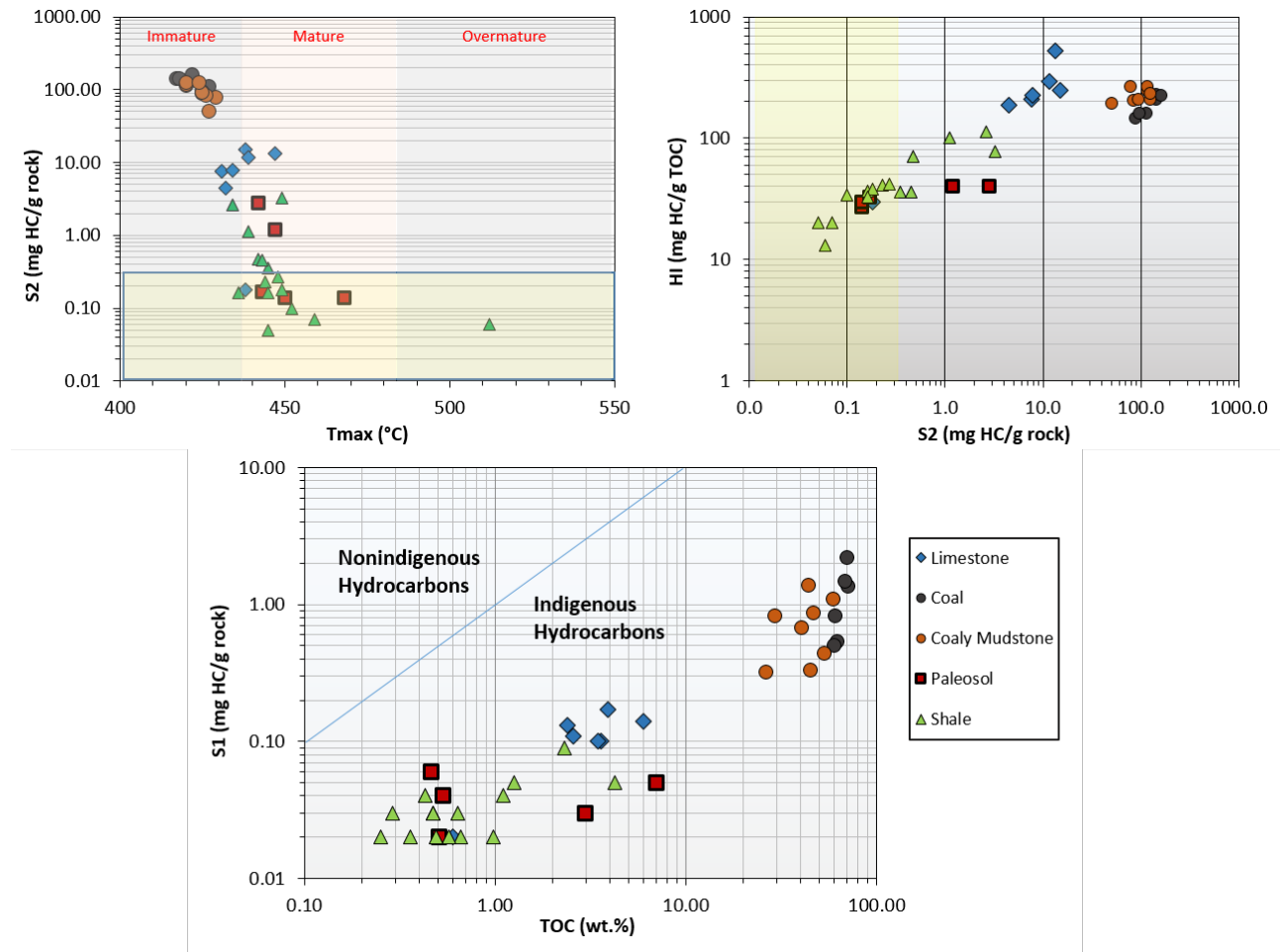


Figure 7. Bulk pyrolysis of the Joggins Fm samples. Low S2 values have caused some T_{max} maturity measures to be inaccurate (light green fields). However, this has likely not resulted in spurious HI measures for equivalent TOC lean samples. Comparisons of SI versus TOC indicates the Joggins Formation organic matter is likely syngeneic.

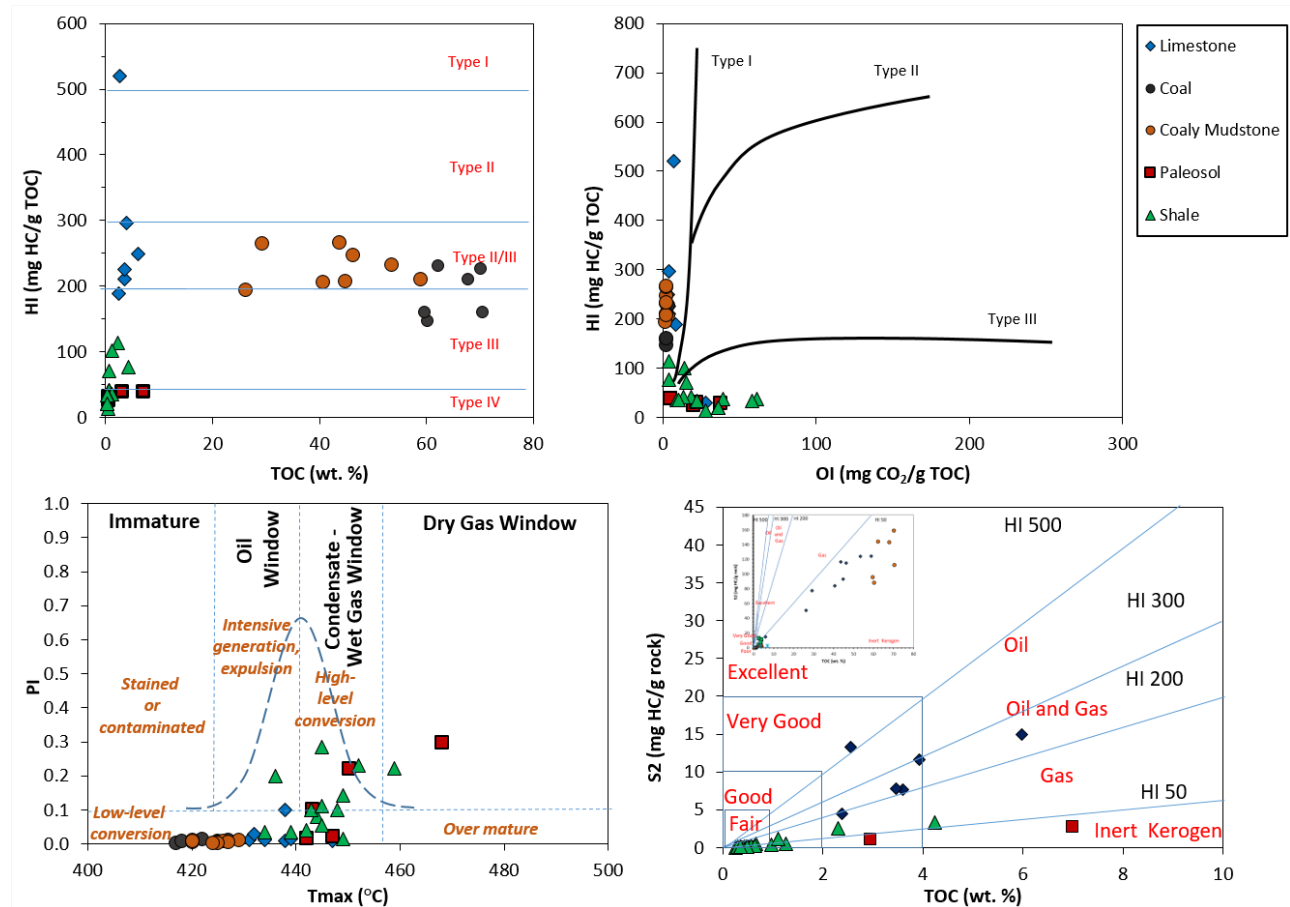


Figure 8. Cross-plots of HI, TOC, OI, PI, T_{max} , and S2 depicting kerogen quality, quantity, type, maturity, and generative potential. The Joggins Formation rocks have variable kerogen types that are lithologically controlled. The remaining petroleum generative potential for the Joggins Formation source rocks are at best very good to excellent for oil and gas formation. Coal samples (figure inset) are excellent for gas or are inert (Peters and Cassa, 1994).

5.2. Carbon and Nitrogen Stable Isotopes

Bulk carbon and nitrogen stable isotopes were measured on all decarbonated powdered sediment fractions (Figure 10; Appendix IV). Carbon and nitrogen isotope values are relatively uniform across the stratigraphic section (avg. $\delta^{13}\text{C}$ -24.26‰; SD 1.97‰ and $\delta^{15}\text{N}$ 3.61‰; SD 0.85‰, respectively). Carbon isotopes of bulk organic matter indicate the collective source of organic carbon within the bitumen and kerogen of the prospective source rocks and the carbon fixation pathways this pool was created. Carbon isotope compositions also reflect the secular global changes in dissolved inorganic carbon over geologic time and therefore have been loosely used to benchmark the age of source rocks that have generated crude oils (i.e. Kvenvolden and Squires, 1967). Nitrogen isotope ratios in sedimentary organic matter generally reflect the biomass from which it is derived, with terrestrial plants having slightly lower average $\delta^{15}\text{N}_{\text{atm}}$ values than marine plankton (Fogel and Cifuentes, 1993). The values of $\delta^{15}\text{N}$ generally decrease slightly during diagenesis due to bacterial utilization of short-chain peptides following peptide bond hydrolysis (Macko, et al., 1993).

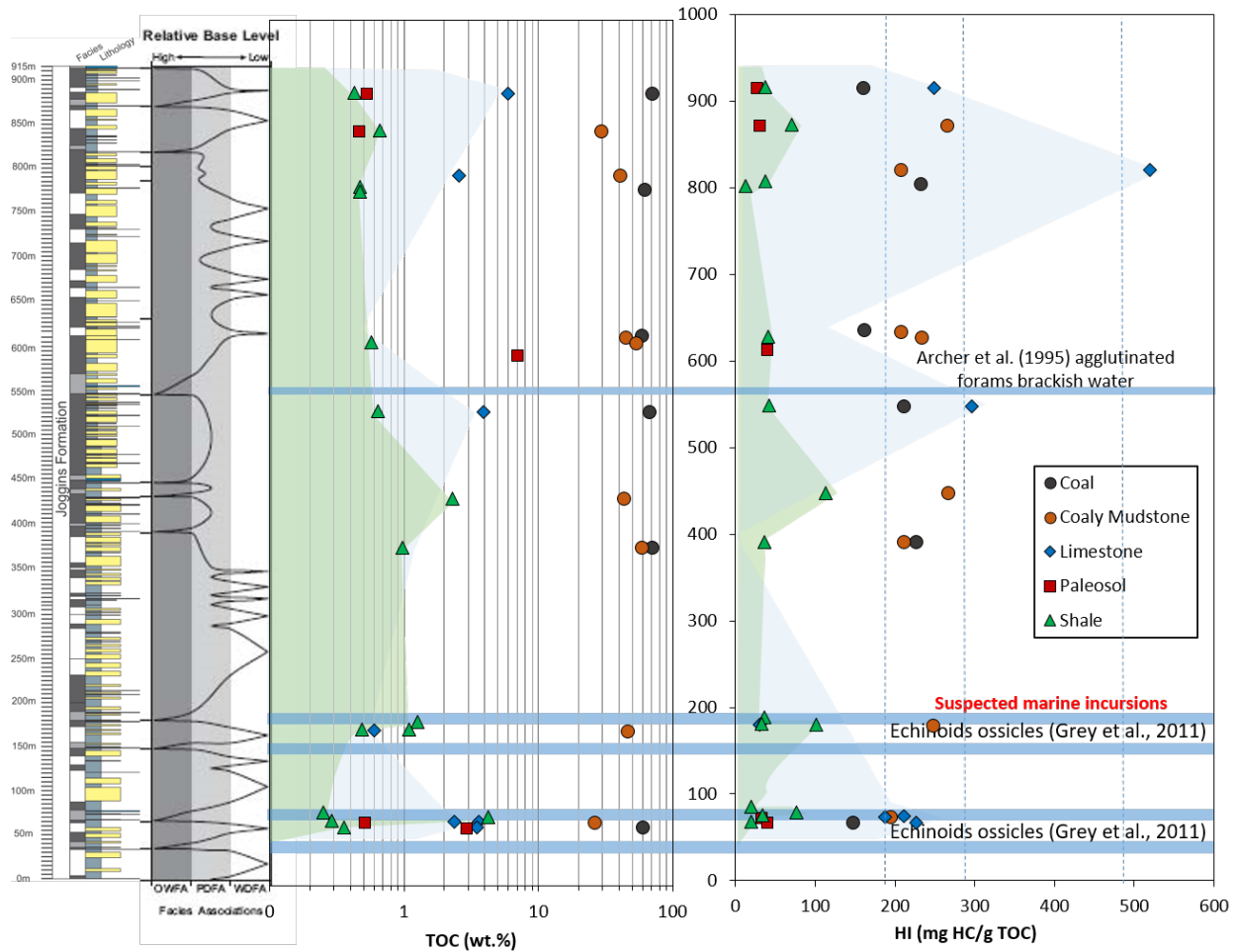


Figure 9. Stratigraphic trends in TOC and HI for the Joggins Formation samples. Blue bars indicate the stratigraphic position of agglutinated forams (Archer et al., 1995) and echinoid ossicles (Grey et al., 2011), which are strong indicators of marine conditions in the depositional environment.

With the exception of the upper-most stratigraphic sample (915.2m), the limestone units have slightly more depleted carbon isotope (avg. $\delta^{13}\text{C}$ -26.48‰) compositions and more enriched nitrogen isotope (avg. $\delta^{15}\text{N}$ 4.01) values (Figure 10). The carbon isotopic composition of terrestrial C3 plants typically ranges from -25 to -30 ‰. The average value for the Joggins Fm coals is slightly more enriched at -23.85‰, which is consistent with the global average coal values of the Carboniferous (Suto and Kawashima, 2016) reflecting low CO_2 concentrations (Graham et al., 1995) with high stomatal density and conductance rate (Beerling and Woodward, 2001). The isotopic composition of marine plants typically ranges from -20 to -28‰ and is in the range observed for the Joggins Fm limestones. Additionally, the most depleted Joggins Fm sample, JF-820.25m ($\delta^{13}\text{C}$ -29.8‰), records the highest HI value (520 mg HC/gTOC). For the limestone and shale lithologies, the $\delta^{13}\text{C}$ values display a moderately, positively correlated trend ($r^2 = 0.61$ and 0.49 , respectively; Figure 11) that likely indicates increasing algal input with elevated microbial activity under more reducing conditions (See section 6.3.3 Elemental ratios for redox conditions and salinity).

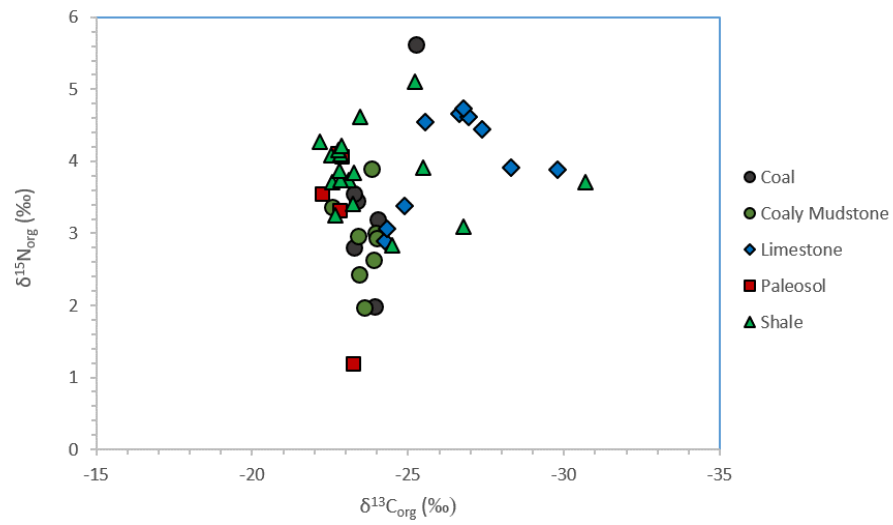


Figure 10. Cross-plot of carbon and nitrogen stable isotope values for the Joggins Formation samples.

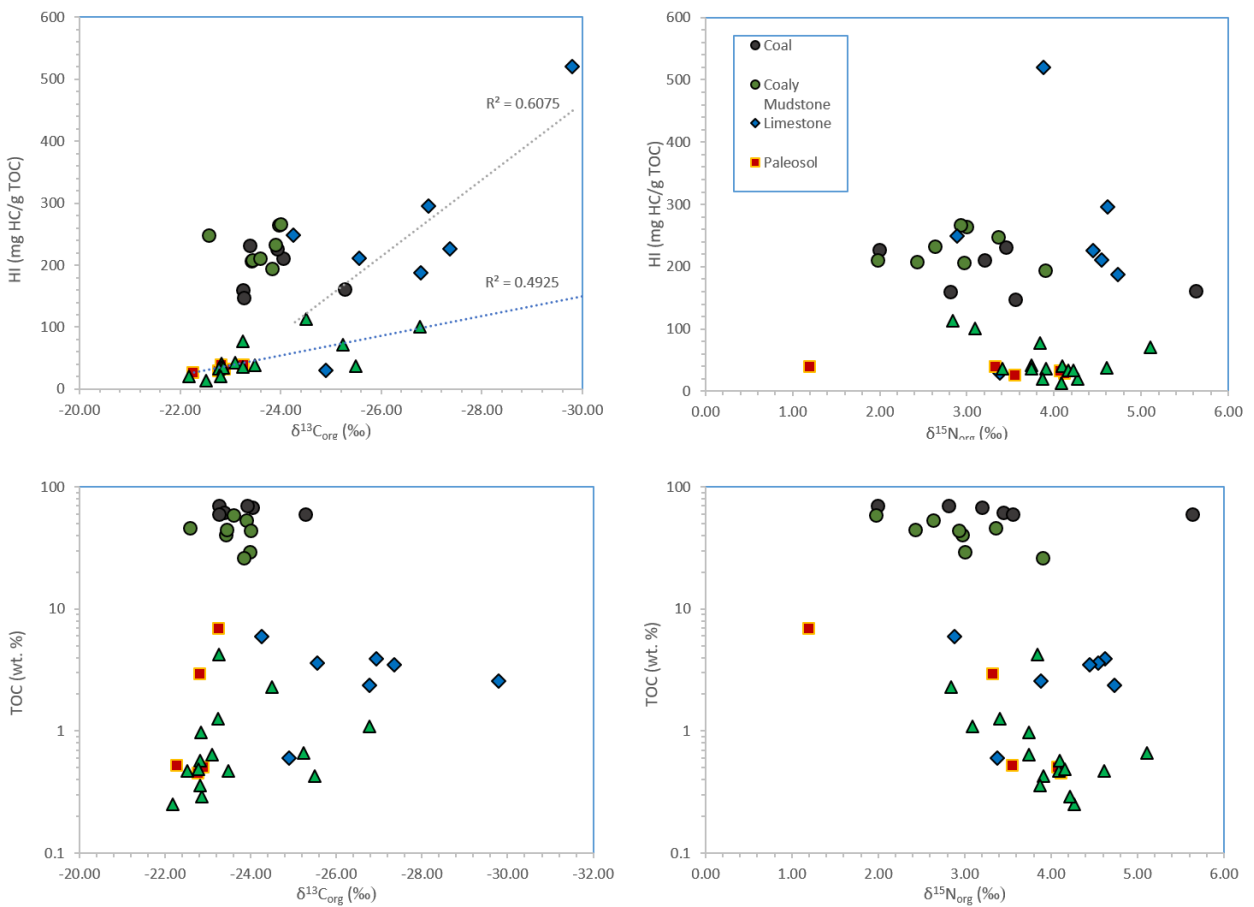


Figure 11. Cross-plots of carbon and nitrogen isotope versus the bulk pyrolysis parameters of TOC and HI.

5.3. Petroleum Biomarkers

The GC×GC-FID chromatograms (Figure 12) display other compound series, such as monomethyl alkanes, alkylcyclohexane, alkylcyclopentanes, alkylbenzenes, and methylalkylbenzenes. Cyclic terpenoids included tricyclic (cheilanthanes), tetracyclic (steranes), and pentacyclic (hopanes) terpanes. Aromatic components of the samples include alkylated naphthalenes, indenes, fluorenes, and phenanthrenes (Figure 12). Common organosulfur compounds, such as benzothiophenes and dibenzothiophenes, were typically observed in low abundance and frequently below detection limits. Their alkylated derivatives were generally more abundant, but not quantified in this study. The relative abundance of unsubstituted polycyclic aromatic hydrocarbons was also generally very low compared to their substituted homologs (monomethyl-, dimethyl-, and trimethyl-). This suggests the low abundance of unsubstituted organosulfur compounds and polycyclic aromatic hydrocarbons is, in part, a function of the overall low maturity of the organic matter (See sections 5.1 Bulk Rock Geochemistry and 5.4. Organic Matter Thermal Maturity Based on Molecular Parameters).

Quantitation of all biomarkers, aromatic hydrocarbons, and organosulfur compounds was made from the GC×GC-FID chromatogram. The identification of the elution position of all target compounds in the FID trace was determined by comparison with samples run using GC×GC-ToFMS with the tentative identification of the specific analyte being made by mass spectral analysis and through comparison of analyte elution position as documented in the literature. The monitoring of specific diagnostic fragment ions is indicated below for the respective compound class.

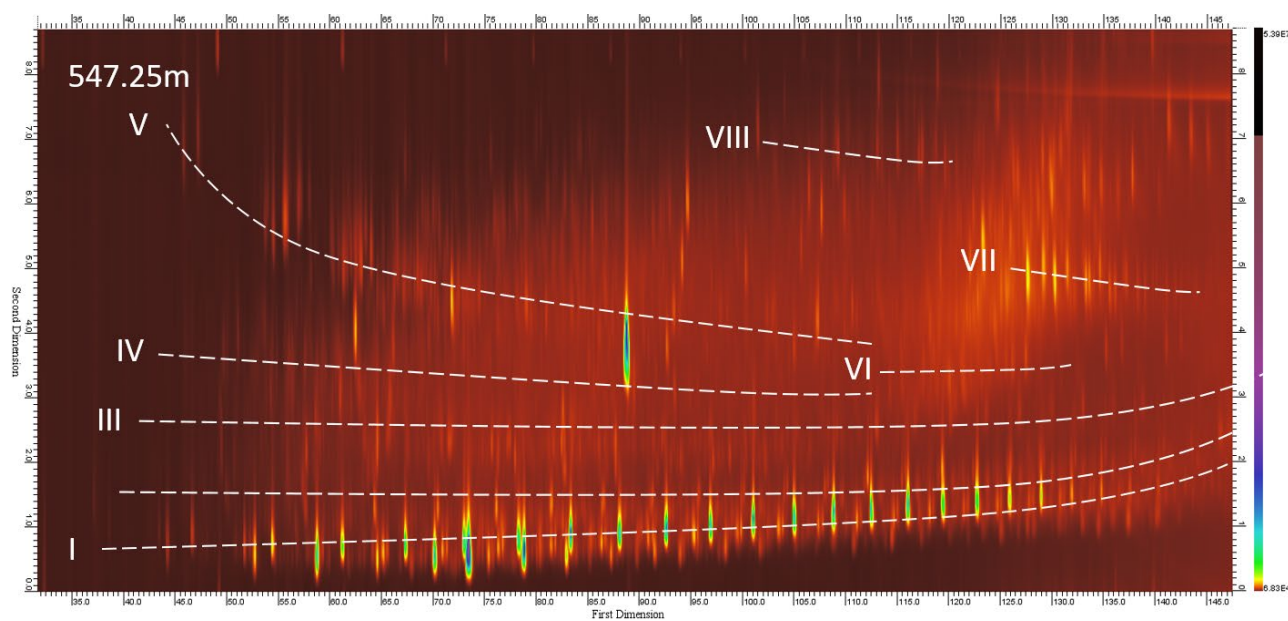


Figure 12. GC×GC-FID chromatogram of a limestone apolar extract from JF-547.25m (dotted lines indicate the elution direction for various compound classes used in the biomarker analyses). From bottom to top the elution of n-alkanes and acyclic isoprenoids (I), cycloalkanes (II), tricyclic terpanes and alkylbenzenes (III), indenes (IV), naphthalenes (V), steranes (VI), and hopanes (VII), triaromatic steranes (VIII).

5.3.1. Normal alkanes and acyclic isoprenoids

Normal alkanes and acyclic isoprenoids were monitored using m/z 57 and 183 mass chromatograms. All of the Joggins Fm samples contain homologous series of n -alkanes ranging from n -C₁₂ to n -C₃₆ and pseudohomologous series of acyclic isoprenoids such as farnesane, norpristane, pristane (Pr), and phytane (Ph). The distribution of n -alkanes is specific to sample lithology. Coals and coaly mudstones have higher abundances of lower molecular weight (n -C₁₂ to n -C₁₉) n -alkanes. Limestones have a broader distribution with two samples at JF-820.25m and JF-179.75m having pronounced high n -alkane abundances. The shale and paleosol samples display distinct bimodal patterns of elevated low and high molecular weight homologs (Figure 13).

Carbon preference index (CPI) is a parameter frequently used to measure the degree of input of terrestrial sourced higher plant waxes that have an odd predominance of higher molecular weight n -alkanes (Eglinton and Hamilton, 1966; Douglas and Eglinton, 1966). This parameter can also be used to track organic matter maturation. As source rocks become heated with deeper burial, the CPI of their associated bitumens decreases due to cracking of n -alkanes (Figure 14). Most of the Joggins Fm source rocks contain CPI values >1 indicating they are immature. However, several samples also have CPI values that are close to 1 suggesting higher maturity levels.

The acyclic isoprenoids Pr and Ph are abundant biomarkers in bitumens and oils. Although these compounds can derive from various sources; it is common to treat them as being exclusively the diagenetically altered photosynthetic carotenoid inputs of chlorophyll a (phytol) that has undergone differential oxidative and reductive steps due to the redox conditions within the depositional environment (e.g. Didyk et al., 1978). As such, the Pr/Ph ratio is frequently used as paleo-redox measure. In this regard, high Pr/Ph ratios indicate sediment deposition in oxic conditions. For example, Pr/Ph ratios >3 may indicate deposition of terrestrial organic matter under oxic conditions (Peters et al., 2005). The Joggins Fm coals and coaly mudstones have Pr/Ph ratios that range from 3.06 to 12.05 (avg. 6.4) suggesting sediment deposition in fully oxic conditions. The limestone units range from 0.3 to 3.88 (avg. 1.77) falling largely within an oxic water column overlying anoxic sediments (Figure 14). However, sample JF-872.3m and JF-189m have low Pr/Ph ratios (0.38 and 0.30, respectively) that indicate anoxic or hypersaline conditions. The shale units range from 0.33 to 5.73 (avg. 1.90) largely also representative of burial in oxic conditions. Furthermore, comparisons of the Pr/ n -C₁₇ and Ph/ n -C₁₈ ratios suggests good agreement with the source of bitumens and their associated kerogens with redox conditions. However, this ratio can be impacted by other factors including source, generation rate, maturity, and analytical uncertainty (e.g. ten Haven et al., 1987; Volkman and Maxwell, 1986; de Graaf et al., 1992; Navale, 1994).

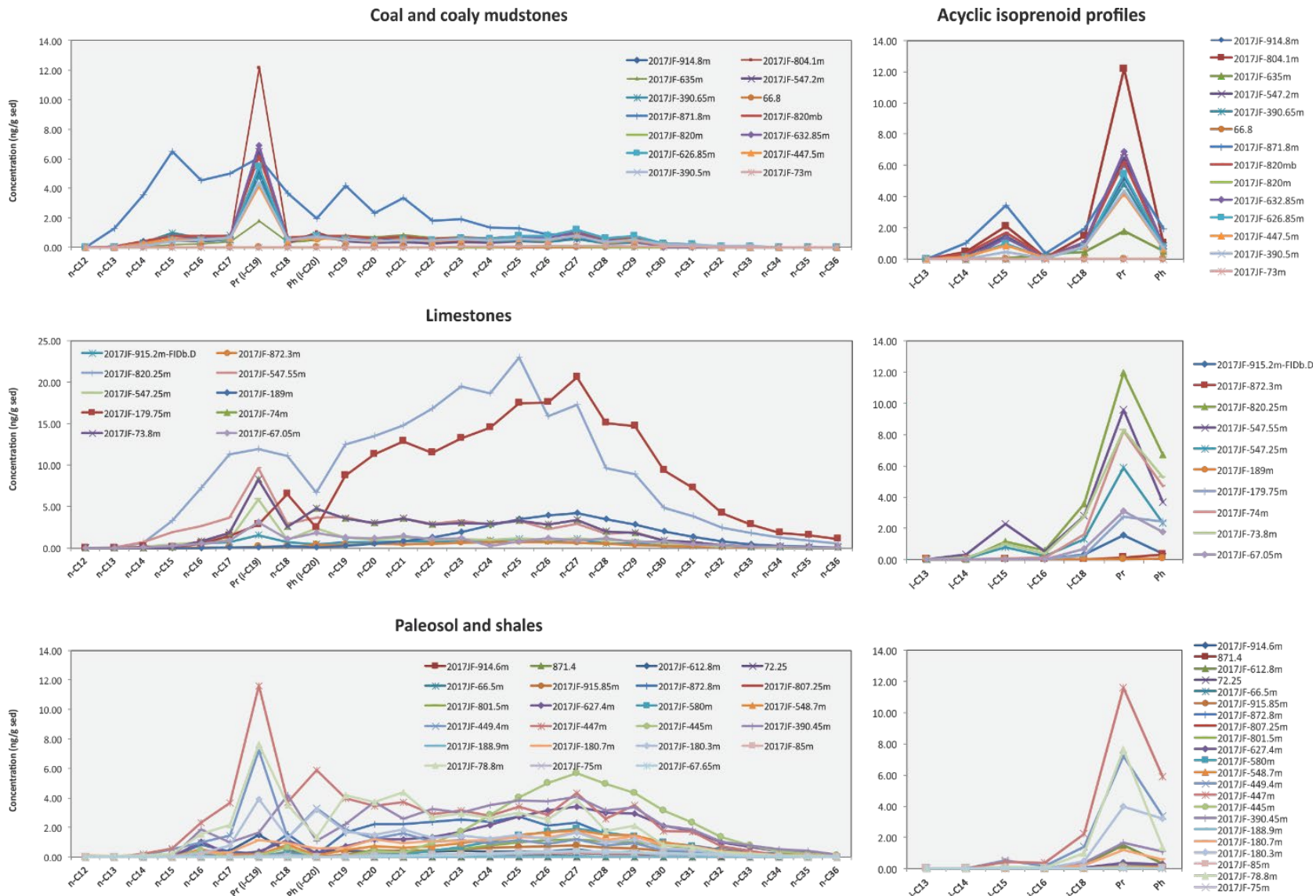


Figure 13. Concentration profiles for n-alkane and the acyclic isoprenoids pristane (Pr) and phytane (Ph; See Appendix IV) for the Joggins Formation lithologic groups.

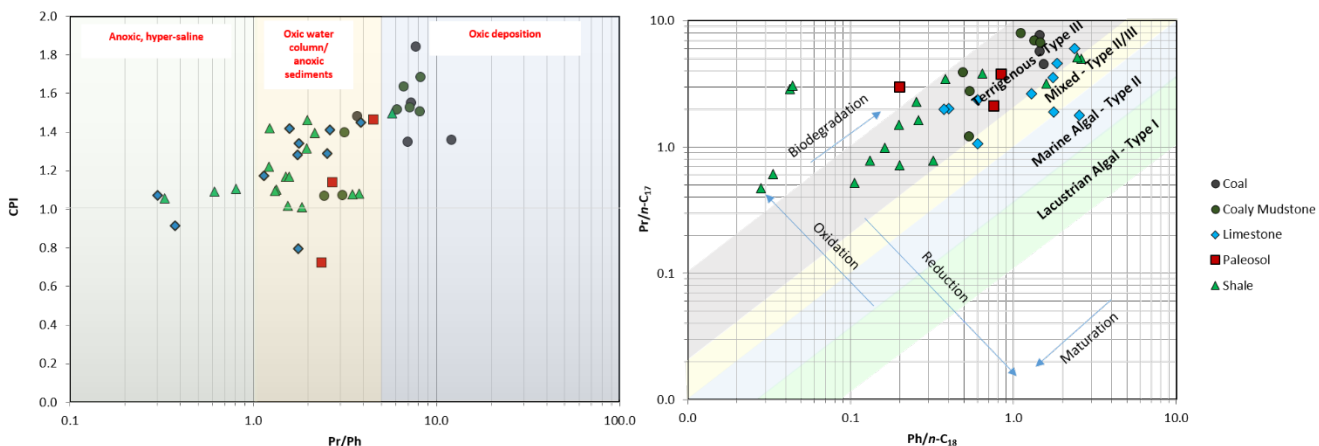


Figure 14. Cross-plots of CPI versus Pr/Ph and Pr/n-C₁₇ versus Ph/n-C₁₈ ratios indicating the Joggins Formation samples have inputs of terrestrial sources higher plant waxes and were likely deposited under suboxic to oxic conditions.

5.3.2. Tricyclic terpanes (chielanthanes)

Tricyclic terpanes were monitored using the m/z 123 and 191 mass chromatograms. Tricyclic terpanes were present in all samples and ranged from C₁₉ to C₂₉ (Moldowan and Seifert, 1983) and are dominated by the C₂₃ homolog. The source organisms of these compounds is unclear (Ourisson et al., 1982; Brocks and Summons, 2005), however, their abundance is consistent with a late release from thermally mature kerogens (Peters and Moldowan, 1993; Farrimond et al., 1999).

5.3.3. Steroidal biomarkers

Steroid biomarkers were monitored using the m/z 217 and 218 extracted ion chromatograms. For all samples steranes ranged in carbon number from C₂₆ to C₂₉. Both regular and rearranged steranes occur in all of the Joggins Fm samples. However, the relative abundances between cholestane (C₂₇), ergostane (C₂₈), and stigmastane (C₂₉) biomarkers is lithologically controlled. Coals and coaly mudstones have higher relative abundances of C₂₉ stigmastanes than that of the limestone, shales, and paleosols. Limestone samples JF-73.8m and JF-547.55m as well as shale samples JF-75m and JF-390.45m have higher relative abundance of C₂₇ steranes (Figure 15) that is consistent with organic matter sourced from algae living in marine or lacustrine environments (Huang and Meinschein, 1979; Grantham and Wakefield, 1988). Limestone sample JF-547.55m is stratigraphically close to the discovery of agglutinated forams at ~550m by Archer et al. (1995). The C₂₇-C₂₉ $\alpha\beta$ -diasteranes are a minor steroid hydrocarbon in the Joggins Fm samples indicating that acid clay catalysis was not a significant factor during organic matter diagenesis. The concentrations of diasterane and regular sterane sequentially increase with higher carbon numbered homologs (i.e. C₂₇<C₂₈<C₂₉).

5.3.4. Hopanoid biomarkers

Bacterial hopanoid biomarkers have been tabulated for the Joggins Fm samples. Dominant hopanoids include C₂₉ norhopane, C₃₀ hopane and gammacerane and C₃₁ to C₃₅ homohopanes. The relative abundance of these bacterial inputs relative to eukaryotic additions is lithofacies specific. For example, the limestone units consistently have lower sterane/hopane ratios compared to coals and coaly mudstones suggesting a larger bacterial influence during carbonate cementation (Figure 16). The ratio of C₂₉ norhopane/hopane has been used to evaluate oils deriving from siliciclastic (values less than 0.5) and marine carbonate environments (values >0.5; Figure 16). This proxy does not seem to work for the Joggins Fm samples as several of the coaly

mudstone samples record high (>0.5) ratios. Most of the limestone and shale samples narrowly straddle the carbonate and siliciclastic fields (0.4> and <0.6).

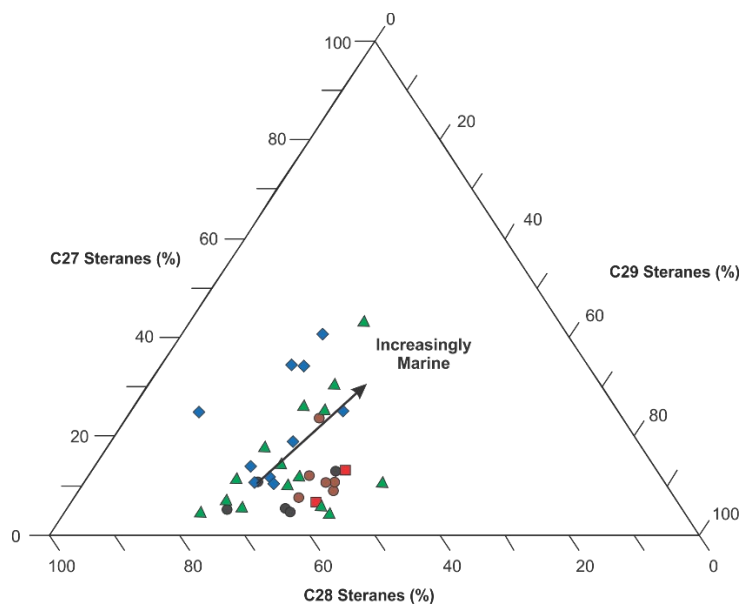


Figure 15. Ternary diagram indicating the relative abundance of C_{27} , C_{28} , and C_{29} regular steranes.

Gammacerane is abundant in most of the Joggins bitumens. Gammacerane is believed to be the geologically preserved hydrocarbon skeleton of tetrahymanol (Haven et al., 1989), which is found in bacterivorous ciliates that feed within anaerobic microenvironments (Sinninghe Damsté et al., 1995) and in cultures of purple non-sulfur bacteria including, *Rhodospseudomonas palustris* (Kleemann et al., 1990; Rashby et al., 2007). The gammacerane index ($GI = \text{gammacerane}/\text{hopane}$) is used as a proxy for evaluating elevated water-column stratification. For the Joggins Fm, the limestone units have a range of GI values, which are positively correlated to the ratio of bisnorhopane to hopane ($BNH/(BNH+H)$); Figure 16) suggesting that elevated water column stratification may be linked to redox changes.

Many of the bitumens have relatively high levels of 2α - and 3β -methylhopanes, monitored on the m/z 205 mass chromatogram. The 2α -methylhopanes are commonly believed to derive from 2α -methylhopanepolyols, which are found in many cyanobacteria (Summons and Jahnke, 1990, 1992; Summons et al., 1999) and some rhizobial bacteria including strains of the anoxygenic phototroph *Rhodospseudomonas palustris* (Rashby et al., 2007). High relative abundances of these compounds measured by the 2α -methylhopane index ($2\alpha\text{-MHI} = 2\alpha\text{-methylhopane}/2\alpha\text{-methylhopane}+\text{hopane}$) can indicate increased nutrient loading in the environment. The Joggins Fm samples have low 2α -MHI values suggesting little algal competition of the biological oxygen demand of the water column and sediments. These compounds are also not correlated to the sterane/hopane (Figure 16).

The 3β -methylhopane series is believed to be diagenetic products of 3β -methylbacteriohopanepolyols derived from aerobic and microaerophilic Type I methanotrophs (Neunlist and Rohmer, 1985; Cvejić et al., 2000; Farrimond et al., 2004) and some acetic acid bacteria (Simonin et al., 1994) and can indicate lacustrine conditions (Grice et al., 2014). The relative abundances of these compounds can be measured using the 3β -

methylhopane index ($3\beta\text{-MHI} = 3\beta\text{-methylhopane}/3\beta\text{-methylhopane}+\text{hopane}$) can indicate increased nutrient loading in the environment. The abundance of these biomarkers suggest high levels of microbial activity consistent with outcrop observations of abundant stromatolite or other microbial mat derived sedimentary structures (Figure 16). For the limestone units, the $3\beta\text{-MHI}$ is weakly correlated ($r^2=0.34$) to the sterane/hopane ratio possibly suggesting increased lacustrine conditions are equally associated with elevated algal input (Figure 16).

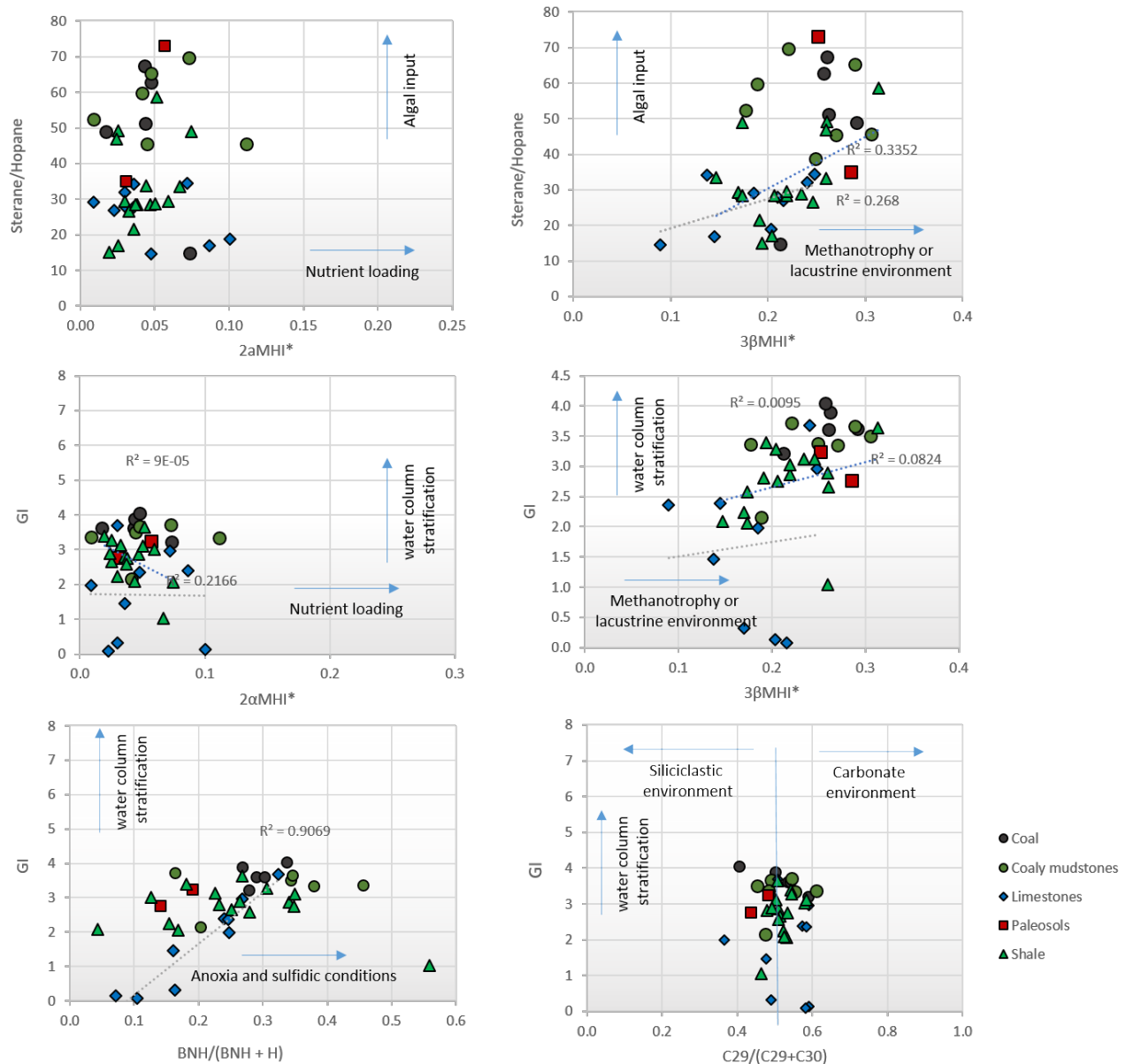


Figure 16. Cross-plots of various triterpenoid biomarkers relating to bacterial inputs of organic matter. Gammacerane index is a measure of water column stratification. The $3\beta\text{-}$ and $2\alpha\text{-methylhopane}$ indices do not have diagnostic trends of either photosynthesis and methylotrophy or lacustrine conditions. The sterane/hopane ratio measures the relative proportion of bacterial to eukaryotic (predominately algal input).

5.4. Organic Matter Thermal Maturity Based on Molecular Parameters

Thermal maturity describes the extent to which heat-driven reactions convert sedimentary organic matter into petroleum. Most molecular maturity parameters span a specific range of maturity (Farrimond et al., 1998) and a survey of several parameters is required to gain a meaningful assessment (i.e. Sykes et al., 2012). Various biomarker hydrocarbon thermal maturity parameters were assessed to determine the thermal maturation of the extracted bitumens (Figure 17; Appendix IV). The hopane ratios $C_{31} \alpha\beta$ hopane 22S/ $C_{31} \alpha\beta$ hopane 22(S+R) and the hopanes/morotane average 0.55 and 0.3, respectively. The sterane ratios $C_{29} \alpha\alpha\alpha$ / $C_{29} \alpha\alpha\alpha$ (S+R) and $C_{29} \alpha\beta\beta$ (S+R)/($C_{29} \alpha\beta\beta$ (S+R) + $C_{29} \alpha\alpha\alpha$ (S+R)) average 0.4 and 0.42, respectively. Collectively, these maturity parameters indicate the sedimentary organic matter is thermally immature (Seifert, 1986; Peters et al., 2005). The sterane and hopane biomarkers are consistent with the CPI (Figure 14), as well as T_{max} (Figure 7) measures, which provides a strong indication that the Joggins Fm organic matter is generally early mature and the detected hydrocarbons represent syngenic material.

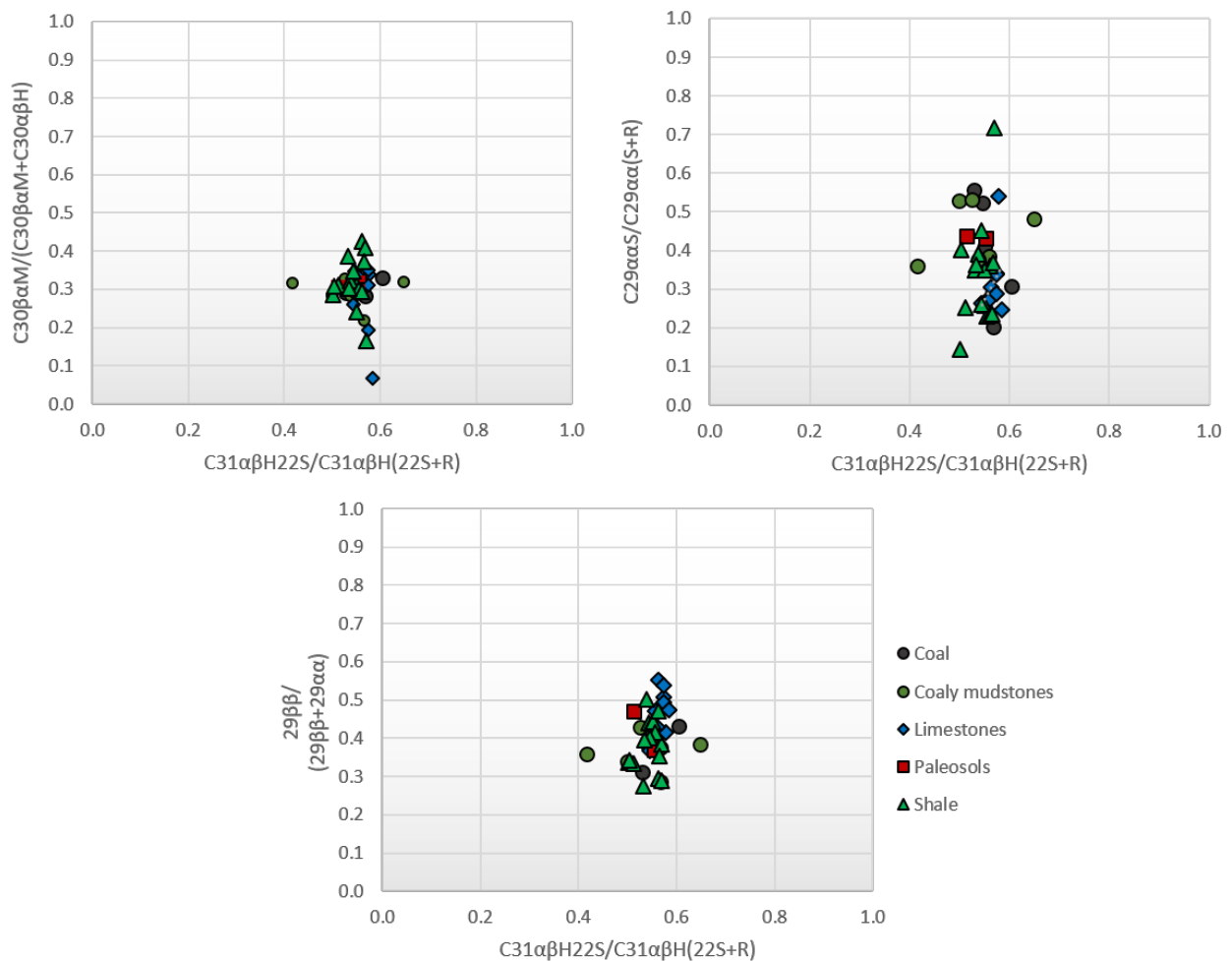


Figure 17. Cross-plot of four sterane and hopane thermal maturity parameters.

5.5. Elemental Geochemistry

Various trace element indices and ratios can be used to inform interpretations of provenance, paleoenvironment, and redox conditions during sediment deposition. For example, the elements Si, Ti, K, Sr, Al, Rb, Sr, Zr are independent of TOC complexes and are important constituents of sediments derived from terrigenous settings. The abundance of these relative to other elements can therefore reveal changes in sediment supply, provenance, and mineralogy. Elements concentrations monitored by pXRF included S, P, Cl, K, Ca, Ti, V, Cr, Mn, Fe, Co, Ni, Cu, Zn, As, Se, Rb, Sr, Y, Zr, Nb, Mo, Ag, Cd, Sn, Sb, Ba, La, Ce, Pr, Nd, Sm, W, Hg, Pd, Bi, Th, U, Si, Hf, and Le (Appendix V and VI). The most abundant measured chalcophile elements were S, Pb, Zn, and Ti. The most abundant siderophile elements were Fe, Mn, Ni, and Co and, lastly, the most abundant lithophile elements were Si, Ca, V, Sr, Ti, and Ba. Apart from Si, the most abundant element measured was S followed by Fe, Ca, and Cl with levels higher than 100 ppm. Total sulfur (including pyritic, sulfate, and organic bound sulfur) ranged up to 10.4% in the shales and paleosols, up to 9.6% in the limestone units, and as high as 24.2% in the coals and coaly mudstone samples. Total sulfur values are further reviewed in the discussion section covering the sulfurization of organic matter. Elemental salinity and redox proxies are also discussed below.

6. Discussion

6.1. Caveats about Marine Microscopic Bioclast Indicators in the Joggins Formation

Even though the echinoderm and brachiopod fragments reported by Grey et al. (2011) are potentially strong indicators of marine conditions, some important caveats and alternative explanations should also be considered. It is possible that these microscopic bioclasts represent reworked material from older, marine sedimentary units in the basin such as the Windsor Group. Currently, such units are exposed in salt-cored anticlinal structures that were active due to salt tectonics just before and during Joggins Fm deposition (Jutras et al., 2015; Craggs et al., 2017; Waldron et al., 2013). Additionally, there were also ongoing crustal tectonic processes related to the broader Appalachian orogeny that could have uplifted and eroded Windsor Group or even older Paleozoic marine rocks in the basin. As an example of this potential, Utting et al. (2010) reported sporadic Visean and lower Serpukhovian palynomorphs in Pennsylvanian strata at Joggins, implying erosion of slightly older Carboniferous strata somewhere in the sediment source areas. Furthermore, likely Windsor clasts are also reported from the underlying Boss Point Formation near Joggins (Rygel et al., 2015). Reworking of bioclasts could be tested by looking for other microscopic components of such a hypothetical Windsor Group fauna that might survive transportation. This could include a search for age-specific conodonts (Von Bitter and Plint, 1987). Alternatively, conodonts could occur in situ within the Joggins Fm, in which case they would be confirmation of marine conditions and potentially be useful independent biostratigraphic tools.

A second issue is the nature of the brachiopod fragments illustrated by Grey et al. (2011), which are described as punctate brachiopods, but also strongly resemble the shell structure of the spirorbiform microconchids found frequently at Joggins (compare Figure 5B of Zaton et al., 2014 to Figure 9 of Grey et al., 2011). If the punctate brachiopods of Grey et al. (2011) are misidentified microconchids, then they cannot be a marine indicator, leaving only the echinoderm fragments as diagnostic of such conditions. Since, neither of these hypotheses have been tested, this study accepts the marine indicators of Grey et al. (2011) for the purposes of further discussion.

6.2. Sulfurization of Organic Matter

The enrichment of sulfur in mudstones is a common attribute of the biogeochemical sulfur cycle. Under low oxygen conditions, porewater sulfate is microbially reduced during or immediately following sediment deposition, producing 2 mol S/mol of consumed C (Luckge et al., 1999). The original proportion of organic matter flux at the time of deposition can be derived by: $TOC_{initial} = TOC_M + TOC_{SR}$, where TOC_m is the measured TOC value, and TOC_{SR} is the amount of organic carbon mineralised through sulfate reduction, determined by multiplying the measured S value by 0.75 to account for the molar ratio of C to S. This is multiplied again by 1.33 to account for a ~ 25% diffusion of S into porewater or the water column, following the method of Veto et al. (1997, 2000) and Luckge et al. (1999). Comparison of TOC_m and $TOC_{initial}$ results in higher divergence in these values near the base of the Joggins Fm (Figure 17).

Sulfurization occurs during early diagenesis and represents a pathway for kerogen formation. However, neither TOC nor HI are shown to correlate with total sulfur values. As such, SOM does not appear to have influenced either the quantity or quality of organic matter in the Joggins Fm. Due to the weaker bond strength of S-S and S-C bonds compared to C-C bonds it can be expected that SOM will result in the generation and expulsion of hydrocarbons at lower burial depths. Comparison of T_{max} with total sulfur values (Figure 19) show a negative correlation whereby T_{max} values of the Joggins Fm kerogens increases with increasing total sulfur concentrations. The increase cannot be ascribed to stratigraphic changes in TOC and total sulfur values as these do not systematically decrease up the section. However, this trend is lithologically controlled with S-rich coals and coaly mudstones being less thermally mature. Therefore, it is uncertain whether some degree of SOM affected the Joggins Fm source rocks.

Consistent with the SOM is a partial change in the preservation of labile forms of organic matter such as proteins and carbohydrates (Sinninghe Damsté et al., 1998). Within marine environments where SOM occurs these components can be altered to thiophenes and other organo-sulfur compounds and locked within the kerogen before they are degraded by microbial activity (Brassell et al., 1986; Sinninghe Damsté, et al., 1990). Compared to lipids, marine carbohydrates and proteins are isotopically heavy up to -18‰ (van Dongen et al., 2002). Therefore, it can be expected that the bulk carbon isotope signature of sulfurized sedimentary marine organic matter will be heavier than that of terrestrially-sourced organic matter. These heavy values are not observed in the Joggins Fm samples. It is therefore unlikely that SOM resulted in significant preservation of more labile forms of organic matter.

6.3. Marine Incursions and Paleoredox

6.3.1. Molecular evidence of marine and paleoredox conditions

Strictly marine sourced biomarkers include C_{30} 24-*n*-propylcholestane (Peters, 1986; Moldowan et al., 1990), dinosterane (23,24-dimethylcholestane; Moldowan and Talyzina, 1998; Robinson et al., 1984), mid-chain monomethylalkanes (i.e. Summons and Walter, 1990), C_{25} and C_{30} highly branched isoprenoids (HBI, i.e. Nichols et al., 1988); and crenarchaeol (Sinninghe Damsté et al., 2002). The 4-methyl-cholestane, ergostane and stigmastane (Volkman 2003) as well as 4,4-dimethylcholestane and $C_{20}+C_{25}$ HBIs can be sourced in both marine and lacustrine settings. With the exception of methylsteranes and crenarchaeol that were not searched for, none of the above list of compounds were detected in any of the samples.

Various combinations of biomarkers and other types of hydrocarbons are also frequently used to assess sediment deposition under marine conditions. For example, the relative abundances of regular steranes plotted as ternary diagram (Figure 15) is frequently used to determine primary sources of organic matter. Interpretation of the depositional environment can also be made by way of a cross-plot of the Pr/Ph versus DBT/P (dibenzothiophene/phenanthrene) ratios (Figure 20; Hughes et al., 1995). For this plot, the samples that reside in Zones 1a and 1b are likely sourced from marine carbonates and or mixed carbonate and lacustrine

environments that are sulfate-rich. Interestingly, sample JF-547.55m, which has a high cholestane content with a marine algal source also has Pr/Ph and DBT/P values that plot in Zone 1a. Zone 4 a field associated with source rocks deposited within fluvial or deltaic environments. In this regard, the sample has similar Pr/Ph and DBT/P values are largely coals and coaly mudstones as well as several shale samples (Figure 20).

High C₃₅-homohopane indices [C₃₅/(C₃₁-C₃₅)] are typical of petroleum generated from source rocks deposited under anoxic marine conditions, where the C₃₅ backbone of the precursor bacteriohopanetetrol is preferentially preserved (Peters and Moldowan, 1991). None of the Joggins Fm samples have elevated C₃₅ distributions (Figure 21). However, the Joggins Fm samples do have C₃₄ homologues that have slightly higher relative abundances compare to their C₃₃ and C₃₅ partners that could result from different types of bacterial input or suboxic exposure resulting in partial oxidation of the bacteriohopanetetrol side chain (Peters and Moldowan, 1991). These data are consistent with other redox determinations based on biomarkers (Pr/Ph) and elemental parameters (see below).

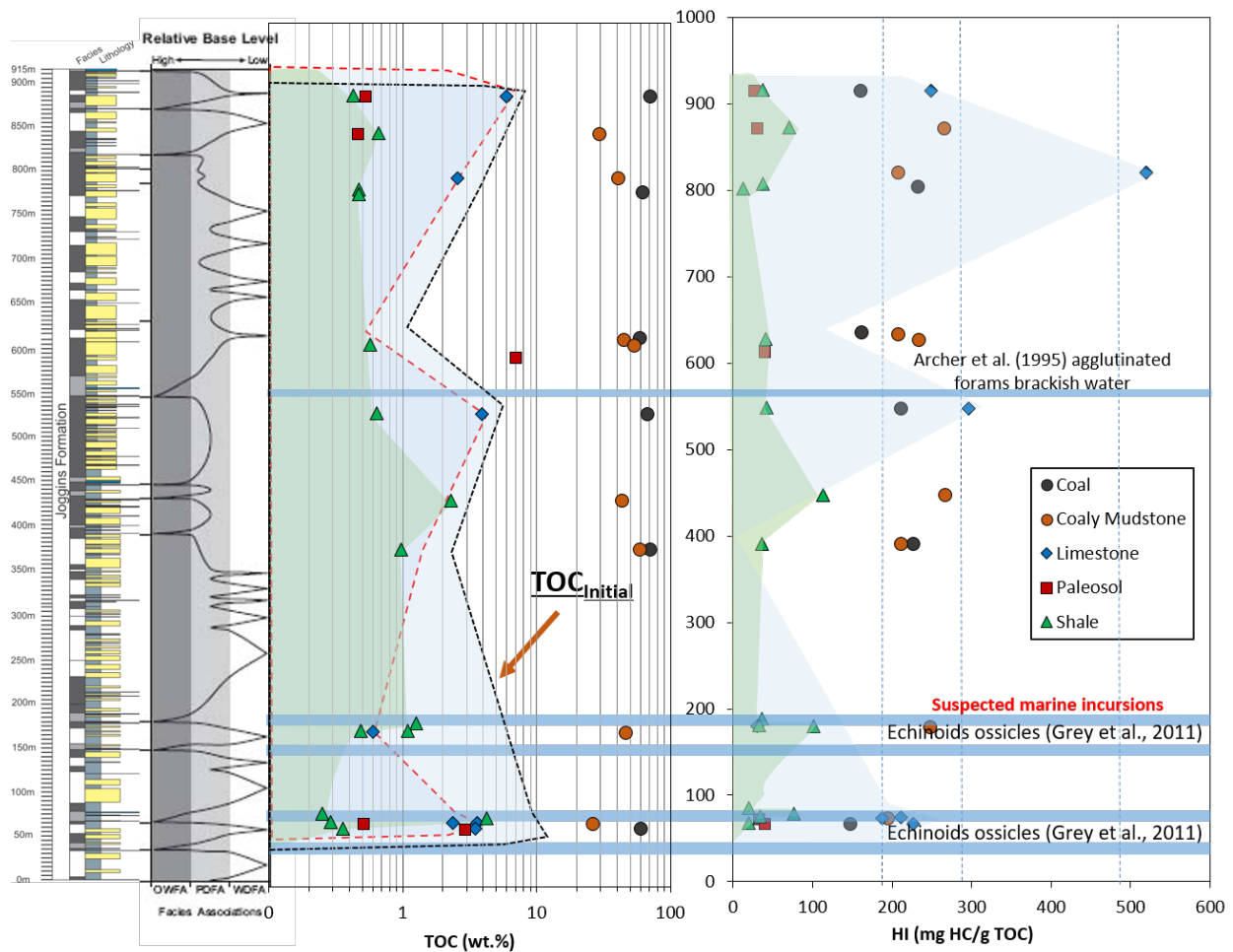


Figure 18. Stratigraphic trends in TOC, TOC_{initial}, and HI for the Joggins Formation samples. Blue bars indicate the stratigraphic position of agglutinated forams (Archer et al., 1995) and echinoid ossicles (Grey et al., 2011), which are strong indicators of marine conditions in the depositional environment.

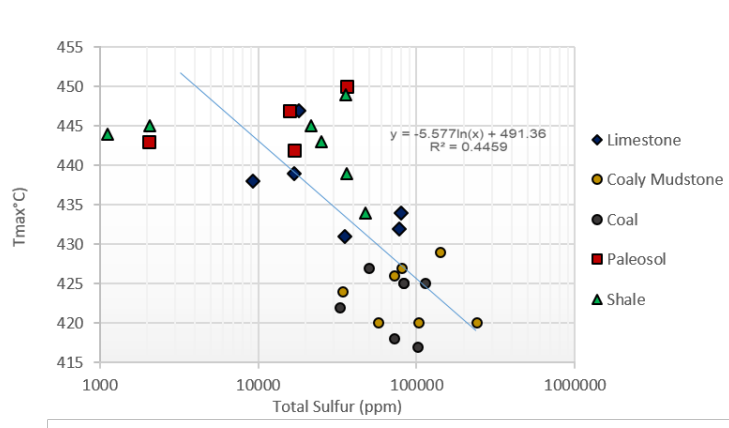
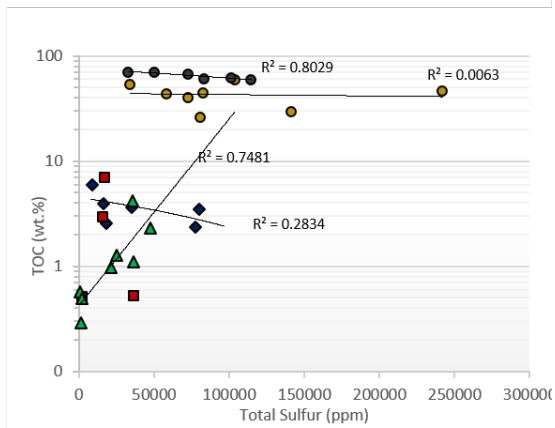
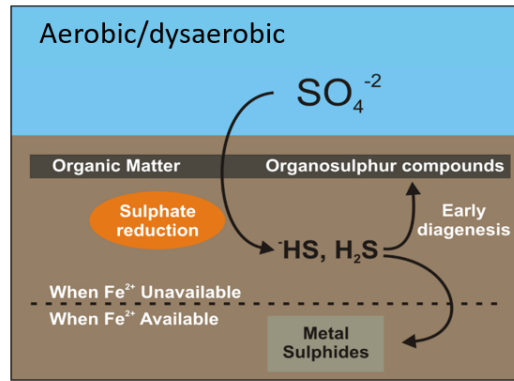
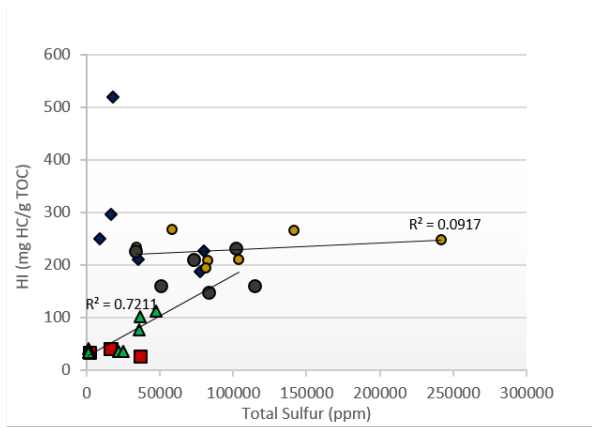


Figure 19. Cross-plots of bulk rock pyrolysis richness, quantity, and maturity parameters versus total sulfur measurements.

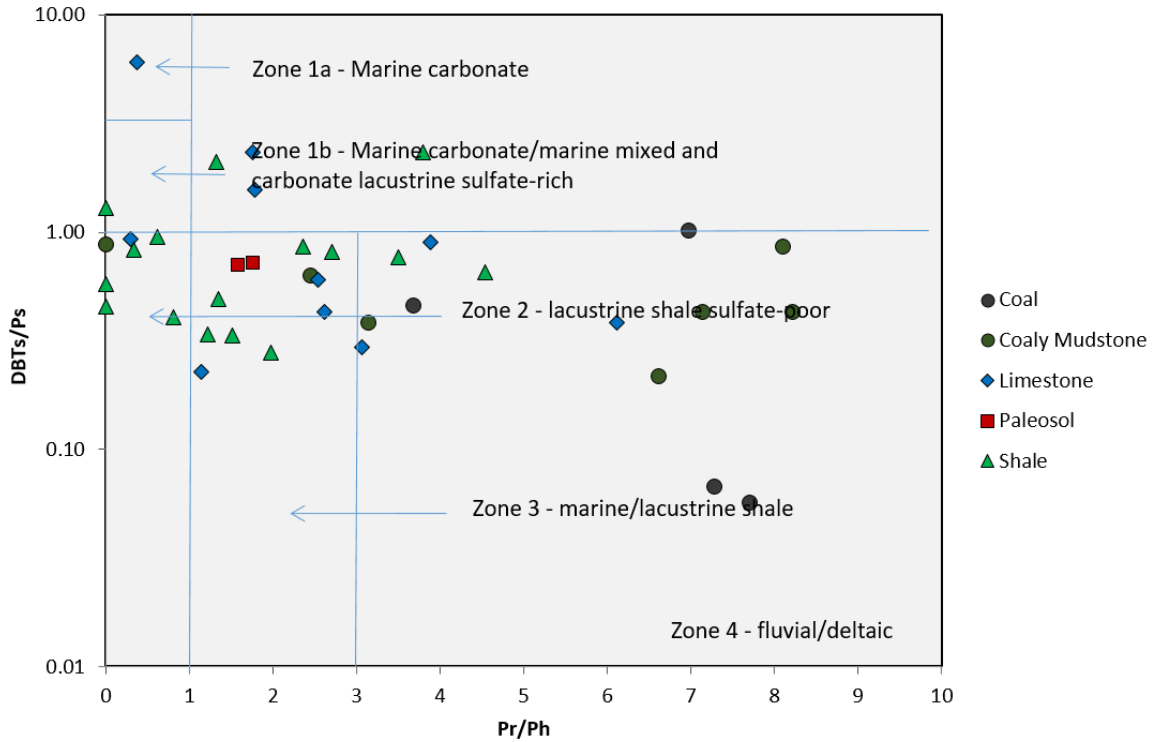


Figure 20. Cross-plot of the Pr/Ph and dibenzothiophene/phenanthrene (DBTs/Ps) ratio indicating potential Paleoenvironmental conditions of the depositional environment.

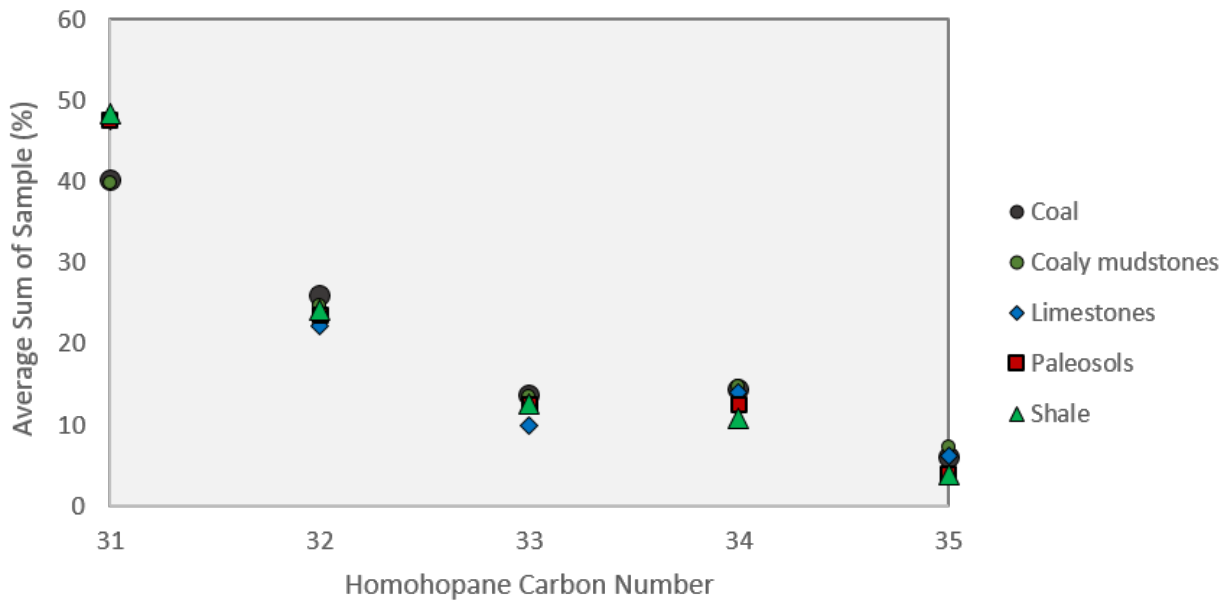


Figure 21. Cross-plot of the average sample abundance of C₃₁ to C₃₅ homohopanes.

6.3.2. Elemental concentrations and salinity and redox conditions

Hierarchical cluster analysis was performed on several groups of the Joggins Fm samples using mean centroid linkage with various groupings of elements for each of the three dominant lithofacies (coals and coal mudstones, limestones, and paleosols and shales). The HCA dendrograms for the Joggins Fm limestones (Figure 22) indicate distinct differences from in the elemental compositions of various samples. Samples JF-179.75m, JF-73.8m, and JF-67.05m form a branched cluster based on elements associated with seawater and marine sediments (S, Cl, V, Sr, K, Ti, Mn, Ba, Cr). These samples are close to the limestone units identified as having echinoderm fossils (Grey et al., 2011). Interestingly, sample JF-189m, which is close to the limestone unit identified as having echinoderm fossils also forms a cluster with sample JF-872.3m. This limestone unit displays a unique gammacerane signature, is adjacent to a limestone unit with a high HI value (indicating Type II kerogen), and has elemental ratios that are consistent with marine influence (see below). In the field it is also one of the densest limestones seen in the section.

The HCA dendrograms for the shale and paleosol sample subset (Figure 21) was measured using elements associated with seawater and marine sediments (S, Cl, V, Sr, K, Ti, Mn, Ba, Cr) as well as for all measured elements that excluded S and Si. For the analysis of marine associated elements, samples JF-78.8m, JF-180.3m, JF-449.4m, JF-807.25m, and JF-915.85m have distinct elemental differences from the other shales and paleosols. Interestingly some of these samples appear to be close to regions in which echinoderm fossils have been detected (Grey et al. 2011). The majority of the remaining samples have very similar compositions of elemental concentrations based on the close branch distances of the HCA dendrogram.

Dendrograms of coals and coaly mudstones were also constructed using HCA. For the set of elements including S, Cl, K, Ca, Ti, Cr, Mn, Fe, Cu, Zn, Sr, Mo, Ba, Pb, Th, and U the profiles produce one dominant cluster and one outlier (JF-178.8m; Figure 22). The weighting of this outlier is focused on this sample having the highest S, Fe, and Mo concentrations for the coal and coal mudstone samples. Sample JF-178m is a coaly mudstone with a TOC of 43.7wt.% and a moderately high HI value of 248mg HC/gTOC. Excluding S, Fe, and Mo results in a new distribution whereby the least similar samples are coaly mudstones JF-632.85m, JF-820m, JF-447.5m, and JF-73m.

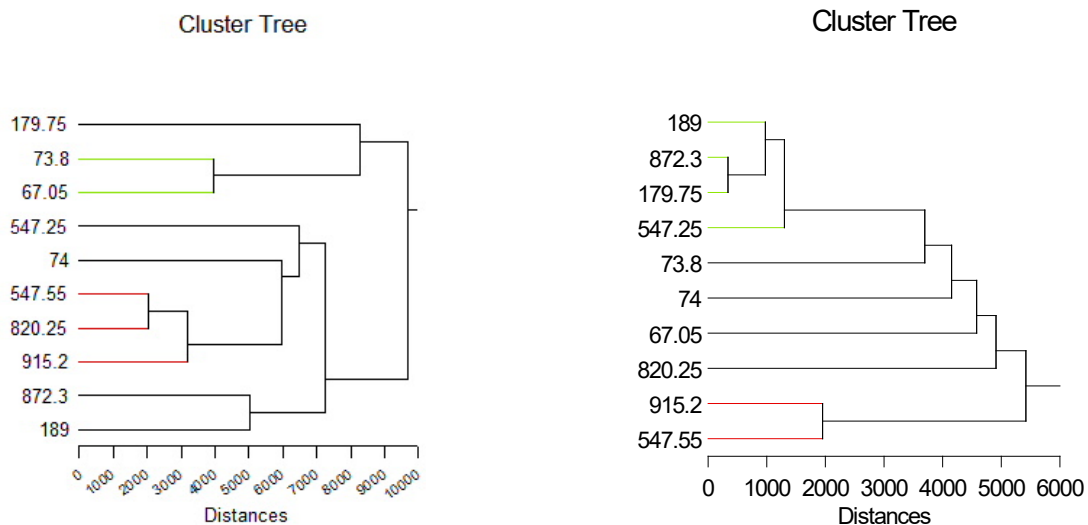


Figure 22. Hierarchical cluster analysis of the Joggins Formation limestone (“clam coal”) samples of common elements found in seawater and marine sediments (Left; S, Cl, V, Sr, K, Ti, Mn, Ba, Cr). Dendrogram for all elements excluding Si and S (Right).

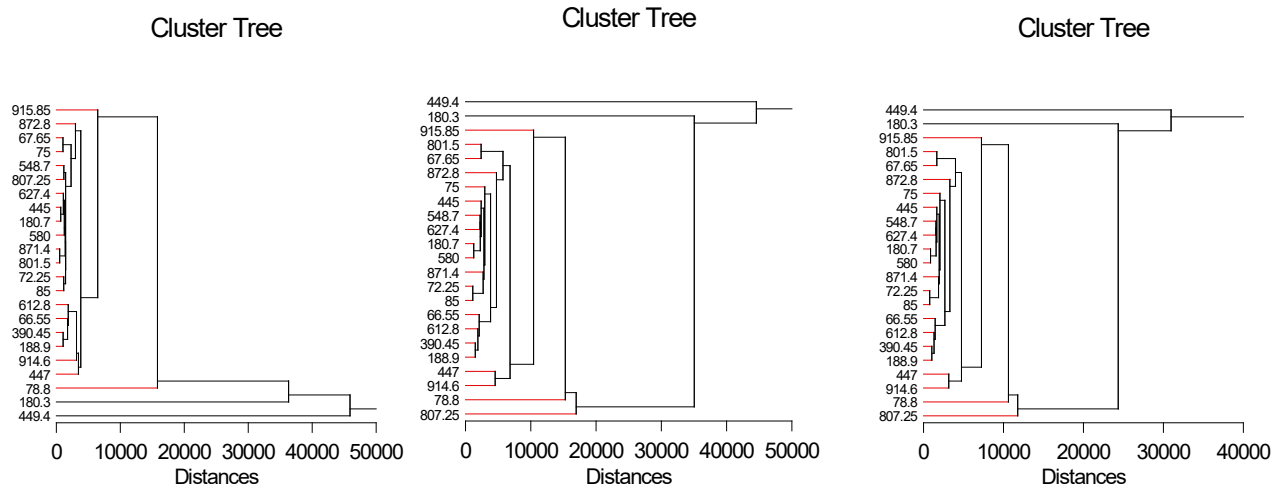


Figure 23. Hierarchical cluster analysis of the Joggins Formation shales and paleosol samples of common elements found in seawater and marine sediments (left; S, Cl, V, Sr, K, Ti, Mn, Ba, Cr). Dendrogram for all (middle). Dendrogram for all elements excluding Si and S (right).

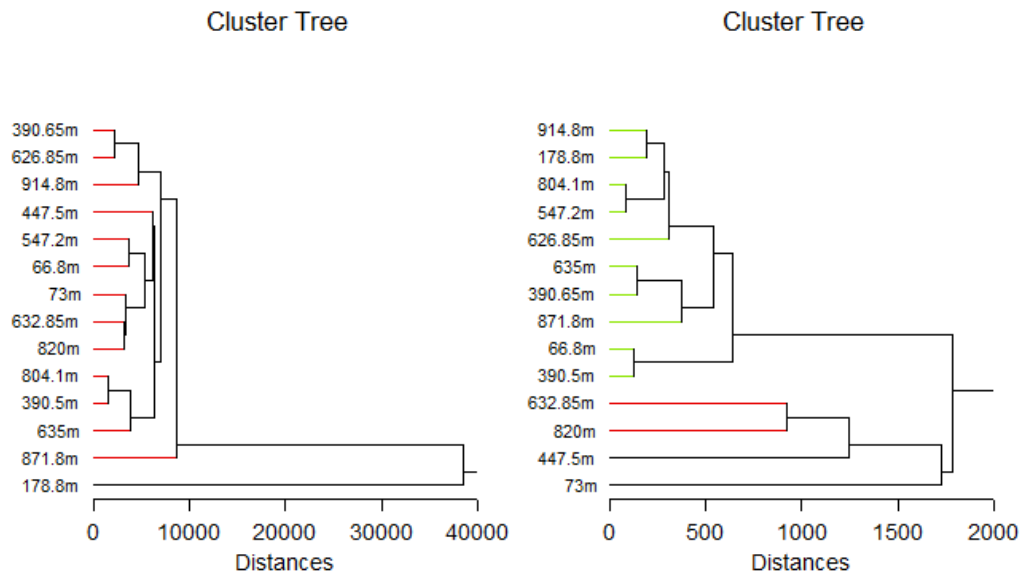


Figure 24. Dendrograms produced by hierarchical cluster analyses of the Joggins Formation coals and coaly mudstones. A) Elements included are S, Cl, K, Ca, Ti, V, Ni, Cr, Mn, Fe, Zn, Cu, Sr, Mo, Ba, Pb, Th, U and B, the same selection without S, Fe, and Mo.

6.3.3. Elemental ratios for redox conditions and salinity

Decreased oxygenation and associated reducing conditions in either the water column or sediment pore-waters increases organic carbon burial and preservation in marine basins. With concomitant microbial sulfate reduction comes syngenetic and diagenetic pyrite formation (Rimmer, 2004; Brumsack, 2006). These processes facilitate the export and sequestration of trace metals in sediments and are responsible for most trace-metal enrichments under dysoxic to anoxic conditions (Brumsack, 2006). Elemental ratios can be useful as proxies in chemostratigraphy for investigation of salinity variation (Rb/K), redox state (V/Cr), or provenance (Zr/Ti) according to Scheffler et al. (2003).

These processes facilitate the export and sequestration of trace metals in sediments and are responsible for most trace-metal enrichments under dysoxic to anoxic conditions (Brumsack, 2006). Biomarker and elemental ratios were used to infer the redox conditions within the sedimentary environment. Pr/Ph ratios indicated sediment deposition an aerobic water column containing oxic to anoxic surface sediments (Figure 14). Elemental paleo-redox indicators V/Ni and V/Cr similarly indicate oxic to marginally suboxic/dysoxic water column conditions. V/Ni ratios indicate oxic conditions pervaded the water column with high values of 4-6 being anoxic. Although, U/Th values should be good indicators of redox as U commonly complexes with carbonates in reducing environments U was only detected in 5 coals and coaly mudstones and is not useful for sedimentation in aquatic systems.

The solubility of SrSO₄ is relatively high and thus Sr is assumed to migrate and precipitate in the open marine basin or in saline lakes. Therefore, elemental salinity proxies are reported in the form of Sr/Ca, Sr/Br and Mn/Ca ratios (Figure 25). Although Sr/Ca ratios may be reasonable proxies for siliciclastic sediments, they are not useful for carbonate rocks. Nonetheless, the highest Sr/Ca ratios are reported for a paleosol at 72.25m and a shale sample collected at 390.45m up from the base of the formation. Sr/Ba ratios can be expected to gradually increase from the coast to the center of the lake/sea. In general, Sr/Br >1.0 indicate saline water. For the Joggins Fm, Sr/Ba ratios of the limestone samples are negatively correlated with V/Ni suggesting that more saline conditions commonly accompany oxic water conditions. Additionally, many of the samples that have higher Sr/Br ratios are limestone units that occur lower in the section (the exception being sample 872.3m, which as the highest Sr/Br ratio).

Manganese in sedimentary rocks is controlled by the source rock geochemistry and redox of the environment. Manganese may occur in detrital phases such as mafic silicates, magnetite and ilmenite, but the largest proportion is typically held in secondary Mn⁺⁴ oxides that form either discrete concretions or surface coatings on primary minerals and lithic fragments. Carbonate rocks can contain high Mn contents. Mn⁺² highly soluble in reducing conditions. Has a low affinity for organic ligands. Shale unit with low Mn/Ca ratio (indicative of reduced terrestrial input) are found lower in the Joggins Fm. These unit also tend to have slightly higher Sr/Ba ratios.

The second uppermost limestone unit (JF-872.3m) includes elemental ratios that are consistent with marine conditions. These include markedly high Sr/Ba and Mo/S coupled with low Mn/Ca, Fe/S, and V/Ni values. Interestingly, the limestone unit stratigraphically immediately underneath this sample also contains the highest HI value (520 mgHC/gTOC; Fig. 8; Appendix III) and the most depleted carbon isotope composition (-29.8‰; Figure. 9; Appendix IV).

Stratigraphic trends of several proxies are plotted as a function of three lithofacies assignment (Figure 26). With the exception of the coals no systematic trends are evident. The coals display a potential bimodal trend of progressively higher Fe/S ratios at 66.8m and 635m to 804.1m that is matched by an equivalent trend in total S concentrations. Inverse to this is lower Sr/Ba, Sr/Rb, and Mo/S ratios peaking at 447.2m and 914.8m. These changes are likely a function of the peat mire environment. Sulfur in coal is derived primarily from two sources: the original plant materials and ambient fluids in the coal-forming environment. High sulfur coals typically form from brackish or marine-influenced environments. Excursion in the elemental ratios of the are

observed at the stratigraphic intervals of 189m, 547.55m, and 872.3m for the limestones and at 180.3m and 447m for the shales.

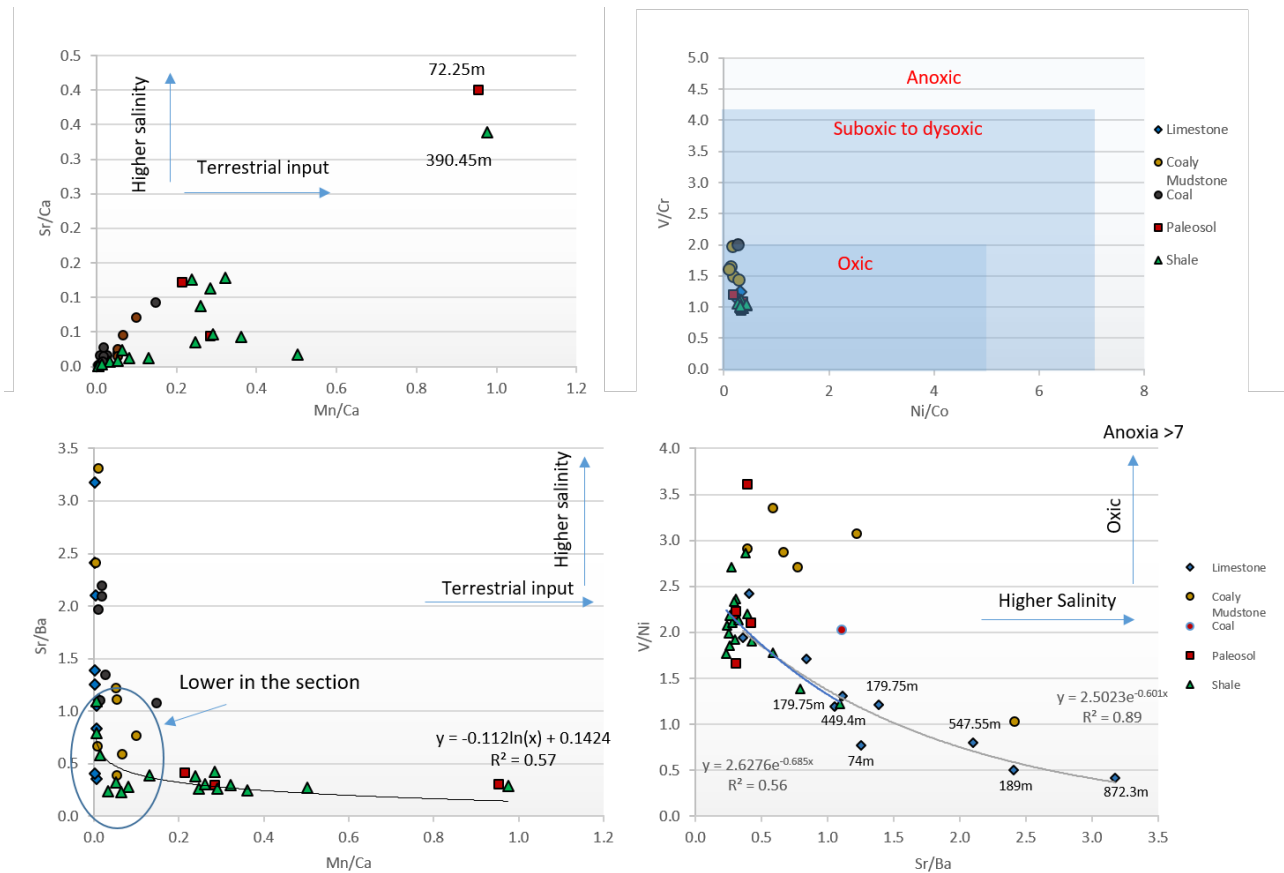


Figure 25. Cross-plots of Sr/Ca, Mn/Ca, V/Cr, Ni/Co, Sr/Ba, and V/Ni derived from pXRF analyses of rock powders. Similar to the Pr/Ph ratios (Figure 9), the elemental ratios of V/Cr, Ni/Co, and V/Ni indicate deposition under predominately oxic conditions. Elevated salinity for some Joggins Formation source rocks is indicated for several of the limestone samples.

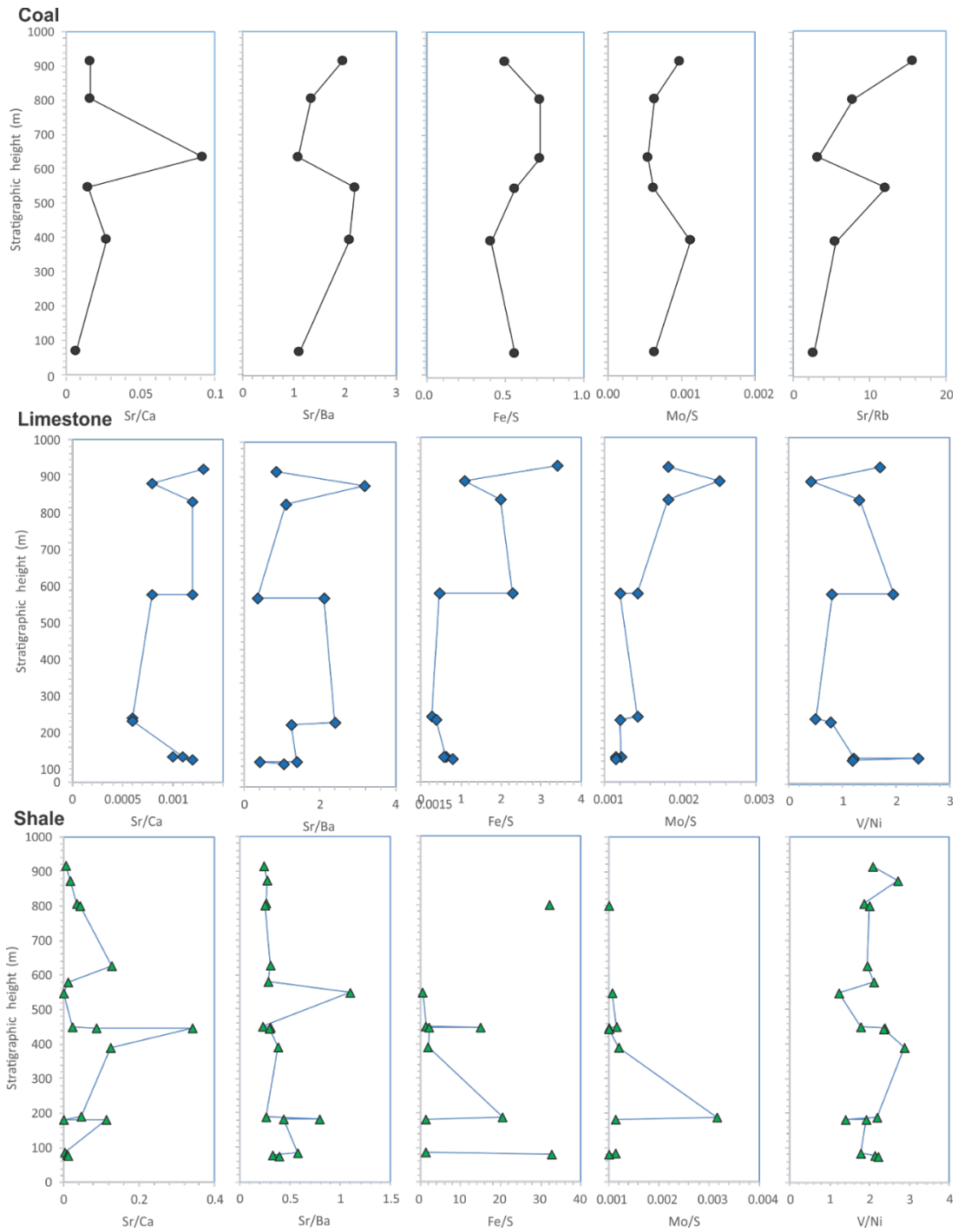


Figure 26. Stratigraphic profile of pXRF determined elemental ratios.

7. Summary and conclusions

This study provides the first comprehensive chemostratigraphic study of the Joggins Fm. The Joggins Formations source rocks were subdivided by lithology into shales, paleosols, limestones, coaly mudstones, and coals. Several trends appear to be present in the current data that can be attributed to source rock properties, paleoenvironmental conditions during sediment deposition, evidence for marine incursions, and the SOM. These attributes have effected the quality, quantity, and maturity of the organic matter.

Description of organic matter:

- With the exception of one limestone sample, the limestones, coals and coaly mudstones contain Type II/III organic matter. The generative potentials for these limestones is very good to excellent for oil and gas. However, the coals and coaly mudstone are inert. The outlier limestone samples contains Type I kerogen sourced from lacustrine environments and has excellent potential for generating oil. The shales and paleosols have Type III and IV kerogens capable of generating gas or are completely inert.
- The limestones have organic matter compositions that are distinctly different from that of the other lithofacies. In this respect, the organic matter was not inherited or migrated from closely associated organic-rich coal and coaly mudstone units.
- The determination of organic matter maturity was based on bulk pyrolysis and molecular biomarker analyses that produced similar results. Despite its age, the organic matter of the Joggins Fm is thermally immature to early mature indicating a shallow burial for these rocks.
- The biomarker and trace metal data (V/Ni, Ni/Co, and V/Cr ratios) for all sample lithofacies indicates a predominant pattern of sediment deposition in an oxic water column and/or near surface sediments.

Evidence of SOM and marine transgression:

- Geochemical evidence of marine incursions is thus far less compelling. Some of the limestone units have Type II kerogens that can be sourced from marine organic matter or a mix of lacustrine and terrestrial organic matter.
- The low relative abundance of C₂₇ steranes in most shales and limestones points to terrestrial and lacustrine conditions for the Joggins Fm. A notable exception is the limestone sample JF-547.55m, which is stratigraphically close to the discovery of agglutinated forams at ~550m by Archer et al. (1995). This sample also has a low Pr/Ph and high DBT/Ps ratio that is indicative of oils formed from marine source rocks.
- Organosulfur compounds such as benzothiophene and dibenzothiophenes, which would likely arise from SOM are of low abundance in the extracted bitumens. The elevated abundance of their alkylated counterparts in all samples also strongly suggest that the low maturity of the organic matter may account for this.
- The coals and coaly mudstones typically have higher sulfur concentrations compared to the other documented lithologies. This presents the possibility that stratigraphically similar lithologies may have inherited their sulfur through leaching. As such, the sulfur concentrations of many shales and limestones may not reflect microbial sulfate reduction.
- The coals and coaly mudstones have low T_{max} values and high sulfur concentrations. Many of these are stratigraphically adjacent to shales and limestone units of higher maturity. The discontinuity in maturities is likely the result of increased cracking from matrix affects relating to low organic matter contents, the lower chemical bond strength associated with carbon-sulfur and sulfur-sulfur linkages, and the elevated presence of free sulfur radicals that can cleave carbon-carbon bonds in the kerogen.
- Nonetheless, total sulfur measures were used to calculate the initial, pre-SRB degraded TOC values. These results indicate a stratigraphic pattern whereby greater heterotrophic activity appears to have occurred at the base of the section than in other parts of the formation.

- This, in addition to elevated Sr/Ba value for limestones, as well as low Mn/Ca ratios for shale units is also consistent with brackish or more marine conditions.

Collectively, the data supports higher saline conditions in sediments deposited at the base of the section (approximately 73-180m) and additional transgressive events at 447.55 – 550m and near the top of the Joggins Fm at 872.3m. These results provide evidence that some level of SOM likely occurred within some of the Joggins Fm source rocks. However, its effects appear to be limited to maturation of the organic matter with no additional impact being observed in the quality or quantity of organic matter that was preserved. Consistent evidence between bulk organic, molecular, and inorganic indicators indicate oxic conditions prevailed within the water column and much of the surface sediments. The geochemical data is in many cases consistent with brackish to marine conditions being present during the initial basin fill marking portions of the lower limestone and shale intervals within the section. Additionally, geochemical evidence also points to an additional transgressive event near the top of the Joggins Formation. However, little evidence was obtained that these events significantly affected the petroleum generative potentials of the Joggins source rocks. Together, these data provide a clearer picture of the geochemical conditions occurring in this section.

7.1. Significance to Hydrocarbon Exploration and Development

The potential to identify SOM within prospective source rocks has implication for the reconstruction of timing and sedimentological fill of the conjugate margin and the resulting geochemistry of the resulting source rocks. The presence of known (Sydney Basin, southern Grand Banks), and speculated (Georges Bank and LaHave Platform) Paleozoic rocks beneath the Mesozoic of the Scotian Basin makes the better characterization of potential Paleozoic source rocks in the region a useful calibration point for assessing the source of known hydrocarbon occurrences in the Atlantic region. The geochemical conditions for the documented and potential occurrences may therefore effect the prospectivity of these regions.

7.2. Future Work Possibilities

More work still needs to be done. We have yet to fully calibrate the molecular, isotope, and elemental proxies. Additional localities also holds promise for continued study. The limitations of the pXRF unit used in this study (particularly Al and lighter elements) are a significant impediment to further analyses of the bulk rock inorganic geochemistry. Reanalysis of the existing powdered samples using a more capable desktop unit would be helpful to better inform this study.

Although broad trends were detected at the formation scale and within individual cyclothems, there may be finer-scale variations within the “clam coal” limestones at cm scale that are not consistently sampled and could reflect shorter-term fluctuations in the character of the aquatic environment during these relatively time-condensed intervals. Macroscopically, clam, fish, and ostracod concentrations vary greatly and shale versus limestone compositional variations are reflected in cm-scale lamination. These variations could be sampled for bulk rock inorganic and organic geochemistry. A clearer understanding of the chemo-microstratigraphy of individual beds might help to account for some of the statistical variation seen between samples at a larger scale.

Given its unusual nature and more marine indications in multiple analyses, the limestone beds at 547.55m and 872.3m could be investigated further, such as by searching for microfossils in thin section using the same techniques as Grey et al. (2011) or by processing it to search for conodonts. The possibility of reworked material in the intervals studied by Grey et al. (2011) should also be tested. The Sr-isotope study of Brand (1994) should be repeated within the intervals with possible marine indicators both from Grey et al. (2011)

and this study to determine if they show isotopic signatures more in line with the established marine Sr-isotope curve for the Carboniferous.

Acknowledgements

This project was made possible by the support of the Offshore Energy Research Association (grant # 171010). Access to the Joggins Fossil Cliffs was facilitated by Melissa Grey, Sean McKeane, Jordan LeBlanc, and Katherine Odgen, and Sam Bolton of the Joggins Fossil Institute and the Communities, Culture and Heritage Department (permit number P2017NS07). Acquisition of elemental data was made possible by Chris White of the Nova Scotia Geoscience and Mines Branch. Carbon and nitrogen stable isotope data were provided by Karem Azmy of Memorial University. Matt Stimson, of SMU, helped with sample collection and field mapping. Sample preparation and extraction was done by Yaisa Owino of Saint Mary's University (SMU). John Mischael Dooma also of SMU provided help with GC-Image data processing.

References

- Archer, A.W., Calder, J.H., Gibling, M.R., Naylor, R.D., Reid, D.R. and Wightman, W.G., 1995. Invertebrate trace fossils and agglutinated foraminifera as indicators of marine influences within the classic Carboniferous section at Joggins, Nova Scotia, Canada. *Canadian Journal of Earth Sciences*, 32, 2027–2039.
- Beerling, D.J., Woodward, F.I., 2001. *Vegetation and the Terrestrial Carbon Cycle*. United Kingdom at the University, Cambridge.
- Bell, J.S., and Howie, R.D., 1990. Ch. 4: Paleozoic Geology. *Geology of the Continental Margin of Eastern Canada*. Geological Survey of Canada, *Geology of Canada no.2, Volume I-1 of the Decade of North American Geology*, pp.141-165.
- Brassell, S.C., Lewis, C.A., de Leeuw, J.W., de Lange, F. Sinninghe Damsté, J. S., 1986. Isoprenoid thiophenes: novel products of sediment diagenesis? *Nature* 320, 160–162.
- Brand, U., 1994. Continental hydrology and climatology of the Carboniferous Joggins Formation (lower Cumberland Group) at Joggins, Nova Scotia: evidence from the geochemistry of bivalves. *Palaeogeography, Palaeoclimatology, Palaeoecology*, 106, 307-321.
- Bray, E.E., Evans, E.D., 1961. Distribution of n-paraffin hydrocarbons in nature. Woods Hole Oceanographic Institution Reference No. 66-34, 55 pp.
- Brocks, J.J., Summons, R.E., 2005. In: *Treatise on Geochemistry. Sedimentary Hydrocarbons, Biomarkers for Early Life*. Vol. 8. Biogeochemistry (Ed. Schesinger, W.H.). Elsevier, Oxford, pp. 63-115.
- Brumsack, H. J., 2006. The trace metal content of recent organic carbon-rich sediments: implications for Cretaceous black shale formation. *Palaeogeography, Palaeoclimatology, Palaeoecology*, 232(2), 344-361.

- Calder, J.H., 1998. The Carboniferous evolution of Nova Scotia. In: Blundell, D.J. and Scott, A.C. (eds.), *Lyell: The Past is the Key to the Present*. Geological Society of London, Special Publication 143, 261-302.
- Carpenter, D.K., Falcon-Lang, H.J., Benton, M.J., Grey, M., 2015. Early Pennsylvanian (Langsettian) fish assemblages from the Joggins Formation, Canada, and their implications for palaeogeography. *Palaeontology* 58, 661-690.
- Craggs, S., Keighley, D., Waldron, J.W.F., and Park, A., 2017. Salt tectonics in an intracontinental transform setting: Cumberland and Sackville basins, southern New Brunswick, Canada. *Basin Research*, 29, 266-283.
- Cvejic J. H., Bodrossy L., Kovács K. L., and Rohmer M., 2000. Bacterial triterpenoids of the hopane series from the methanotrophic bacteria *Methylocaldum* spp: Phylogenetic implications and Methylhopanoids: Ancient bacteria and petroleum correlation 3881 first evidence for an unsaturated aminobacteriohopanepolyol. *FEMS Microbiol. Lett.* 182, 361–365.
- Davies, S.J. and Gibling, M.R., 2003. Architecture of coastal and alluvial deposits in an extensional basin: the Carboniferous Joggins Formation of eastern Canada. *Sedimentology*, 50, 414-439.
- Davies, S.J., Gibling, M.R., Rygel, M.C., Calder, J.H., and Skilliter, D.M., 2005. The Pennsylvanian Joggins Formation of Nova Scotia: Sedimentological log and stratigraphic framework of the historic fossil cliffs: *Atlantic Geology*, 41, 115–142.
- de Graaf, W., Sinninghe Damsté, J.S., and de Leeuw, J.W., 1992. Laboratory simulation of natural sulphurization. I. Formation of monomeric and oligomeric isoprenoid polysulphides by low-temperature reactions of inorganic polysulphides with phytol and phytadienes. *Geochimica et Cosmochimica Acta* 56, 4321–4328.
- Deptuck, M.E. and Altheim, B., 2018. Rift basins of the central LaHave Platform, offshore Nova Scotia. Canada-Nova Scotia Geoscience Open File Report, 2018-001MF, 54pp.
- Didyk, B.M., Simoneit, B.R.T., Brassell, S.C., and Eglinton, G., 1978. Organic geochemical indicators of palaeoenvironmental conditions of sedimentation. *Nature* 272, 216–222.
- Douglas, A.G. and Eglinton, G., 1966. The distribution of alkanes. In: Swain, T. (Ed.). *Comparative Phytochemistry*. Academic Press, London, pp. 57–78.
- Duff, P.McL.D and Walton, E.K., 1973. Carboniferous sediments at Joggins, Nova Scotia. In: Josten, K. (ed.), *Septième Congrès International de Stratigraphie et de Géologie du Carbonifère : Krefeld*, 23.-28. Aug. 1971. *Competes Rendus, Geologisches Landesamt Nordrhein-Westfalen*, v.2, pp.365-379.
- Eglinton, G. and Hamilton, R.J., 1967. Leaf epicuticular waxes. *Science* 156, 1322–1335.
- Espitalié, J., 1982. Institut Français du Pétrole, *Syntheses Geologiques et Geochimie* 7020, dated April 28, 1982.
- Espitalié, J., Madec, M., Tissot, B., Mennig, J.J., and Leplat, P., 1977. Source rock characterization method for petroleum exploration. *Proceedings of the 9th Annual Offshore Technology Conference*. pp. 439–448.
- Falcon-Lang, H.J., 2006. A history of research at the Joggins Fossil Cliffs of Nova Scotia, Canada, the world's finest Pennsylvanian section. *Proceedings of the Geologists' Association*, 117, 377-392.

- Farrimond, P., Bevan, J.C., Bishop, A.N., 1999. Tricyclic terpane maturity parameters: response to heating by an igneous intrusion. *Organic Geochemistry* 30, 1011-1019.
- Farrimond, P., Talbot, H. M., Watson, D. F., Schulz, L. K., Wilhelms, A., 2004. Methylhopanoids: Molecular indicators of ancient bacteria and a petroleum correlation tool. *Geochimica et Cosmochimica Acta*. 68(19), 3873-3882.
- Farrimond, P., Taylor, A., and Telnæs, N., 1998. Biomarker maturity parameters: the role of generation and thermal degradation. *Organic Geochemistry* 29, 1181–1197.
- Fogel, M. L. and M. L. Cifuentes., 1993. Isotope Fractionation during Primary Production. in *Organic Geochemistry: Principles and Applications*, ed. M. H. Engel and S. A. Macko. 73-98. New York: Plenum.
- Grey, M., Pufahl, P.K., Aziz, A.A., 2011. Using multiple environmental proxies to determine degree of marine influence and paleogeographical position of the Joggins Fossil Cliffs, UNESCO World Heritage Site. *Palaios*, 26, 256-263.
- Gibling, M.R. and Kalkreuth, W.D., 1991. Petrology of selected carbonaceous limestones and shales in Late Carboniferous coal basins of Atlantic Canada. *International Journal of Coal Geology*, 17, 239-271.
- Gibling, M.R. and Wightman, W.G., 1994. Paleovalleys and protozoan assemblages in a Late Carboniferous cyclothem, Sydney Basin, Nova Scotia. *Sedimentology*, 41, 699-719.
- Gibling, M.R., Calder, J.H., Ryan, R.M., Van De Poll, H.W., and Yeo, G.M., 1992, Late Carboniferous and Early Permian drainage patterns in Atlantic Canada: *Canadian Journal of Earth Sciences*, 29, 338–352.
- Gibling, M.R., Culshaw, N., Rygel, M.C., and Pascucci, V., 2008. Ch. 6: The Maritimes Basin of Atlantic Canada: Basin creation and destruction in the collisional zone of Pangea. In: Miall, A.D. (ed.), *The Sedimentary Basins of the United States and Canada*, pp.211-244.
- Grice, K., Eiserbeck, C., 2014. The analysis and application of biomarkers. In: *Treatise on Geochemistry*. Second Edition. Elsevier Ltd. Pg. 47-78.
- Hines, B.R., Grazley, M.F., Collins, K.S., Bland, K.J., Crampton, J.S., Ventura, G.T., 2019. Chemostratigraphic resolution of widespread reducing conditions in the Southwest Pacific Ocean during the Late Paleocene. *Chemical Geology*. *Chemical Geology* 504, 236-252.
- Hower, J.C., Calder, J.H., Eble, C.F., Scott, A.C., Robertson, J.D., Blanchard, L.J., 2000. Metalliferous coals of the Westphalian A Joggins Formation, Cumberland Basin, Nova Scotia, Canada: petrology, geochemistry, and palynology. *International Journal of Coal Geology* 42, 185–206.
- Huang, W. and Meinschein, W.G., 1979. Sterols as ecological indicators. *Geochimica et Cosmochimica Acta* 43, 739–745.
- Hughes, W.B., Holba, A.G., and Dzou, L.I.P., 1995. The ratios of dibenzothiophene to phenanthrene and pristane to phytane as indicators of depositional environment and lithology of petroleum source rocks. *Geochimica et Cosmochimica Acta* 59, 3581–3598.
- Jarvie, D.M., and Tobey, M.H., 1999. TOC, Rock-Eval, or SR Analyzer Interpretive Guidelines. Humble, TX: Humble Geochemical Services. Application Note 99–4.

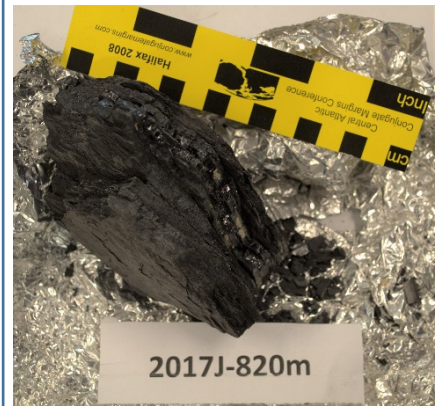
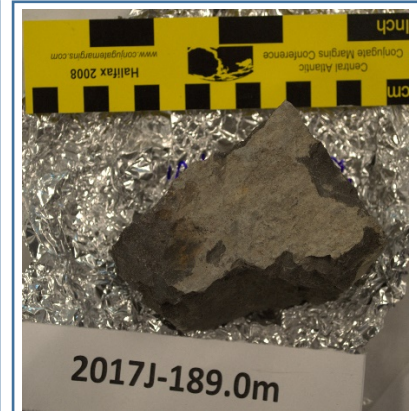
- Jutras, P., McLeod, J.R., and Utting, J., 2015. Sedimentology of the lower Serpukhovian (upper Mississippian) Mabou Group in the Cumberland Basin of eastern Canada: tectonic, halokinetic, and climatic implications. *Canadian Journal of Earth Sciences*, 52, 1150-1168.
- Kvenvolden, K.A. and Squires, R.M., 1967. Carbon isotopic composition of crude oil from Ellenburger group (Lower Ordovician), Permian Basin, west Texas and eastern New Mexico. *Am. Assoc. Pet. Geol., Bull.*, 5(7), 1293--1303.
- Kleemann, G., Poralla, K., Englert, G., Kjoesen, H., Liaaen-Jensen, S., Neunlist, S., Rohmer, M., 1990. Tetrahymanol from the phototrophic bacterium *Rhodospseudomonas palustris*: first report of a gammacerane triterpene from a prokaryote. *J. Gen. Microbiol.* 136(12), 2551-3.
- Lückge, A., Ercegovac, M., Strauss, H., & Littke, R., 1999. Early diagenetic alteration of organic matter by sulfate reduction in Quaternary sediments from the northeastern Arabian Sea. *Marine Geology*, 158(1), 1-13.
- McArthur, J.M., Howarth, R.J., and Bailey, T.R., 2001. Strontium isotope stratigraphy: LOWESS Version 3: Best fit to the marine Sr-isotope curve for 0-509Ma and accompanying look-up table for deriving numerical age. *Journal of Geology*, 109, 155-170.
- Macko, S. A., E. M. H. and P. L. Parker., 1993. Early diagenesis of organic matter in sediments: assessment of mechanisms and preservation by the use of isotopic molecular approaches. In *Organic Geochemistry: Principles and Applications*, Vol. M. H. Engel and S. A. Macko. ed., pp. 211-223. New York: Plenum Press.
- Moldowan, J.M., Seifert, W.K., Gallergos, E.J., 1983. Identification of an extended series of tricyclic terpanes in petroleum. *Geochimica et Cosmochimica Acta* 47(8), 1531-4.
- Mukhopadhyay, P. K., Hatcher, P.G., Calder, J. H. 1991. Hydrocarbon generation from deltaic and intermontane fluviodeltaic coal and coaly shale from the Tertiary of Texas and Carboniferous of Nova Scotia. In *Coal and Terrestrial Organic Matter as a Source Rock for Petroleum* (Mukhopadhyay, P. K. et al. editors), *Org. Geochem.* v. 17, No. 6., p. 765-784. Pergamon Press. Oxford.
- Mukhopadhyay, P. K. 1991. Source rock potential and maturation of Paleozoic sediments (Devonian-Carboniferous) from onshore Nova Scotia. 186 pages, 11 maps, Open File Report of the Department of Natural Resources 91-012.
- Navale, V., 1994. Comparative study of low and high temperature hydrous pyrolysis products of monoglyceryl diether lipid from archaeobacteria. *Journal of Analytical and Applied Pyrolysis*, 29 33–43.
- Naylor, R.D., Archer, A.W., Chandler, F.W. and Fralick, P.W., 1998. Fluvio-estuarine sedimentation in the Late Carboniferous Malagash Formation of Nova Scotia, Canada. Nova Scotia Department of Natural Resources, Report of Activities 1998, p.71-89.
- Neunlist S. and Rohmer M., 1985. Novel hopanoids from the methylotrophic bacteria *Methylococcus capsulatus* and *Methylomonas methanica*. *Biochem. J.* 231, 635–639.
- Ourisson, G., Rohmer, M., 1982. Prokaryotic polyterpenes: phylogenetic precursors of sterols. *Curr. Top. Membr. Transp.* 17, 153-82.

- Peters, K.E. and Cassa, M.R., 1994. Applied source rock geochemistry. In: Magoon, L.B. and Dow, W.G. (Eds.) *The Petroleum System – From Source to Trap*: Tulsa, OK. pp. 93–117.
- Peters, K.E., Moldowan, J.M., 1991. Effects of source, thermal maturity, and biodegradation on the distribution and isomerization of homohopanes in petroleum. *Organic Geochemistry* 17, 47-61.
- Peters, K.E., Moldowan, J.M., 1993. *The Biomarker Guide. Interpreting Molecular Fossils in Petroleum and Ancient Sediments*. Prentice Hall, New York.
- Peters, K.E., Walters, C.C., and Moldowan, J.M., 2005. *The Biomarker Guide, 2nd Edition, Volume 2. Biomarkers and Isotopes in Petroleum Exploration and Earth History*. Cambridge University Press, Cambridge, pp. 475–1155.
- Rashby, S.E., Sessions, A.L., Summons, R.E., Newman, D.K., 2007. Biosynthesis of 2-methylbacteriohopanepolyols by an anoxygenic phototroph. *Proc. Nat. Acad. Sci. U.S.A.* 104(38), 15099-15104.
- Rimmer, S. M., 2004. Geochemical paleoredox indicators in Devonian–Mississippian black shales, central Appalachian Basin (USA). *Chemical Geology*, 206(3), 373-391.
- Rygel, M.C., Sheldon, E.P., Stimson, M.R., Calder, J.H., Ashley, K.T. and Salg, J.L., 2014. The Pennsylvanian Springhill Mines Formation: sedimentological framework of a portion of the Joggins Fossil Cliffs UNESCO World Heritage Site. *Atlantic Geology*, 50, 249-289.
- Rygel, M.C., Lally, C., Gibling, M.R., Ielpi, A., Calder, J.H., and Bashforth, A.R., 2015. Sedimentology and stratigraphy of the type section of the Pennsylvanian Boss Point Formation, Joggins Fossil Cliffs, Nova Scotia, Canada. *Atlantic Geology*, 51, 1-43.
- Scotese, C.R., and McKerrow, W.S., 1990. Revised world maps and introduction, In McKerrow, W.S., and Scotese, C.R., eds., *Palaeozoic Palaeogeography and Biogeography: Geological Society of London Memoirs*, 12, 1–21.
- Seifert, W.K. and Moldowan, J.M., 1986. Use of biological markers in petroleum exploration. In: *Methods in Geochemistry and Geophysics* (R. B. Johns, ed.) Vol. 24. pp. 261-290.
- Simonin, P., Tindall B., and Rohmer M., 1994. Structure elucidation and biosynthesis of 31 methylhopanoids from *Acetobacter europaeus*. *Eur. J. Biochem.* 225, 765–771.
- Sinninghe Damsté, J.S., Kenig, F., Koopmans, M.P., Koster, J., Schouten, S., Hayes, J.M., de Leeuw, J.W., 1995. Evidence for gammacerane as an indicator of water column stratification. *Geochimica Cosmochimica Acta* 59, 9, 1895-1900.
- Sinninghe Damsté, J.S., et al., 1998. Sulfurized carbohydrates: an important sedimentary sink for organic carbon? *Earth and Planetary Science Letters*, 164(1-2), 7-13.
- Sinninghe Damsté, J.S., Kohnen, M.E.L., de Leeuw, J.W., 1990. Thiophenic biomarkers for palaeoenvironmental assessment and molecular stratigraphy. *Nature* 345:6276, pages 609-611.
- Stankiewicz, B.A., Scott, A.C., Collinson, M.E., Finch, P., Mosle, B., Briggs, D.E.G., Evershed, R.P., 1998. Molecular taphonomy of arthropod and plant cuticles from the Carboniferous of North America: implication for the origin of kerogen. *Journal of the Geological Society, London* 155, 453-462.

- Summons, R.E., Hope J.M, Swart R. and Walter M.R., 2008. Origins of bitumens from the Nama Basin: Petroleum Derived from Permian Lacustrine Basins Traversing southwestern Gondwana. *Org. Geochem* 39, 589-607.
- Summons, R.E., Janke, L.L., 1990. Identification of the methyl-hopane in sediments and petroleum. *Geochimica Cosmochimica Acta* 54, 247-251.
- Summons, R.E., Janke, L.L., 1992. Hopenes and hopanes methylated in ring-A: Correlation of the hopanoids from extant methylotrophic bacteria with their fossil analogues. In: *Biological Markers in Sediments and Petroleum* (eds. J.M. Moldowan, P. Albrecht, and R.P. Philp). Prentice-Hall, pp. 182-200.
- Summons, R.E., Janke, L.L., Hope, J.M., Logan, G.A., 1999. 2-Methylhopanoids as biomarkers for cyanobacterial oxygenic photosynthesis. *Nature* 400, 554-557.
- Suto, N., Kawashima, H., 2016. Global mapping of carbon isotope ratios in coal. *Journal of Geochemical Exploration*, 167, 12-19.
- Sykes, R., Zink, K.-G., Rogers, K.M., Phillips, A., and Ventura, G.T., 2012. New and updated geochemical databases for New Zealand petroleum samples, with assessments of genetic oil families, source age, facies and maturity. New Zealand unpublished Petroleum Report 4515. Ministry of Business, Innovation and Employment, 29 p + 2 appendices.
- ten Haven, H.L., de Leeuw, J.W., Rullkötter, J., and Sinninghe Damsté, J.S., 1987. Restricted utility of the pristane/phytane ratio as a palaeoenvironmental indicator. *Nature* 330, 641–643.
- Tibert, N.E. and Scott, D.B., 1999. Ostracodes and agglutinated foraminifera as indicators of palaeoenvironmental change in an Early Carboniferous brackish bay, Atlantic Canada. *Palaios*, 14, 246-260.
- Utting, J., Giles, P.S., and Dolby, G., 2010. Palynostratigraphy of Mississippian and Pennsylvanian rocks, Joggins area, Nova Scotia and New Brunswick, Canada.
- van Dongen, B.E., Schouten, S., Sinninghe Damsté, J.S., 2002. Carbon isotope variability in monosaccharides and lipids of aquatic algae and terrestrial plants. *Marine Ecology Progress Series*. 232, 83–92.
- Vetö, I., Demény, A., Hertelendi, E., & Hetényi, M., 1997. Estimation of primary productivity in the Toarcian Tethys—a novel approach based on TOC, reduced sulphur and manganese contents. *Palaeogeography, Palaeoclimatology, Palaeoecology*, 132(1), 355-371.
- Vetö, I., Hetényi, M., Hámor-Vidó, M., Hufnagel, H., & Haas, J. 2000. Anaerobic degradation of organic matter controlled by productivity variation in a restricted Late Triassic basin. *Organic Geochemistry*, 31(5), 439-452.
- Volkman, J.K., and Maxwell, J.R., 1986. Acyclic isoprenoids as biological markers. In: Johns, R.B. (Ed.), *Biological Markers in the Sedimentary Record*, Elsevier, New York, pp. 1–42.
- von Bitter, P.H. and Plint, H.A., 1987. Conodonts of the Windsor Group (Lower Carboniferous), Magdalen Islands, Quebec, Canada. *Journal of Paleontology*, 61(2), 346-362.
- Wade, J.A., 1990. Part 1: The stratigraphy of Georges Bank Basin and relationships to the Scotian Basin. In: Keen, M.J. and Williams, G.L. (eds), *Geology of the Continental Margin of Eastern Canada*.

- Geological Survey of Canada, *Geology of Canada no.2, Volume I-1 of the Decade of North American Geology*, pp.171-190.
- Waldron, J.W.F., Rygel, M.C., Gibling, M.R., Calder, J.H., 2013. Evaporite tectonics and the late Paleozoic stratigraphic development of the Cumberland Basin, Appalachians of Atlantic Canada. *Geological Society of America Bulletin*, 125, 945-960.
- Waples, D., 1985. *Geochemistry in petroleum exploration*, International Human Resources development corporation, Boston. 232 p.
- Wightman, W.G., Scott, D.B., Medioli, F.S., and Gibling, M.R., 1994. Agglutinated foraminifera and thecameobians from the late Carboniferous Sydney Coalfield, Nova Scotia: paleoecology, paleoenvironments and paleogeographical implications. *Palaeogeography, Palaeoclimatology, Palaeoecology*, 106: 187-202.
- Zaton, M., Grey, M., and Vin, O., 2014. Microconchid tubeworms (Class Tentaculita) from the Joggins Formation (Pennsylvanian), Nova Scotia, Canada. *Canadian Journal of Earth Sciences*, 51, 669-676.

Appendix I: Examples of samples collected for study



Examples of coal

Examples of coaly mudstone

Examples of shale

Examples of limestones
(clam coals)

Appendix II: Sample analyses

Sample Name	Distance from base of section (m)	Cycle	Paleoenvironment			Processing Steps				Data Analysis						
			Grey/Red Beds	Lithology	Number	Microwave Extracted	Polar	Sulfur removal	Apol	Petro-graphic	Rock-Eval	pXRF	G×GC-FID	GC×GC-ToFMS	Carbon Isotopes	Nitrogen Isotopes
17J-915.85	915.85	15	Grey bed	Mudstone	OWFA	X	X	X	X		X	X	X		X	X
17J-915.2	915.20	15	Grey bed	Clam coal limestone	OWFA	X	X	X	X	X	X	X	X		X	X
17J-914.8	914.80	15	Grey bed	Coal	PDFA	X	X	X	X	X	X	X	X		X	X
17J-914.6	914.60	15/14?	Grey bed	Paleosol		X	X	X	X	X	X	X	X		X	X
17J-872.8	872.80	14	Grey bed	Shale	OWFA	X	X	X	X		X	X	X		X	X
17J-872.3	872.30	14	Grey bed	Clam coal limestone	OWFA	X	X	X	X			X	X		X	X
17J-871.8	871.80	14	Grey bed	Coal	PDFA	X	X	X	X		X	X	X		X	X
17J-871.4	871.40	13	Red bed	Paleosol	OWFA	X	X	X	X		X	X	X		X	X
17J-820.25	820.25	13	Grey bed	Limestone	OWFA	X	X	X	X		X	X	X		X	X
17J-820	820.00	12	Grey bed	Coaly mudstone	OWFA/PDFA	X	X	X	X			X	X		X	X
17J-807.25	807.25	12	Grey bed	Mudstone	PDFA	X	X	X	X		X	X	X		X	X
17J-804.1	804.10	12	Grey bed	Coal	PDFA	X	X	X	X		X	X	X		X	X
17J-801.5	801.50	11	Grey bed	Mudstone	PDFA	X	X	X	X		X	X	X		X	X
17J-635	635.00	10	Grey bed	Shale	PDFA	X	X	X	X		X	X	X		X	X
17J-632.85	632.85	10	Grey bed	Shale	PDFA	X	X	X	X		X	X	X		X	X
17J-627.4	627.40	10	Grey bed	Shale	PDFA	X	X	X	X		X	X	X		X	X
17J-626.85	626.85	10	Grey bed	Coaly mudstone	PDFA	X	X	X	X		X	X	X		X	X
17J-612.8	612.80	9	Red bed	Shale	WDFA	X	X	X	X		X	X	X		X	X
17J-580	580.00	9		Mudstone		X	X	X	X			X	X		X	X
17J-449.4	449.40	9	Grey bed	Mudstone	OWFA	X	X	X	X			X	X		X	X
17J-548.7	548.70	9	Grey bed	Mudstone	OWFA	X	X	X	X		X	X	X		X	X
17J-547.55	547.55	9	Grey bed	Org-rich limestone	OWFA	X	X	X	X			X	X		X	X
17J-447.5	447.50	9	Grey bed	Carbonaceous Shale	OWFA	X	X	X	X		X	X	X		X	X
17J-547.25	547.25	8	Grey bed	Org-rich limestone	OWFA	X	X	X	X			X	X		X	X
17J-547.2	547.20	7	Grey bed	Bituminous coal	PDFA	X	X	X	X			X	X		X	X
17J-447	447.00	7	Grey bed	Grey shale	PDFA	X	X	X	X		X	X	X		X	X
17J-445	445.00	7	Grey bed	Grey shale	PDFA	X	X	X	X			X	X		X	X
17J-390.65	390.65	6	Grey bed	Coal	PDFA	X	X	X	X		X	X	X		X	X
17J-390.5	390.50	6	Grey bed	Carbonaceous Shale	PDFA	X	X	X	X		X	X	X		X	X
17J-390.45	390.45	6	Grey bed	Mudstone	PDFA	X	X	X	X		X	X	X		X	X
17J-189.0	189.00	5	Grey bed	Org-rich limestone	OWFA	X	X	X	X			X	X		X	X
17J-188.9	188.90	5	Grey bed	Shale	OWFA	X	X	X	X		X	X	X		X	X

17J-180.7	180.70	5	Grey bed	Shale (marine?)	OWFA	X	X	X	X		X	X	X	X	X	
17J-180.3	180.30	5	Grey bed	Bituminous shale	OWFA	X	X	X	X		X	X	X	X	X	
17J-179.75	179.75	4	Grey bed	Org-rich limestone	PDFFA	X	X	X	X		X	X	X	X	X	
17J-178.8	178.80	4	Grey bed	Coal	PDFFA	X	X	X	X		X	X	X	X	X	
17J-85	85.00	3	Red bed	Shale	PDFFA/Terrestrial shallow water	X	X	X	X		X	X	X	X	X	
17J-78.8	78.80	3	Grey bed	Shale	OWFA/Drowning event	X	X	X	X		X	X	X	X	X	
17J-75	75.00	3	Grey bed	Shale	PDFFA/OWFA	X	X	X	X		X	X	X	X	X	
17J-74	74.00	3	Grey bed	Org-rich limestone	PDFFA	X	X	X	X	X	X	X	X	X	X	
17J-73.8	73.80	3	Grey bed	Org-rich limestone	PDFFA	X	X	X	X	X	X	X	X	X	X	
17J-73	73.00	3	Grey bed	Coaly mudstone	PDFFA/Wetland	X	X	X	X	X	X	X	X	X	X	
17J-72.25	72.25	3	Grey bed	Paleosol	PDFFA	X	X	X	X	X	X	X	X	X	X	
17J-67.65	67.65	3	Grey bed	Shale	PDFFA	X	X	X	X		X	X	X	X	X	
17J-67.05	67.05	3	Grey bed	Limestone	PDFFA	X	X	X	X	X	X	X	X	X	X	
17J-66.8	66.80	3	Grey bed	Coal	PDFFA	X	X	X	X	X	X	X	X	X	X	
17J-66.55	66.55	2	Grey bed	Paleosol	WDFFA	X	X	X	X	X	X	X	X	X	X	
Number						47	47	47	47	10	41	47	47	15	47	47

- Colored fields denote samples collected from similar parasequences.
- Darker blue fields are samples that were collected within the stratigraphic intervals reported to have experienced marine influence during sediment deposition.

Appendix III: Bulk pyrolysis measurements

Sample name	Formation	Lithology	Stratigraphic height (m)	S1	S2	Tmax (cTemp) (°C)	S3 (mg CO ₂ /g rock)	TOC (wt%)	HI (mg HC/g TOC)	OI (mg CO ₂ /g TOC)	PI	BI (mg HC/g TOC)	S1/S2	S1+S2
				(vTPH)	(pTPH)									
				(mg HC/g rock)										
2017J-914.8	Joggins	Coal	914.80	1.37	112.54	427	1.3	70.4	160	2	0.01	2	0.01	113.91
2017J-804.1	Joggins	Coal	804.10	0.54	144.25	417	1.19	62.2	232	2	0.00	1	0.00	144.79
2017J-635.0	Joggins	Coal	635.00	0.5	96.02	425	1.11	59.6	161	2	0.01	1	0.01	96.52
2017J-547.2	Joggins	Coal	547.20	1.49	143.33	418	1.33	67.8	211	2	0.01	2	0.01	144.82
2017J-390.65	Joggins	Coal	390.65	2.21	159.28	422	2.38	70.2	227	3	0.01	3	0.01	161.49
2017J-66.8	Joggins	Coal	66.80	0.83	88.34	425	1.13	60.2	147	2	0.01	1	0.01	89.17
2017J-871.8	Joggins	Coaly Mudstone	871.80	0.83	77.61	429	0.59	29.3	265	2	0.01	3	0.01	78.44
2017J-820.0	Joggins	Coaly Mudstone	820.00	0.68	84.18	426	1.09	40.6	207	3	0.01	2	0.01	84.86
2017J-632.85	Joggins	Coaly Mudstone	632.85	0.33	93.14	425	0.7	44.8	208	2	0.00	1	0.00	93.47
2017J-626.85	Joggins	Coaly Mudstone	626.85	0.44	124.16	424	1.24	53.4	233	2	0.00	1	0.00	124.60
2017J-447.5	Joggins	Coaly Mudstone	447.50	1.39	116.65	420	0.69	43.7	267	2	0.01	3	0.01	118.04
2017J-178.8	Joggins	Coaly Mudstone	178.80	0.87	114.96	420	0.89	46.3	248	2	0.01	2	0.01	115.83
2017J-390.5	Joggins	Coaly Mudstone	390.50	1.09	124.35	420	1.07	58.9	211	2	0.01	2	0.01	125.44
2017J-178.8	Joggins	Coaly Mudstone	178.80	0.87	114.96	420	0.89	46.3	248	2	0.01	2	0.01	115.83
2017J-73.0	Joggins	Coaly mudstone	73.00	0.32	50.72	427	0.38	26.2	194	1	0.01	1	0.01	51.04
2017J-915.2	Joggins	Limestone	915.20	0.14	14.90	438	0.15	5.98	249	3	0.01	2	0.01	15.04
2017J-820.25	Joggins	Limestone	820.25	0.11	13.31	447	0.17	2.56	520	7	0.01	4	0.01	13.42
2017J-547.55	Joggins	Limestone	547.55	0.17	11.61	439	0.16	3.92	296	4	0.01	4	0.01	11.78
2017J-179.75	Joggins	Limestone	179.75	0.02	0.18	438	0.17	0.6	30	28	0.10	3	0.11	0.20
2017J-74.0	Joggins	Limestone	74.00	0.1	7.61	431	0.14	3.6	211	4	0.01	3	0.01	7.71
2017J-73.8	Joggins	Limestone	73.80	0.13	4.48	432	0.18	2.38	188	8	0.03	5	0.03	4.61
2017J-67.05	Joggins	Limestone	67.05	0.1	7.83	434	0.13	3.47	226	4	0.01	3	0.01	7.93
2017J-914.6	Joggins	Paleosol	914.60	0.04	0.14	450	0.1	0.53	27	19	0.22	8	0.29	0.18
2017J-871.4	Joggins	Paleosol	871.40	0.06	0.14	468	0.17	0.46	30	37	0.30	13	0.43	0.20
2017J-612.8	Joggins	Paleosol	612.80	0.05	2.79	442	0.31	6.99	40	4	0.02	1	0.02	2.84
2017J-72.25	Joggins	Paleosol	72.25	0.02	0.17	443	0.11	0.51	33	21	0.11	4	0.12	0.19
2017J-66.55	Joggins	Paleosol	66.55	0.03	1.18	447	0.11	2.95	40	4	0.02	1	0.03	1.21
2017J-915.85	Joggins	Shale	915.85	0.04	0.16	436	0.17	0.43	37	39	0.20	9	0.25	0.20
2017J-872.8	Joggins	Shale	872.80	0.02	0.47	442	0.1	0.66	71	15	0.04	3	0.04	0.49
2017J-807.25	Joggins	Shale	807.25	0.03	0.18	449	0.29	0.47	38	61	0.14	6	0.17	0.21
2017J-801.5	Joggins	Shale	801.50	0.03	0.06	512	0.13	0.47	13	28	0.33	6	0.50	0.09

2017J-627.4	Joggins	Shale	627.40	0.02	0.23	444	0.1	0.57	41	18	0.08	4	0.09	0.25
2017J-548.7	Joggins	Shale	548.70	0.03	0.27	448	0.08	0.64	42	13	0.10	5	0.11	0.30
2017J-447.0	Joggins	Shale	447.00	0.09	2.60	434	0.09	2.3	113	4	0.03	4	0.03	2.69
2017J-390.45	Joggins	Shale	390.45	0.02	0.35	445	0.09	0.98	36	9	0.05	2	0.06	0.37
2017J-188.9	Joggins	Shale	188.90	0.05	0.45	443	0.13	1.26	36	10	0.10	4	0.11	0.50
2017J-180.7	Joggins	Shale	180.70	0.02	0.16	445	0.11	0.49	33	22	0.11	4	0.13	0.18
2017J-180.3	Joggins	Shale	180.30	0.04	1.11	439	0.15	1.1	101	14	0.03	4	0.04	1.15
2017J-85.0	Joggins	Shale	85.00	0.02	0.05	445	0.09	0.25	20	36	0.29	8	0.40	0.07
2017J-78.8	Joggins	Shale	78.80	0.05	3.26	449	0.15	4.23	77	4	0.02	1	0.02	3.31
2017J-75.0	Joggins	Shale	75.00	0.03	0.10	452	0.17	0.29	34	58	0.23	10	0.30	0.13
2017J-67.65	Joggins	Shale	67.65	0.02	0.07	459	0.13	0.36	20	36	0.22	6	0.29	0.09

Appendix IV: Biomarker and stable isotope measurements

Table 1. Carbon and nitrogen stable isotope and atomic measures

Sample	Lithology	Stratigraphic height (m)	Carbon and Nitrogen Stable Isotopes		C/N
			$\delta^{13}\text{C}_{\text{bulk}}$ (‰)	$\delta^{15}\text{N}_{\text{bulk}}$ (‰)	
2017J-914.8	Coal	914.80	2.81	-23.25	2.4
2017J-804.1	Coal	804.10	3.45	-23.38	2.9
2017J-635.0	Coal	635.00	5.63	-25.27	16.2
2017J-547.2	Coal	547.20	3.20	-24.04	2.3
JF-390.65m	Coal	390.65	1.99	-23.92	23.5
JF-66.8m	Coal	66.80	3.56	-23.26	3.1
JF-871.8m	Coaly Mudstone	871.80	3.00	-23.97	2.5
JF-820.0m	Coaly Mudstone	820.00	2.97	-23.41	0.4
JF-632.85m	Coaly Mudstone	632.85	2.43	-23.44	2.0
JF-626.85m	Coaly Mudstone	626.85	2.63	-23.89	2.7
JF-447.5m	Coaly Mudstone	447.50	2.93	-24.00	2.9
JF-390.5m	Coaly Mudstone	390.50	1.97	-23.59	2.1
JF-178.8m	Coaly Mudstone	178.80	3.36	-22.57	19.4
JF-73.0m	Coaly mudstone	73.00	3.90	-23.83	2.8
JF-915.20m	Limestone	915.20	2.89	-24.25	3.3
JF-872.3m	Limestone	872.30	4.66	-26.64	4.3
JF-820.25m	Limestone	820.25	3.88	-29.80	2.1
JF-547.55m	Limestone	547.55	3.91	-28.30	1.7
JF-547.25m	Limestone	547.25	4.62	-26.94	0.4
JF-189m	Limestone	189.00	3.07	-24.32	5.5
JF-179.75m	Limestone	179.75	3.38	-24.89	3.3
JF-74.0m	Limestone	74.00	4.55	-25.56	3.1
JF-73.8m	Limestone	73.80	4.73	-26.78	16.5

JF-67.05m	Limestone	67.05	4.45	-27.36	2.5
JF-914.6m	Paleosol	914.60	3.55	-22.25	2.9
JF-871.4m	Paleosol	871.40	4.11	-22.75	5.5
JF-612.8m	Paleosol	612.80	1.19	-23.24	1.7
JF-72.25m	Paleosol	72.25	4.07	-22.88	2.5
JF-66.55m	Paleosol	66.55	3.32	-22.80	2.8
JF-915.85m	Shale	915.85	3.91	-25.49	1.9
JF-872.8m	Shale	872.80	5.11	-25.23	2.8
JF-807.25m	Shale	807.25	4.61	-23.48	1.1
JF-801.5m	Shale	801.50	4.09	-22.52	5.4
JF-627.4m	Shale	627.40	4.10	-22.82	3.4
JF-580.0m	Shale	580.00	3.71	-22.57	3.8
JF-548.7m	Shale	548.70	3.74	-23.09	5.6
JF-449.4m	Shale	449.40	3.71	-30.69	2.7
JF-447.0m	Shale	447.00	2.84	-24.50	7.7
JF-445.0m	Shale	445.00	3.25	-22.68	4.1
JF-390.45m	Shale	390.45	3.74	-22.83	1.1
JF-188.9m	Shale	188.90	3.41	-23.24	1.9
JF-180.70m	Shale	180.70	4.16	-22.78	3.5
JF-180.3m	Shale	180.30	3.09	-26.77	1.9
JF-85.0m	Shale	85.00	4.27	-22.18	1.9
JF-78.8m	Shale	78.80	3.84	-23.25	2.0
JF-75.0m	Shale	75.00	4.22	-22.86	3.3
JF-67.65m	Shale	67.65	3.87	-22.81	2.1

Table 2. Normal alkane and acyclic isoprenoid FID concentrations

Sample	Stratigraphic level (m)	Lithology	n-C12	n-C13	n-C14	n-C15	n-C16	n-C17	n-C18	n-C19	n-C20	n-C21	n-C22	n-C23	n-C24	n-C25
2017JF-914.8m	914.8	Coal	0.00	0.03	0.40	0.78	0.66	0.67	0.51	0.56	0.47	0.54	0.46	0.56	0.45	0.48
2017JF-804.1m	804.1	Coal	0.00	0.00	0.24	0.43	0.39	0.59	0.37	0.44	0.34	0.43	0.33	0.37	0.36	0.42
2017JF-635m	635	Coal	0.00	0.00	0.03	0.17	0.24	0.40	0.32	0.82	0.71	0.86	0.62	0.68	0.62	0.75
2017JF-547.2m	547.2	Coal	0.00	0.04	0.27	0.55	0.42	0.51	0.33	0.39	0.29	0.36	0.28	0.37	0.32	0.42

2017JF-390.65m	390.65	Coal	0.00	0.03	0.31	0.97	0.62	0.84	0.46	0.57	0.41	0.49	0.40	0.55	0.40	0.47
2017JF-871.8m	871.8	Coaly Mudstone	0.00	1.29	3.55	6.49	4.54	4.99	3.64	4.20	2.31	3.33	1.82	1.92	1.33	1.31
2017JF-820mb	820	Coaly Mudstone	0.00	0.07	0.44	0.78	0.75	0.78	0.69	0.77	0.61	0.73	0.56	0.66	0.63	0.72
2017JF-820m	820	Coaly Mudstone	0.00	0.00	0.00	0.00	0.00	0.00	0.01	0.00	0.01	0.01	0.02	0.02	0.02	0.03
2017JF-632.85m	632.85	Coaly Mudstone	0.00	0.00	0.26	0.59	0.55	0.68	0.47	0.51	0.43	0.50	0.49	0.58	0.61	0.71
2017JF-626.85m	626.85	Coaly Mudstone	0.00	0.00	0.15	0.47	0.45	0.54	0.44	0.50	0.44	0.52	0.47	0.59	0.59	0.75
2017JF-447.5m	447.5	Coaly Mudstone	0.00	0.03	0.25	0.56	0.52	0.60	0.47	0.52	0.43	0.50	0.41	0.50	0.47	0.55
2017JF-390.5m	390.5	Coaly Mudstone	0.00	0.00	0.08	0.43	0.53	0.65	0.49	0.52	0.44	0.49	0.44	0.57	0.47	0.56
2017JF-73m	73	Coaly Mudstone	0.00	0.00	0.00	0.00	0.01	0.00	0.01	0.00	0.01	0.01	0.03	0.04	0.05	0.07
2017JF-915.2m	915.2	Limestone	0.00	0.00	0.00	0.16	0.47	0.65	0.66	0.73	0.72	0.79	0.79	0.90	0.87	1.08
2017JF-872.3m	872.3	Limestone	0.00	0.00	0.00	0.00	0.01	0.06	0.18	0.28	0.50	0.41	0.55	0.56	0.72	0.65
2017JF-820.25m	820.25	Limestone	0.00	0.00	0.61	3.31	7.24	11.26	11.14	12.46	13.53	14.78	16.77	19.45	18.63	22.99
2017JF-547.55m	547.55	Limestone	0.00	0.07	0.73	1.89	2.63	3.62	2.86	3.71	2.91	3.59	2.92	3.27	2.77	3.31
2017JF-547.25m	547.25	Limestone	0.00	0.00	0.10	0.45	0.71	0.97	0.97	1.26	0.99	1.27	0.94	1.07	0.97	1.14
2017JF-189m	189	Limestone	0.00	0.00	0.00	0.00	0.00	0.01	0.20	0.28	0.55	0.75	1.21	1.88	2.68	3.46
2017JF-179.75m	179.75	Limestone	0.00	0.00	0.17	0.04	0.51	1.38	6.46	8.70	11.30	12.86	11.49	13.18	14.51	17.44
2017JF-74m	74	Limestone	0.00	0.00	0.00	0.09	0.79	1.79	2.53	3.54	2.96	3.53	2.79	3.04	2.89	3.30
2017JF-73.8m	73.8	Limestone	0.00	0.02	0.18	0.72	1.40	4.66	2.08	2.53	1.90	2.48	1.72	1.97	1.83	2.27
2017JF-67.05m	67.05	Limestone	0.00	0.00	0.02	0.20	0.55	0.88	1.02	1.21	1.17	1.40	1.07	1.19	0.26	0.75
2017JF-914.6m	914.6	Paleosol	0.00	0.00	0.00	0.01	0.15	0.04	0.23	0.08	0.16	0.10	0.13	0.13	0.16	0.21
2017JF-612.8m	612.8	Paleosol	0.00	0.00	0.03	0.14	0.28	0.40	0.40	0.45	0.38	0.43	0.36	0.41	0.35	0.39
2017JF-66.5m	66.5	Paleosol	0.00	0.00	0.00	0.01	0.02	0.03	0.03	0.04	0.05	0.05	0.06	0.07	0.06	0.07
2017JF-915.85m	915.85	Shale	0.00	0.00	0.00	0.00	0.05	0.01	0.37	0.17	0.45	0.37	0.50	0.52	0.61	0.69
2017JF-872.8m	872.8	Shale	0.00	0.00	0.00	0.00	0.82	0.39	1.58	1.66	2.21	2.24	2.39	2.53	2.39	2.74
2017JF-807.25m	807.25	Shale	0.00	0.00	0.00	0.00	0.06	0.02	0.14	0.08	0.13	0.10	0.13	0.15	0.18	0.21
2017JF-801.5m	801.5	Shale	0.00	0.00	0.00	0.00	0.00	0.00	0.23	0.07	0.47	0.25	0.47	0.51	0.77	1.00
2017JF-627.4m	627.4	Shale	0.00	0.00	0.00	0.00	1.06	0.17	1.14	0.71	1.17	1.17	1.37	1.72	2.19	2.75
2017JF-580m	580	Shale	0.00	0.00	0.00	0.01	0.17	0.02	0.30	0.02	0.20	0.15	0.41	0.67	1.06	1.43
2017JF-548.7m	548.7	Shale	0.00	0.00	0.05	0.01	0.55	0.18	0.84	0.48	0.72	0.61	0.75	0.95	1.21	1.52
2017JF-449.4m	449.4	Shale	0.00	0.00	0.10	0.51	0.99	1.44	1.28	1.88	1.24	1.63	1.02	1.15	0.93	1.15
2017JF-447m	447	Shale	0.00	0.00	0.20	0.60	2.33	3.65	3.71	3.96	3.47	3.75	2.90	3.16	2.81	3.42
2017JF-445m	445	Shale	0.00	0.00	0.00	0.01	0.44	0.03	0.61	0.05	0.40	0.33	0.95	1.71	2.87	4.05
2017JF-390.45m	390.45	Shale	0.00	0.00	0.05	0.03	1.84	1.01	4.18	2.25	3.74	2.59	3.24	3.01	3.51	3.83
2017JF-180.7m	180.7	Shale	0.11	0.05	0.12	0.07	0.25	0.31	0.93	0.61	1.21	0.95	1.08	1.09	1.13	1.35
2017JF-180.3m	180.3	Shale	0.00	0.00	0.00	0.01	0.28	0.77	1.31	1.70	1.51	1.86	1.29	1.44	1.24	1.50
2017JF-85m	85	Shale	0.00	0.00	0.00	0.00	0.00	0.00	0.00	0.00	0.07	0.05	0.14	0.16	0.26	0.31
2017JF-78.8m	78.8	Shale	0.08	0.04	0.13	0.23	1.55	2.20	3.49	4.16	3.74	4.41	2.68	2.96	2.62	3.02

2017JF-75m	75	Shale	0.00	0.00	0.00	0.00	0.06	0.03	0.17	0.08	0.16	0.12	0.16	0.15	0.19	0.23
2017JF-67.65m	67.65	Shale	0.00	0.00	0.00	0.00	0.00	0.00	0.00	0.01	0.07	0.05	0.12	0.14	0.23	0.31

Sample	n-C26	n-C27	n-C28	n-C29	n-C30	n-C31	n-C32	n-C33	n-C34	n-C35	n-C36	i-C13	i-C14	i-C15	i-C16	i-C18	Pr	Ph
2017JF-914.8m	0.44	0.55	0.30	0.34	0.14	0.10	0.04	0.03	0.00	0.00	0.00	0.00	0.24	1.49	0.06	0.94	5.18	0.74
2017JF-804.1m	0.38	0.53	0.28	0.31	0.13	0.00	0.00	0.00	0.00	0.00	0.00	0.00	0.46	2.09	0.08	1.50	12.19	1.01
2017JF-635m	0.67	0.99	0.48	0.57	0.23	0.20	0.08	0.07	0.04	0.03	0.01	0.00	0.00	0.02	0.30	0.45	1.80	0.49
2017JF-547.2m	0.39	0.75	0.30	0.47	0.14	0.12	0.00	0.00	0.00	0.00	0.00	0.00	0.26	1.37	0.05	0.98	6.47	0.84
2017JF-390.65m	0.38	0.56	0.27	0.32	0.14	0.13	0.00	0.00	0.00	0.00	0.00	0.00	0.15	0.95	0.06	0.81	4.84	0.66
2017JF-871.8m	0.88	0.88	0.46	0.44	0.17	0.13	0.00	0.00	0.00	0.00	0.00	0.00	1.01	3.44	0.36	1.95	6.09	1.94
2017JF-820mb	0.70	1.01	0.54	0.69	0.25	0.22	0.00	0.00	0.00	0.00	0.00	0.00	0.35	1.66	0.13	1.08	6.21	0.77
2017JF-820m	0.03	0.03	0.02	0.02	0.01	0.00	0.00	0.00	0.00	0.00	0.00	0.00	0.00	0.00	0.00	0.00	0.01	0.00
2017JF-632.85m	0.65	0.99	0.38	0.42	0.00	0.00	0.00	0.00	0.00	0.00	0.00	0.00	0.00	1.31	0.07	1.07	6.91	0.84
2017JF-626.85m	0.76	1.21	0.60	0.76	0.26	0.21	0.07	0.04	0.00	0.00	0.00	0.00	0.10	0.95	0.05	0.78	5.44	0.76
2017JF-447.5m	0.47	0.82	0.33	0.44	0.18	0.09	0.00	0.00	0.00	0.00	0.00	0.00	0.16	0.88	0.07	0.80	4.19	0.63
2017JF-390.5m	0.51	0.78	0.38	0.52	0.20	0.17	0.12	0.11	0.00	0.00	0.00	0.00	0.00	0.46	0.05	0.82	4.38	0.72
2017JF-73m	0.08	0.09	0.08	0.07	0.05	0.04	0.02	0.01	0.01	0.00	0.00	0.00	0.00	0.00	0.00	0.00	0.02	0.00
2017JF-915.2m	0.80	1.07	0.54	0.59	0.27	0.23	0.11	0.08	0.05	0.03	0.02	0.00	0.00	0.07	0.03	0.32	1.54	0.40
2017JF-872.3m	0.74	0.56	0.50	0.31	0.23	0.12	0.07	0.04	0.02	0.00	0.00	0.00	0.00	0.00	0.00	0.01	0.12	0.33
2017JF-820.25m	15.85	17.31	9.58	8.93	4.87	3.86	2.42	1.77	1.25	0.87	0.49	0.00	0.00	1.17	0.59	3.57	11.94	6.72
2017JF-547.55m	2.30	2.87	1.70	1.87	0.88	0.71	0.32	0.21	0.10	0.07	0.00	0.00	0.34	2.30	0.54	2.77	9.61	3.68
2017JF-547.25m	0.98	1.18	0.85	0.88	0.47	0.38	0.16	0.11	0.00	0.00	0.00	0.00	0.07	0.79	0.20	1.30	5.87	2.31
2017JF-189m	3.95	4.21	3.47	2.83	1.97	1.37	0.76	0.42	0.22	0.12	0.06	0.00	0.00	0.00	0.00	0.00	0.02	0.08
2017JF-179.75m	17.50	20.54	15.01	14.69	9.37	7.26	4.23	2.83	1.84	1.50	1.07	0.00	0.00	0.00	0.00	0.26	2.77	2.42
2017JF-74m	2.81	3.33	2.02	1.84	0.92	0.68	0.29	0.18	0.12	0.08	0.04	0.00	0.00	0.05	0.10	1.63	8.23	4.70
2017JF-73.8m	1.73	2.31	1.34	1.44	0.63	0.49	0.20	0.14	0.08	0.08	0.00	0.00	0.10	1.00	0.40	2.76	8.32	5.29
2017JF-67.05m	1.19	0.89	1.13	0.69	0.78	0.37	0.31	0.15	0.11	0.07	0.06	0.00	0.00	0.00	0.00	0.69	3.13	1.78
2017JF-914.6m	0.24	0.28	0.23	0.23	0.15	0.12	0.06	0.04	0.02	0.00	0.00	0.00	0.00	0.00	0.00	0.02	0.12	0.05
2017JF-612.8m	0.36	0.53	0.27	0.35	0.13	0.11	0.04	0.00	0.00	0.00	0.00	0.00	0.00	0.08	0.02	0.26	1.51	0.33
2017JF-66.5m	0.05	0.05	0.02	0.02	0.00	0.00	0.67	0.41	0.00	0.00	0.00	0.00	0.00	0.00	0.00	0.01	0.06	0.02
2017JF-915.85m	0.73	0.77	0.63	0.58	0.40	0.30	0.17	0.10	0.06	0.04	0.01	0.00	0.00	0.00	0.00	0.00	0.01	0.01
2017JF-872.8m	2.14	2.32	1.56	1.47	0.95	0.76	0.49	0.34	0.22	0.16	0.01	0.00	0.00	0.00	0.00	0.02	0.20	0.17
2017JF-807.25m	0.24	0.26	0.22	0.21	0.15	0.13	0.07	0.05	0.03	0.02	0.01	0.00	0.00	0.00	0.00	0.00	0.02	0.02
2017JF-801.5m	1.14	1.19	1.06	0.98	0.78	0.61	0.41	0.27	0.17	0.12	0.08	0.00	0.00	0.00	0.00	0.00	0.00	0.01
2017JF-627.4m	3.17	3.39	2.98	2.95	2.13	1.78	1.00	0.68	0.37	0.25	0.11	0.00	0.00	0.00	0.00	0.06	0.39	0.29
2017JF-580m	1.72	1.92	1.64	1.40	0.99	0.72	0.40	0.23	0.12	0.05	0.00	0.00	0.00	0.00	0.00	0.01	0.05	0.01

2017JF-548.7m	1.69	1.81	1.51	1.44	1.00	0.75	0.43	0.26	0.17	0.11	0.00	0.00	0.00	0.00	0.03	0.18	0.14	
2017JF-449.4m	0.87	1.17	0.78	0.93	0.45	0.37	0.12	0.00	0.00	0.00	0.00	0.00	0.00	0.54	0.16	1.39	7.23	3.34
2017JF-447m	2.83	4.32	2.59	3.54	1.78	1.72	0.72	0.43	0.14	0.09	0.00	0.00	0.00	0.40	0.39	2.22	11.62	5.90
2017JF-445m	4.99	5.69	4.96	4.35	3.15	2.33	1.33	0.78	0.40	0.22	0.10	0.00	0.00	0.00	0.00	0.02	0.09	0.03
2017JF-390.45m	3.75	4.11	3.16	3.35	2.15	1.85	1.02	0.76	0.51	0.42	0.19	0.00	0.00	0.00	0.00	0.38	1.65	1.09
2017JF-180.7m	1.30	1.69	1.16	1.40	0.77	0.76	0.36	0.29	0.14	0.11	0.05	0.00	0.00	0.03	0.03	0.21	1.17	0.60
2017JF-180.3m	1.19	1.67	0.98	1.18	0.56	0.47	0.20	0.14	0.07	0.07	0.00	0.00	0.00	0.00	0.49	3.95	3.22	
2017JF-85m	0.38	0.37	0.34	0.29	0.24	0.19	0.11	0.07	0.04	0.03	0.02	0.00	0.00	0.00	0.00	0.00	0.00	0.00
2017JF-78.8m	2.55	3.88	1.78	2.11	0.85	0.67	0.30	0.22	0.12	0.09	0.05	0.00	0.00	0.09	0.04	0.99	7.62	1.33
2017JF-75m	0.26	0.31	0.25	0.26	0.17	0.15	0.09	0.07	0.04	0.03	0.02	0.00	0.00	0.00	0.00	0.01	0.05	0.03
2017JF-67.65m	0.38	0.41	0.38	0.34	0.28	0.21	0.14	0.08	0.05	0.04	0.03	0.00	0.00	0.00	0.00	0.00	0.00	0.00

Table 3. Normal alkane and acyclic isoprenoid parameters

Sample	Stratigraphic Interval (m)	Lithology	Pr/Ph	Pr/nC17	Ph/nC18	nC14/(iC15+nC14)	nC17/(nC17+Pr)	nC18/(nC18+Ph)	waxiness		(Pr/n-C17)/(Ph/n-C18))	n-C17/(n-C17+n-C27)	Carbon number preference indices			
									(nC23 to nC36)/(nC12 to nC22)	(nC29 to nC31)/((nC17 to nC19)+(nC29 to nC31))			CPI ¹	CPI(1)	OEP(1)	OEP(2)
2017JF-914.8m	914.8	Coal	6.98	7.70	1.44	0.21	0.11	0.41	0.67	0.25	5.33	0.55	1.35	1.29	1.21	1.37
2017JF-804.1m	804.1	Coal	12.05	20.70	2.76	0.10	0.05	0.27	0.78	0.24	7.51	0.53	1.36	1.32	1.13	1.50
2017JF-635m	635	Coal	3.68	4.53	1.54	0.58	0.18	0.39	1.30	0.39	2.95	0.29	1.48	1.36	1.14	1.58
2017JF-547.2m	547.2	Coal	7.71	12.59	2.58	0.17	0.07	0.28	0.95	0.37	4.88	0.41	1.84	1.66	1.25	1.97
2017JF-390.65m	390.65	Coal	7.28	5.77	1.44	0.25	0.15	0.41	0.63	0.24	3.99	0.60	1.55	1.44	1.32	1.60
2017JF-66.85m	66.8	Coal	N/A	N/A	N/A	N/A	N/A	N/A	N/A	N/A	N/A	N/A	N/A	N/A	N/A	N/A
2017JF-871.8m	871.8	Coaly Mudstone	3.14	1.22	0.53	0.51	0.45	0.65	0.21	0.05	2.29	0.85	1.40	1.24	1.28	1.31
2017JF-820mb	820	Coaly Mudstone	8.10	7.97	1.11	0.21	0.11	0.47	0.87	0.34	7.21	0.44	1.51	1.35	1.13	1.50
2017JF-820m	820	Coaly Mudstone	2.44	2.76	0.54	N/A	0.27	0.65	3.55	0.69	5.12	0.11	1.07	1.10	0.91	1.14
2017JF-632.85m	632.85	Coaly Mudstone	8.21	10.19	1.81	0.16	0.09	0.36	0.97	0.20	5.63	0.41	1.68	1.44	1.08	1.72
2017JF-626.85m	626.85	Coaly Mudstone	7.14	10.05	1.73	0.14	0.09	0.37	1.47	0.45	5.79	0.31	1.53	1.43	1.14	1.61
2017JF-447.5m	447.5	Coaly Mudstone	6.61	6.95	1.34	0.22	0.13	0.43	0.89	0.31	5.18	0.42	1.64	1.48	1.15	1.85
2017JF-390.5m	390.5	Coaly Mudstone	6.11	6.70	1.46	0.15	0.13	0.41	1.07	0.35	4.59	0.46	1.52	1.44	1.23	1.61
2017JF-73m	73	Coaly Mudstone	3.06	3.93	0.49	N/A	0.20	0.67	8.08	0.89	8.05	0.04	1.07	1.07	0.94	1.10
2017JF-915.2m	915.2	Limestone	3.88	2.37	0.61	0.00	0.30	0.62	1.34	0.35	3.91	0.38	1.45	1.33	1.10	1.51
2017JF-872.3m	872.3	Limestone	0.38	1.90	1.77	N/A	0.35	0.36	2.27	0.56	1.07	0.10	0.91	0.89	0.87	0.87
2017JF-820.25m	820.25	Limestone	1.78	1.06	0.60	0.34	0.49	0.62	1.41	0.34	1.76	0.39	1.34	1.25	1.09	1.33
2017JF-547.55m	547.55	Limestone	2.61	2.65	1.29	0.24	0.27	0.44	0.82	0.25	2.06	0.56	1.41	1.31	1.16	1.40
2017JF-547.25m	547.25	Limestone	2.54	6.05	2.38	0.12	0.14	0.30	1.07	0.35	2.55	0.45	1.29	1.22	1.16	1.25
2017JF-189m	189	Limestone	0.30	2.01	0.40	N/A	0.33	0.71	9.16	0.93	5.05	0.00	1.07	1.06	1.00	1.06
2017JF-179.75m	179.75	Limestone	1.15	2.00	0.37	1.00	0.33	0.73	2.66	0.65	5.35	0.06	1.17	1.15	1.05	1.19
2017JF-74m	74	Limestone	1.75	4.61	1.86	0.00	0.18	0.35	1.20	0.30	2.48	0.35	1.28	1.20	1.10	1.30
2017JF-73.8m	73.8	Limestone	1.57	1.79	2.54	0.15	0.36	0.28	0.82	0.22	0.70	0.67	1.42	1.32	1.16	1.44
2017JF-67.05m	67.05	Limestone	1.76	3.56	1.75	1.00	0.22	0.36	1.06	0.37	2.04	0.50	0.79	1.00	1.75	0.73

2017JF-871.4m	914.6	Paleosol	2.70	3.02	0.20	N/A	0.25	0.83	2.09	0.58	15.20	0.13	1.14	1.09	0.92	1.11
2017JF-914.6m	871.4	Paleosol	N/A	N/A	N/A	N/A	N/A	N/A	N/A	N/A						
2017JF-612.8m	612.8	Paleosol	4.54	3.79	0.84	0.25	0.21	0.54	1.02	0.32	4.53	0.43	1.46	1.37	1.16	1.56
2017JF-72.25m	72.25	Paleosol	N/A	N/A	N/A	N/A	N/A	N/A	N/A	N/A						
2017JF-66.5m	66.5	Paleosol	2.36	2.14	0.75	N/A	0.32	0.57	4.97	0.16	2.84	0.34	0.72	1.31	1.05	1.50
2017JF-915.85m	915.85	Shale	0.62	0.61	0.03	N/A	0.62	0.97	2.94	0.70	18.34	0.02	1.09	1.06	0.94	1.08
2017JF-872.8m	872.8	Shale	1.22	0.52	0.11	N/A	0.66	0.90	1.60	0.47	4.93	0.14	1.22	1.17	1.06	1.23
2017JF-807.25m	807.25	Shale	0.81	0.78	0.13	N/A	0.56	0.88	2.91	0.67	5.91	0.07	1.11	1.07	0.97	1.07
2017JF-801.5m	801.5	Shale	0.33	0.47	0.03	N/A	0.68	0.97	6.07	0.88	16.77	0.00	1.06	1.03	0.88	1.04
2017JF-627.4m	627.4	Shale	1.34	2.27	0.25	N/A	0.31	0.80	3.75	0.77	8.97	0.05	1.10	1.07	1.00	1.06
2017JF-580m	580	Shale	3.79	2.87	0.04	N/A	0.26	0.96	9.64	0.90	67.69	0.01	1.08	1.06	0.95	1.07
2017JF-548.7m	548.7	Shale	1.32	0.99	0.16	1.00	0.50	0.86	3.06	0.68	6.11	0.09	1.10	1.08	1.00	1.08
2017JF-449.4m	449.4	Shale	2.17	5.03	2.60	0.16	0.17	0.28	0.78	0.27	1.93	0.55	1.39	1.33	1.24	1.38
2017JF-447m	447	Shale	1.97	3.19	1.59	0.33	0.24	0.39	1.12	0.38	2.00	0.46	1.46	1.37	1.15	1.52
2017JF-445m	445	Shale	3.49	3.05	0.04	N/A	0.25	0.96	13.13	0.93	69.52	0.01	1.08	1.06	0.96	1.07
2017JF-390.45m	390.45	Shale	1.51	1.64	0.26	1.00	0.38	0.79	1.67	0.50	6.24	0.20	1.17	1.09	0.91	1.15
2017JF-188.9m	188.9	Shale	N/A	N/A	N/A	N/A	N/A	N/A	N/A	N/A						
2017JF-180.7m	180.7	Shale	1.95	3.83	0.64	0.79	0.21	0.61	2.04	0.61	5.95	0.15	1.32	1.22	1.00	1.31
2017JF-180.3m	180.3	Shale	1.23	5.12	2.45	N/A	0.16	0.29	1.22	0.37	2.09	0.32	1.42	1.33	1.18	1.46
2017JF-85m	85	Shale	1.85	0.78	0.32	N/A	0.56	0.76	10.29	0.99	2.45	0.00	1.01	0.97	0.83	0.97
2017JF-78.8m	78.8	Shale	5.73	3.47	0.38	0.58	0.22	0.72	0.93	0.27	9.11	0.36	1.50	1.38	1.19	1.64
2017JF-75m	75	Shale	1.57	1.51	0.20	N/A	0.40	0.84	2.84	0.67	7.64	0.10	1.17	1.12	0.91	1.17
2017JF-67.65m	67.65	Shale	1.55	0.71	0.20	1.00	0.58	0.83	11.85	0.99	3.57	0.00	1.02	1.00	0.86	1.01

¹ Carbon Preference Index (1) = $[(C_{25}+C_{27}+C_{29}+C_{31}+C_{33}) / (C_{26}+C_{28}+C_{30}+C_{32}+C_{34}) + [(C_{25}+C_{27}+C_{29}+C_{31}+C_{33}) / [(C_{24}+C_{26}+C_{28}+C_{30}+C_{32})]] / 2$ measured by GCMS using the *m/z* 57 mass chromatogram (Bray and Evans, 1961).

Table 4. Biomarker source and maturity parameters

Sample	Lithology	Stratigraphic height (m)	Source specific biomarker proxies											
			35 α β / (31+32+33+34+35) α β (R+S)	29 α β / 30 α β	BNH/ (BNH+30 α β)	C35 α β / (C31 α β +C35 α β) (S+R)	G \times 10 / (G+30 α β)	Steranes / (steranes+hopanes) (%)	27 / (27+28+29) α α R steranes	28 / (27+28+29) α α R steranes	29 / (27+28+29) α α R steranes	29 / (27+28+29) α α R steranes (%)	29 / (27+30) α α R steranes	27 / (27+28+29) α α R + α α S + β β S steranes
JF-914.8m	Coal	914.8	0.06	0.53	0.29	0.15	3.61	67.63	0.19	0.13	0.68	67.83	3.58	0.12
JF-804.1m	Coal	804.1	0.06	0.59	0.28	0.13	3.21	14.80	0.08	0.05	0.87	86.93	10.81	0.06
JF-635m	Coal	635	0.13	0.54	0.30	0.25	3.62	49.10	0.08		0.92	92.43	12.20	0.13
JF-547.2m	Coal	547.2	0.02	0.50	0.27	0.05	3.89	51.52	0.11	0.16	0.73	72.88	6.86	0.06
JF-390.65m	Coal	390.65	0.03	0.41	0.34	0.09	4.05	63.04	0.07	0.30	0.63	62.72	8.73	0.04
JF-871.8m	Coaly Mudstone	871.8	0.13	0.55	0.38	0.27	3.35	45.69	0.09		0.91	91.25	10.43	0.15
JF-820m	Coaly Mudstone	820		0.61	0.46		3.36	52.65	0.10	0.26	0.64	63.77	6.51	0.27
JF-632.85m	Coaly Mudstone	632.85	0.02	0.47	0.20	0.09	2.16	59.95		0.48	0.52	51.70		0.12
JF-626.85m	Coaly Mudstone	626.85	0.02	0.54	0.16	0.04	3.72	70.04	0.11	0.15	0.74	73.80	6.69	0.11
JF-447.5m	Coaly Mudstone	447.5	0.01	0.45	0.34	0.03	3.50	45.86	0.09	0.39	0.52	52.06	5.61	0.07
JF-390.5m	Coaly Mudstone	390.5	0.01	0.49	0.35	0.03	3.66	65.49	0.21	0.20	0.60	59.50	2.85	0.08
JF-73m	Coaly Mudstone	73		0.48			3.38	38.96		0.35	0.65	65.18		
JF-915.2m	Limestone	915.2	0.04	0.51	0.32	0.10	3.68	31.95	0.10	0.39	0.51	51.45	5.21	0.18
JF-872.3m	Limestone	872.3	0.02	0.48	0.16	0.03	1.46	34.27	0.04	0.37	0.58	58.32	13.16	0.17
JF-820.25m	Limestone	820.25	0.13	0.37	0.25	0.30	1.98	29.11	0.15	0.22	0.64	63.58	4.31	0.35
JF-547.55m	Limestone	547.55	0.19	0.49	0.16	0.36	0.32	28.03	0.12	0.32	0.57	56.78	4.93	0.15
JF-547.25m	Limestone	547.25	0.14	0.57	0.24	0.25	2.39	16.94	0.05	0.34	0.62	61.66	13.46	0.05
JF-189m	Limestone	189	0.04	0.59	0.27	0.08	2.96	34.52	0.10		0.90	89.95	8.95	0.11
JF-179.75m	Limestone	179.75	0.02	0.59	0.07	0.04	0.14	18.81	0.07		0.93	92.74	12.78	0.17
JF-74m	Limestone	74	0.04	0.58	0.11	0.07	0.08	26.91	0.07		0.93	93.07	13.43	0.15
JF-73.8m	Limestone	73.8	0.10	0.51		0.14		27.86	0.12	0.37	0.52	51.66	4.42	0.38
JF-67.05m	Limestone	67.05	0.06	0.59	0.25	0.12	2.36	14.53	0.08		0.92	92.20	11.83	0.15
JF-914.6m	Paleosol	914.6	0.09	0.44	0.14	0.28	2.77	35.26	0.13	0.08	0.79	79.22	5.98	0.08
JF-612.8m	Paleosol	612.8	0.02	0.48	0.19	0.04	3.24	73.32	0.16	0.33	0.51	51.15	3.22	0.16
JF-915.85m	Shale	915.85	0.08	0.54	0.18	0.19	3.39	15.02		0.21	0.79	79.11		0.30
JF-872.8m	Shale	872.8	0.05	0.54	0.31	0.10	3.28	16.94	0.03	0.10	0.88	87.57	34.70	0.19
JF-807.25m	Shale	807.25	0.09	0.46	0.56	0.12	1.04	33.47		0.08	0.92	92.49		
JF-801.5m	Shale	801.5	0.08	0.52	0.15	0.12	2.24	29.38	0.06	0.24	0.71	70.73	12.33	0.24
JF-627.4m	Shale	627.4	0.16	0.51	0.34	0.33	2.86	28.46	0.08	0.37	0.56	55.51	6.96	0.16

JF-580m	Shale	580	0.21	0.53	0.17	0.30	2.06	49.26	0.37	0.63	63.06			0.14
JF-548.7m	Shale	548.7	0.11	0.48	0.23	0.29	2.81	21.55	0.04	0.03	0.93	93.15	26.28	0.06
JF-449.4m	Shale	449.4	0.16	0.52	0.04	0.39	2.08	33.75	0.09	0.27	0.64	63.61	6.95	0.08
JF-447m	Shale	447	0.14					74.03						0.71
JF-445m	Shale	445	0.02	0.50	0.23	0.04	3.12	26.59	0.08	0.30	0.62	62.13	7.85	0.07
JF-390.45m	Shale	390.45	0.04	0.51	0.25	0.10	2.66	49.34	0.26	0.20	0.54	54.19	2.11	0.35
JF-180.7m	Shale	180.7	0.04	0.53	0.35	0.08	2.75	28.41	0.12	0.14	0.75	74.88	6.46	0.11
JF-180.3m	Shale	180.3	0.09	0.51	0.28	0.14	2.57	28.39	0.09		0.91	91.22	10.39	0.13
JF-85m	Shale	85		0.58	0.13		3.02	29.50		0.16	0.84	83.91		0.06
JF-78.8m	Shale	78.8	0.02	0.51	0.27	0.03	3.64	58.77	0.07		0.93	93.32	13.97	0.04
JF-75m	Shale	75	0.06	0.49	0.26	0.12	2.89	47.05	0.14	0.32	0.54	53.77	3.79	0.23
JF-67.65m	Shale	67.65		0.58	0.35		3.11	28.80	0.08	0.22	0.70	69.57	8.33	0.11

Sample	Source specific biomarker proxies (continued)													
	28/ (27+28+29) $\alpha\alpha R + \alpha\alpha S + \beta\beta S$ steranes	29/ (27+28+29) $\alpha\alpha R + \alpha\alpha S + \beta\beta S$ steranes	27/ (27+28+29) $\alpha\alpha + \beta\beta$ (S+R) (%)	28/ (27+28+29) $\alpha\alpha + \beta\beta$ (S+R) (%)	29/ (27+28+29) $\alpha\alpha + \beta\beta$ (S+R) (%)	3 β MHI	2 α MHI	27Dster(S+R)/ (27DS S+R +27RegSter)	C31%/ (C31- C35)	C32%/ (C31- C35)	C33%/ (C31- C35)	C34%/ (C31- C35)	C35%/ (C31- C35)	(DBT+all M- & DMDBTs)/ (P+all M- ,DM-, & ET- Ps)
JF-914.8m	0.35	0.54	12.70	37.64	49.65	0.11	0.17	0.21	0.36	0.22	0.19	0.16	0.06	0.57
JF-804.1m	0.22	0.72	5.05	24.89	70.06	0.05	0.08	0.65	0.39	0.29	0.17	0.09	0.06	0.82
JF-635m	0.27	0.60	10.95	26.57	62.48	0.10	0.05	0.17	0.40	0.21	0.08	0.18	0.13	1.27
JF-547.2m	0.31	0.62	5.19	33.86	60.95	0.09	0.14	0.50	0.44	0.22	0.09	0.22	0.02	2.22
JF-390.65m	0.33	0.62	4.60	34.79	60.61	0.09	0.13	0.57	0.33	0.39	0.16	0.09	0.03	0.41
JF-871.8m	0.33	0.52	12.08	33.99	53.94	0.06	0.12	0.38	0.35	0.16	0.18	0.19	0.13	0.34
JF-820m	0.26	0.47	23.62	29.80	46.59		0.09	0.09	0.73	0.21		0.06		3.64
JF-632.85m	0.38	0.50	10.32	38.60	51.07		0.16	0.42	0.23	0.36	0.27	0.12	0.02	
JF-626.85m	0.37	0.52	9.01	39.17	51.82	0.08	0.07	0.24	0.55	0.23	0.08	0.12	0.02	1.41
JF-447.5m	0.34	0.59	7.59	34.57	57.84	0.07	0.10	0.54	0.34	0.41	0.14	0.11	0.01	0.45
JF-390.5m	0.40	0.52	10.66	37.11	52.23	0.11	0.15	0.42	0.30	0.44	0.14	0.12	0.01	5.06
JF-73m	0.43	0.57		50.06	49.94				0.74	0.26				0.22
JF-915.2m	0.35	0.47	25.32	32.60	42.08	0.12	0.04	0.49	0.37	0.29	0.15	0.15	0.04	0.38
JF-872.3m	0.27	0.55	18.81	28.14	53.04	0.10	0.12	0.46	0.60	0.19	0.07	0.12	0.02	0.29
JF-820.25m	0.19	0.46	34.08	22.13	43.78	0.09	0.01	0.35	0.30	0.27	0.18	0.11	0.13	0.90
JF-547.55m	0.32	0.53	40.66	21.80	37.54	0.09	0.05	0.37	0.33	0.15	0.19	0.14	0.19	6.06
JF-547.25m	0.31	0.64	10.57	26.27	63.16	0.09	0.09	0.52	0.41	0.14	0.16	0.16	0.14	1.57

JF-189m	0.30	0.59	10.46	29.09	60.45	0.09	0.09	0.58	0.49	0.31	0.09	0.07	0.04	0.43
JF-179.75m	0.24	0.59	14.21	23.92	61.87	0.12	0.13	0.40	0.53	0.26	0.11	0.08	0.02	0.60
JF-74m	0.13	0.72	25.12	10.51	64.38	0.10	0.11	0.26	0.56	0.21	0.10	0.08	0.04	0.93
JF-73.8m	0.21	0.40	34.15	20.32	45.53	0.02		0.34	0.58	0.15	0.02	0.16	0.10	0.23
JF-67.05m	0.29	0.57	11.59	28.21	60.20	0.06	0.04	0.54	0.48	0.26	0.10	0.10	0.06	2.33
JF-914.6m	0.34	0.58	6.58	37.78	55.64			0.48	0.24	0.36	0.19	0.12	0.09	0.71
JF-612.8m	0.37	0.48	13.07	39.09	47.84	0.10	0.09	0.18	0.49	0.41	0.03	0.06	0.02	0.72
JF-915.85m	0.21	0.49	25.75	26.23	48.03	0.05	0.03	0.26	0.33	0.32	0.11	0.16	0.08	0.81
JF-872.8m	0.21	0.60	17.72	24.18	58.11	0.10	0.04	0.26	0.42	0.25	0.15	0.12	0.05	1.29
JF-807.25m	0.26	0.74		37.89	62.11	0.38			0.61	0.08	0.07	0.16	0.09	0.66
JF-801.5m	0.23	0.52	25.12	29.74	45.14	0.08	0.06	0.42	0.62	0.10	0.10	0.10	0.08	0.57
JF-627.4m	0.30	0.54	14.14	28.72	57.14	0.08	0.09	0.43	0.33	0.36	0.04	0.11	0.16	0.86
JF-580m	0.25	0.61	11.75	32.59	55.66			0.65	0.50	0.10	0.06	0.12	0.21	0.95
JF-548.7m	0.24	0.70	5.50	26.93	67.56	0.07	0.07	0.66	0.28	0.26	0.18	0.17	0.11	0.34
JF-449.4m	0.24	0.68	6.80	23.79	69.41	0.05	0.09	0.73	0.25	0.17	0.22	0.20	0.16	0.40
JF-447m	0.29		70.97	29.03				0.18			0.72	0.14	0.14	0.83
JF-445m	0.33	0.60	5.63	38.89	55.47	0.10	0.06	0.61	0.52	0.26	0.12	0.08	0.02	0.49
JF-390.45m	0.27	0.38	30.22	28.66	41.12	0.15	0.01	0.18	0.39	0.34	0.11	0.12	0.04	2.34
JF-180.7m	0.34	0.55	9.99	31.69	58.32	0.07	0.07	0.48	0.52	0.27	0.13	0.04	0.04	2.10
JF-180.3m	0.24	0.63	11.06	23.21	65.73	0.06	0.08	0.50	0.55	0.13	0.12	0.10	0.09	
JF-85m	0.30	0.64	4.24	40.96	54.79	0.14		0.78						0.28
JF-78.8m	0.22	0.74	4.36	21.13	74.50	0.12	0.10	0.46	0.57	0.27	0.06	0.08	0.02	0.77
JF-75m	0.37	0.40	43.02	26.82	30.15	0.14	0.03	0.09	0.39	0.38	0.10	0.06	0.06	0.33
JF-67.65m	0.39	0.51	10.37	46.05	43.58	0.11	0.02	0.50	0.54	0.27	0.19			0.45

Sample	Maturity biomarker proxies						
	Ts/ (Ts+Tm)	31αβ 22S/ 31αβ(S+R)	32αβ 22S/ 32αβ(S+R)	30βα/ (30αβ+30βα)	31αβ(S+R)/ (29αβ+30αβ)	29ααS/ 29αα(S+R)	29ββ/ (29ββ+29αα)
JF-914.8m	0.16	0.55	0.50	0.30	0.55	0.52	0.41
JF-804.1m	0.56	0.57	0.46	0.28	0.43	0.20	0.38
JF-635m	0.16	0.60	0.51	0.33	0.49	0.31	0.43
JF-547.2m	0.15	0.55	0.48	0.29	0.73	0.41	0.38
JF-390.65m	0.20	0.53	0.50	0.29	0.82	0.56	0.31
JF-871.8m	0.04	0.56	0.45	0.32	0.48	0.38	0.42
JF-820m		0.50		0.28	0.37	0.53	0.34
JF-632.85m		0.42	0.54	0.32	0.41	0.36	0.36
JF-626.85m	0.04	0.65	0.51	0.32	0.70	0.48	0.38
JF-447.5m	0.23	0.54	0.52	0.28	0.63	0.38	0.39
JF-390.5m	0.58	0.53	0.49	0.33	0.57	0.53	0.43
JF-73m	0.58	0.57		0.22	0.49	0.29	0.29
JF-915.2m	0.94	0.55	0.47	0.35	0.59	0.34	0.38
JF-872.3m	0.28	0.57	0.33	0.19	0.36	0.26	0.51
JF-820.25m	0.04	0.54	0.51	0.26	0.33	0.54	0.37
JF-547.55m	0.72	0.58	0.13	0.34	0.43	0.34	0.42
JF-547.25m	0.20	0.57	0.08	0.35	0.42	0.27	0.49
JF-189m	0.13	0.56	0.46	0.33	0.44	0.27	0.47
JF-179.75m	0.54	0.56	0.47	0.31	0.36	0.25	0.43
JF-74m	0.87	0.59	0.58	0.07	0.43	0.31	0.47
JF-73.8m	0.29	0.56	0.06	0.32	0.47	0.29	0.55
JF-67.05m	0.00	0.57	0.45	0.31	0.30	0.23	0.54
JF-914.6m	0.25	0.55	0.47	0.32	0.50	0.43	0.37
JF-612.8m	0.07	0.51	0.69	0.31	0.54	0.44	0.47
JF-915.85m		0.53	0.44	0.39	0.37	0.35	0.27
JF-872.8m	0.14	0.56	0.53	0.43	0.38	0.36	0.29
JF-807.25m		0.50	0.60	0.29	0.59	0.14	0.34
JF-801.5m	0.22	0.54	0.52	0.31	0.32	0.45	0.44
JF-627.4m	0.26	0.55	0.56	0.31	0.43	0.26	0.44
JF-580m	0.44	0.57	0.39	0.17	0.43	0.72	0.38
JF-548.7m		0.51	0.44	0.31	0.42	0.25	0.33
JF-449.4m	0.34	0.55	0.04	0.24	0.29	0.35	0.44

JF-447m								
JF-445m	0.26	0.50	0.46	0.31	0.46	0.40	0.34	
JF-390.45m		0.54	0.48	0.32	0.37	0.39	0.50	
JF-180.7m	0.35	0.56	0.54	0.30	0.39	0.23	0.41	
JF-180.3m	0.01	0.56	0.02	0.29	0.35	0.23	0.47	
JF-85m	0.25	0.57		0.41	0.34	0.37	0.29	
JF-78.8m	0.03	0.54	0.48	0.35	0.56	0.26	0.40	
JF-75m	0.40	0.53	0.60	0.30	0.42	0.36	0.40	
JF-67.65m	0.36	0.57	0.48	0.37	0.37	0.23	0.35	

List of selected formula and references:

¹ $C_{27}, C_{28}, C_{29} S/(S+R) = 5\alpha(H), 14\alpha(H), 17\alpha(H)\text{-sterane-20S}/(5\alpha(H), 14\alpha(H), 17\alpha(H)\text{-sterane-20S} + 5\alpha(H), 14\alpha(H), 17\alpha(H)\text{-sterane-20R})$ for $C_{27}, C_{28},$ and $C_{29},$ respectively (Seifert and Moldowan, 1986).

² $C_{27} \beta\beta/(\alpha\alpha+\beta\beta) = C_{27} 5\alpha(H), 14\beta(H), 17\beta(H)\text{-cholestane } 20(S+R)/[C_{27} 5\alpha(H), 14\beta(H), 17\beta(H)\text{-cholestane } 20(S+R) + 5\alpha(H), 14\alpha(H), 17\alpha(H)\text{-cholestane } 20(S+R)],$
 $C_{28} \beta\beta/(\alpha\alpha+\beta\beta)$ and $C_{29} \beta\beta/(\alpha\alpha+\beta\beta)$ is calculated from the same equation as $C_{27} \beta\beta/(\alpha\alpha+\beta\beta)$ (Seifert and Moldowan, 1986).

³ $C_{28}/(C_{28}+C_{29}) = [\sum C_{28} 13\beta(H), 17\alpha(H)\text{-diasterane-20}(S+R) + 5\alpha(H), 14\alpha(H), 17\alpha(H)\text{-cholestane } 20(S+R) + 5\alpha(H), 14\beta(H), 17\beta(H)\text{-cholestane-20}(S+R)]/[\sum C_{28} + C_{29} 13\beta(H), 17\alpha(H)\text{-diasterane-20}(S+R) + 5\alpha(H), 14\alpha(H), 17\alpha(H)\text{-cholestane } 20(S+R) + 5\alpha(H), 14\beta(H), 17\beta(H)\text{-cholestane-20}(S+R)]$ (Grantham and Wakefield, 1988).

⁴ $\text{Reg}C_{27}(\%) = [C_{27} 5\alpha(H), 14\alpha(H), 17\alpha(H)\text{-cholestane } 20(S+R) + (C_{27} 5\alpha(H), 14\beta(H), 17\beta(H)\text{-cholestane-20}(S+R))]/[\sum C_{27} \text{ to } C_{29} (5\alpha(H), 14\beta(H), 17\beta(H)\text{-steranes } 20(S+R) + 5\alpha(H), 14\alpha(H), 17\alpha(H)\text{-steranes } 20(S+R))];$ $\text{Reg}C_{28}(\%)$ and $\text{Reg}C_{29}(\%)$ are calculated from the same equation as $\text{Reg}C_{27}(\%)$.

⁵ $\text{Dia}C_{27}(\%) = C_{27} 13\beta(H), 17\alpha(H)\text{-diasterane-20}(S+R)/[C_{27}, C_{28} \text{ and } C_{29} (13\beta(H), 17\alpha(H)\text{-diasterane-20}(S+R))];$ $\text{Dia}C_{28}(\%)$ and $\text{Dia}C_{29}(\%)$ is calculated from the same equation as $\text{Dia}C_{27}(\%)$.

¹ $C_{27}/C_{29} = (T_s + T_m)/C_{29} 17\alpha(H), 21\beta(H)\text{-hopane}; C_{29}/C_{30} = C_{29} 17\alpha(H), 21\beta(H)\text{-hopane} / C_{30} 17\alpha(H), 21\beta(H)\text{-hopane};$
 $C_{30}/C_{31} = C_{30} 17\alpha(H), 21\beta(H)\text{-hopane} / C_{31} 17\alpha(H), 21\beta(H)\text{-hopane } 22(S+R).$

² T_s and $T_m = C_{27} 17\alpha(H)\text{-22,29,30-trisnorhopane}$ and $18\alpha(H)\text{-22,29,30-trisnorhopane},$ respectively.

³ $C_{29}T_s/C_{29}H = C_{29} 17\alpha(H)\text{-22,29,30-trisnorhopane} / C_{29} 17\alpha(H), 21\beta(H)\text{-hopane}.$

⁴ $C_{31}S/(S+R) = C_{31} 17\alpha(H), 21\beta(H)\text{-hopane } 22S / C_{31} 17\alpha(H), 21\beta(H)\text{-hopane } 22(S+R).$

⁵ $C_{30}Mor/C_{30}Hop = C_{30} 17\beta(H), 21\alpha(H)\text{-hopane}/C_{30} 17\alpha(H), 21\beta(H)\text{-hopane}.$

⁸ $\text{Gammacerane Index (GI)} = \text{Gammacerane}/(\text{Gammacerane} + C_{30} 17\alpha(H), 21\beta(H)\text{-hopane})$ (Moldowan *et al.*, 1985).

⁹ $C_{31} 2\alpha\text{-Methylhopane Index (} C_{31} 2\alpha\text{-MHI)} = C_{31} 2\alpha\text{-methylhopane} / (C_{31} 2\alpha\text{-methylhopane} + C_{30} 17\alpha(H), 21\beta(H)\text{-hopane})$ (Summons *et al.*, 1999).

¹⁰ $H/S = [\sum C_{27} 17\alpha(H)\text{-22,29,30-trisnorhopane} + C_{27} 18\alpha(H)\text{-22,29,30-trisnorhopane} + C_{29} 17\alpha(H)\text{-22,29,30-trisnorhopane} + C_{29}\text{-}C_{30} 17\alpha(H), 21\beta(H)\text{-hopane} + C_{31}\text{-}C_{35} 17\alpha(H), 21\beta(H)\text{-hopane } 22(S+R) + C_{31} 2\alpha(H)\text{-methylhopane}] / (\sum C_{27}\text{-}C_{29} 5\alpha(H), 14\alpha(H), 17\alpha(H) \text{ and } 5\alpha(H), 14\beta(H), 17\beta(H)\text{-steranes and } 13\beta(H), 17\alpha(H)\text{-diasteranes}).$

¹¹ $\text{DiaSt}/\text{RegSt} = (\sum C_{27}\text{-}C_{29} 13\beta(H), 17\alpha(H)\text{-diasteranes}) / (\sum C_{27}\text{-}C_{29} 5\alpha(H), 14\alpha(H), 17\alpha(H)\text{- and } 5\alpha(H), 14\beta(H), 17\beta(H)\text{-steranes}).$

Table 5. Key to compound abbreviations

Abbreviation	Compound	Abbreviation	Compound
Sat	saturate fraction	34 α β R	17 α , 21 β , 22(R)-tetrakishomohopane
Aro	aromatic fraction	35 α β S	17 α , 21 β , 22(S)-pentakishomohopane
<i>i</i> -C ₉	iso-nonane	35 α β R	17 α , 21 β , 22(R)-pentakishomohopane
<i>n</i> -C ₉	normal-nonane	21 $\alpha\alpha$	C21-5 α , 14 α , 17 α -pregnane
<i>i</i> -C ₁₀	iso-decane	21 $\beta\beta$	C21-5 α , 14 β , 17 β -pregnane
<i>n</i> -C ₁₀	normal-decane	22 $\alpha\alpha$	C22-5 α , 14 α , 17 α -pregnane
<i>i</i> -C ₁₁	iso-undecane	22 $\beta\beta$	C22-5 α , 14 β , 17 β -pregnane
<i>n</i> -C ₁₁	normal-undecane	27d β S	13 β , 17 α , 20(S)-cholestane
<i>n</i> -C ₁₂	normal-dodecane	27d β R	13 β , 17 α , 20(R)-cholestane
<i>i</i> -C ₁₃	iso-tridecane	27d α R	13 α , 17 β , 20(R)-cholestane
<i>i</i> -C ₁₄	iso-tetradecane	27d α S	13 α , 17 β , 20(S)-cholestane
<i>n</i> -C ₁₃	normal-tridecane	28d β S#1	24-methyl-13 β , 17 α , 20(S)-cholestane #1
<i>i</i> -C ₁₅	iso-pentadecane	28d β S#2	24-methyl-13 β , 17 α , 20(S)-cholestane #2
<i>n</i> -C ₁₄	normal-tetradecane	28d β R#1	24-methyl-13 β , 17 α , 20(R)-cholestane #1
<i>i</i> -C ₁₆	iso-hexadecane	28d β R#2	24-methyl-13 β , 17 α , 20(R)-cholestane #2
<i>n</i> -C ₁₅	normal-pentadecane	28d α R	24-methyl-13 α , 17 β , 20(R)-cholestane
<i>n</i> -C ₁₆	normal-hexadecane	27 $\alpha\alpha$ S	5 α , 14 α , 17 α , 20(S)-cholestane
<i>i</i> -C ₁₈	iso-octadecane	27 $\beta\beta$ R+29d β S	5 α , 14 β , 17 β , 20(R)-cholestane + 24-ethyl-13 β , 17 α , 20(S)-cholestane
<i>n</i> -C ₁₇	normal-heptadecane	27 $\beta\beta$ S	5 α , 14 β , 17 β , 20(S)-cholestane
Pr	pristane (iso-nonadecane)	28d α S	24-methyl-13 α , 17 β , 20(S)-cholestane
<i>n</i> -C ₁₈	normal-octadecane	27 $\alpha\alpha$ R	5 α , 14 α , 17 α , 20(R)-cholestane
Ph	phytane (iso-eicosane)	29d β R	24-ethyl-13 β , 17 α , 20(R)-cholestane
<i>n</i> -C ₁₉	normal-nonadecane	29d α R	24-ethyl-13 α , 17 β , 20(R)-cholestane

Abbreviation	Compound	Abbreviation	Compound
<i>n</i> -C ₂₀	normal-eicosane	28 α α S	24-methyl-5 α , 14 α , 17 α , 20(S)-cholestane
<i>n</i> -C ₂₁	normal-heneicosane	29 α α S	24-ethyl-13 α , 17 β , 20(S)-cholestane
<i>n</i> -C ₂₂	normal-docosane	28 β β R	24-methyl-5 α , 14 β , 17 β , 20(R)-cholestane
<i>n</i> -C ₂₃	normal-tricosane	28 β β S	24-methyl-5 α , 14 β , 17 β , 20(S)-cholestane
<i>n</i> -C ₂₄	normal-tetracosane	28 α α R	24-methyl-5 α , 14 α , 17 α , 20(R)-cholestane
<i>n</i> -C ₂₅	normal-pentacosane	29 α α S	24-ethyl-5 α , 14 α , 17 α , 20(S)-cholestane
<i>n</i> -C ₂₆	normal-hexacosane	29 β β R	24-ethyl-5 α , 14 β , 17 β , 20(R)-cholestane
<i>n</i> -C ₂₇	normal-heptacosane	29 β β S	24-ethyl-5 α , 14 β , 17 β , 20(S)-cholestane
<i>n</i> -C ₂₈	normal-octacosane	29 α α R	24-ethyl-5 α , 14 α , 17 α , 20(R)-cholestane
<i>n</i> -C ₂₉	normal-nonacosane	30 β β S	24-propyl-5 α , 14 β , 17 β , 20(S)-cholestane
<i>n</i> -C ₃₀	normal-triacontane	30 α α R	24-propyl-5 α , 14 α , 17 α , 20(R)-cholestane
<i>n</i> -C ₃₁	normal-hentriacontane	27 β β R	5 α , 14 β , 17 β , 20(R)-cholestane
<i>n</i> -C ₃₂	normal-dotriacontane	27 β β S	5 α , 14 β , 17 β , 20(S)-cholestane
<i>n</i> -C ₃₃	normal-tritriacontane	28 β β R	24-methyl-5 α , 14 β , 17 β , 20(R)-cholestane
<i>n</i> -C ₃₄	normal-tetratriacontane	28 β β S	24-methyl-5 α , 14 β , 17 β , 20(S)-cholestane
<i>n</i> -C ₃₅	normal-pentatriacontane	29 β β R	24-ethyl-5 α , 14 β , 17 β , 20(R)-cholestane
<i>n</i> -C ₃₆	normal-hexatriacontane	29 β β S	24-ethyl-5 α , 14 β , 17 β , 20(S)-cholestane
25nor28 α β	17 α , 21 β -25,28,30-trisnorhopane	30 β β R	24-propyl-5 α , 14 β , 17 β , 20(R)-cholestane
25nor29 α β	17 α , 21 β -25,30-bisnorhopane	30 β β S	24-propyl-5 α , 14 β , 17 β , 20(S)-cholestane
25nor30 α β	17 α , 21 β -25-norhopane	27 δ β S	13 β , 17 α , 20(S)-cholestane
25nor31 α β	17 α , 21 β , 22(R/S)-25-norhomohopane	27 δ β R	13 β , 17 α , 20(R)-cholestane
19C	C19H34 tricyclic terpane	27 α α R	13 α , 17 β , 20(R)-cholestane
IP	isopimarane	27 α α S	13 α , 17 β , 20(S)-cholestane
20C	C20H36 tricyclic terpane	28 δ β S#1	24-methyl-13 β , 17 α , 20(S)-cholestane #1
21C	C21H38 tricyclic terpane	28 δ β S#2	24-methyl-13 β , 17 α , 20(S)-cholestane #2

Abbreviation	Compound	Abbreviation	Compound
23C	C23H42 tricyclic terpane	28dβR#1	24-methyl-13β, 17α, 20(R)-cholestane #1
24C	C24H44 tricyclic terpane	28dβR#2	24-methyl-13β, 17α, 20(R)-cholestane #2
26C	C26H48 tricyclic terpane	28dαR	24-methyl-13α, 17β, 20(R)-cholestane
28C	C28H52 tricyclic terpane	29dβS	24-ethyl-13β, 17α, 20(S)-cholestane
29C	C29H54 tricyclic terpane	28dαS	24-methyl-13α, 17β, 20(S)-cholestane
Ts	18α-22,29,30-trisnorhopane	29dβR	24-ethyl-13β, 17α, 20(R)-cholestane
A	unknown pentacyclic triterpenoid	29dαR	24-ethyl-13α, 17β, 20(R)-cholestane
Tm	17α-22,29,30-trisnorhopane	29dαS	24-ethyl-13α, 17β, 20(S)-cholestane
30C	C30H56 tricyclic terpane	1MN	1-methylnaphthalenes
BNH	17α, 21β-28,30-bisnorhopane	2MN	2-methylnaphthalenes
25-norH	17α, 21β-25-norhopane	1,5DMN	1,5-dimethylnaphthalenes
29αβ	17α, 21β-30-norhopane	2,6DMN	2,6-dimethylnaphthalenes
29Ts	18α-30-norhopane	2,7DMN	2,7-dimethylnaphthalenes
30d	15α-methyl-17α-27-norhopane	EN	ethylnaphthalene
29βα	17β, 21α-30-norhopane	1,3,7TMN	1,3,7-trimethylnaphthalenes
30αβ	17α, 21β-hopane	1,2,5TMN	1,2,5-trimethylnaphthalenes
30βα	17β, 21α-hopane (moretane)	2,3,6TMN	2,3,6-trimethylnaphthalenes
31αβS	17α, 21β, 22(S)-homohopane	1,3,5TMN	1,3,5-trimethylnaphthalenes
31αβR	17α, 21β, 22(R)-homohopane	1,4,6TMN	1,4,6-trimethylnaphthalenes
G	gammacerane	1,3,7TMN	1,3,7-trimethylnaphthalenes
31βα	17β, 21α-homohopane	1,3,6TMN	1,3,6-trimethylnaphthalenes
32αβS	17α, 21β, 22(S)-bishomohopane	P	phenanthrene
32αβR	17α, 21β, 22(R)-bishomohopane	Ps	phenanthrene and anthracene
33αβS	17α, 21β, 22(S)-trishomohopane	1MP	1-methylphenanthrenes
33αβR	17α, 21β, 22(R)-trishomohopane	2MP	2-methylphenanthrenes

Abbreviation	Compound
34 α β S	17 α , 21 β , 22(S)-tetrakishomohopane
MDBT	methyldibenzothiophene
1MDBT	1-methyldibenzothiophenes
4MDBT	4-methyldibenzothiophenes
DMDBTs	dimethyldibenzothiophenes

Abbreviation	Compound
3MP	3-methylphenanthrenes
9MP	9-methylphenanthrenes
DMP	dimethylphenanthrenes
EP	ethylphenanthrene
DBT	dibenzothiophene

Appendix V: Portable-XRF elemental ratios

Sample	Lithology	P/Si	K/P	K/Si	Cr/P	Mo/S	Fe/S	Mn/Fe	Ba/P	Cl/P	Sr/Ba	Sr/Ca	V/Ni	V/Cr	Mn/Ca	Ni/Co	Sr/Rb	Ti/Zr
914.8	Coal	0.0000				0.0005	0.50	0.0027			1.960	0.016			0.010		15.71	24
804.1	Coal	0.0655	0.6500			0.0003	0.72	0.0014	0.040	2.305	1.350	0.016			0.026		7.88	28
635	Coal	0.0407	2.4000	0.07		0.0003	0.72	0.0014	0.050	1.252	1.080	0.092	0.890		0.148		3.32	37
547.2	Coal	0.1656	0.3900			0.0003	0.56	0.0028	0.020	1.342	2.190	0.015			0.018		12.13	32
390.65	Coal	0.0728	1.8100	0.10	0.054	0.0006	0.41	0.0064	0.040	0.835	2.090	0.027	1.280		0.018		5.57	29
66.8	Coal	0.0488	1.8400	0.08		0.0003	0.56	0.0039	0.030	0.424	1.100	0.007	2.030	2.010	0.015	0.25	2.65	29
871.8	Coaly Mudsto	0.2346	0.3900	0.12		0.0001	0.48	0.0163	0.040	0.204	2.410	0.002	1.030	1.230	0.004		40.00	9
820	Coaly Mudsto	0.0099	11.4400	0.14	0.125	0.0006	0.95	0.0027	0.200	0.679	0.390	0.020	2.910	1.980	0.054	0.16	0.80	41
632.85	Coaly Mudsto	0.0184	5.9600	0.12		0.0005	0.78	0.0024	0.090	0.777	0.770	0.070	2.710	1.660	0.100	0.12	1.89	23
626.85	Coaly Mudsto	0.1347	0.6400	0.07		0.0009	0.60	0.0328	0.030	1.658	3.310	0.002			0.011		17.43	15
447.5	Coaly Mudsto	0.0142	9.6700	0.16	0.079	0.0004	0.74	0.0034	0.120	0.904	0.590	0.046	3.350	1.490	0.066	0.17	1.16	36
390.5	Coaly Mudsto	0.0676	1.6800	0.12		0.0003	0.72	0.0031	0.040	0.590	1.220	0.025	3.080	1.610	0.053	0.09	3.76	24
178.8	Coaly Mudsto	0.0838	1.3300			0.0002	0.68	0.0012	0.030	0.829	1.110	0.014			0.054	0.00	5.20	31
73	Coaly mudsto	0.0220	5.8700	0.18		0.0001	0.79	0.0064	0.100	0.471	0.660	0.004	2.870	1.440	0.009	0.27	1.95	28
915.2	Limestone	0.0000		0.16		0.0004	3.40	0.0437			0.840	0.001	1.710	1.240	0.007		2.86	30
872.3	Limestone					0.0008	1.07	0.2897			3.180	0.001	0.420		0.003		136.80	
820.25	Limestone	0.0000		0.21		0.0004	1.99	0.0865			1.110	0.001	1.310	0.980	0.010		4.83	27
547.55	Limestone	0.0000		0.20		0.0002	2.29	0.0216			0.360	0.001	1.950	1.250	0.005	0.31	1.39	34
547.25	Limestone	0.0000		0.19		0.0001	0.46	0.1074			2.100	0.001	0.800	1.470	0.004		25.10	15
189	Limestone	0.0000		0.17		0.0002	0.27	0.3310			2.410	0.001	0.510		0.002			9
179.75	Limestone	0.0000		0.17		0.0001	0.36	0.0455			1.250	0.001	0.780		0.002			11
74	Limestone	0.0307	3.1500	0.23		0.0001	0.61	0.0638	0.130		1.390	0.001	1.210	1.460	0.003		11.75	22
73.8	Limestone	0.0000		0.26		0.0001	0.56	0.0342			0.400	0.001	2.420	3.200	0.003		13.26	23
67.05	Limestone	0.0000		0.28		0.0001	0.77	0.0308			1.050	0.001	1.200	1.140	0.007	0.25	3.99	27
914.6	Paleosol	0.0000		0.17		0.0002	2.08	0.0042			0.310		1.670	0.940		0.33	0.78	37
871.4	Paleosol	0.0080	14.5600	0.15	0.124			0.0173	0.260		0.300	0.044	2.190	1.090	0.285	0.35	0.84	38
612.8	Paleosol	0.0071	19.1400	0.16	0.189	0.0005	3.01	0.0061	0.280		0.390		3.610	1.200		0.18	0.92	32
72.25	Paleosol	0.0061	23.3200	0.18	0.141		23.55	0.0066	0.310		0.310	0.401	2.230	0.970	0.953	0.31	0.74	33
66.55	Paleosol	0.0050	30.7900	0.19	0.187	0.0003	2.80	0.0065	0.360		0.420	0.123	2.110	0.970	0.214	0.36	0.84	34
872.8	Shale	0.0000						0.0101			0.240	0.007	2.080	0.990	0.032		0.68	7

807.25	Shale	0.0126	6.5200	0.11			0.0225	0.150		0.270	0.018	2.710	1.290	0.502		0.97	25	
801.5	Shale	0.0065	18.8800	0.17	0.155		0.0116	0.330		0.260	0.035	1.850	1.060	0.248	0.30	0.68	34	
627.4	Shale	0.0065	10.9800	0.08	0.094	32.34	0.0201	0.190		0.250	0.043	1.990	0.990	0.362	0.36	0.76	26	
580	Shale	0.0065	15.7100	0.12	0.100		0.0069	0.240	0.255	0.300	0.128	1.930	1.020	0.321		0.73	30	
548.7	Shale	0.0065	12.8600	0.10	0.105		0.0210	0.210		0.280	0.013	2.100	1.150	0.081		0.90	22	
449.4	Shale	0.0202	5.4600	0.23		0.0001	0.66	0.0280	0.170	0.554	1.090	0.001	1.220	1.100	0.006		5.57	22
447	Shale	0.0072	18.6500	0.17	0.107	0.0002	1.35	0.0051	0.320		0.230	0.023	1.770	1.020	0.065	0.42	0.68	35
445	Shale	0.0057	15.1500	0.09	0.191		15.15	0.0123	0.240		0.310	0.087	2.370	1.120	0.261	0.33	0.88	30
390.45	Shale	0.0057	23.4100	0.17	0.225		2.27	0.0089	0.390		0.290	0.340	2.340	1.010	0.976	0.31	0.80	38
188.9	Shale	0.0061	23.4400	0.18	0.220	0.0002	2.10	0.0062	0.350		0.380	0.126	2.860	1.090	0.239	0.29	0.90	36
180.7	Shale	0.0070	13.2700	0.11	0.140	0.0022	20.42	0.0160	0.230		0.260	0.047	2.180	1.040	0.291	0.32	0.82	25
180.3	Shale	0.0116	9.9100	0.21	0.101	0.0001	1.34	0.0204	0.180	0.339	0.790	0.001	1.380	0.920	0.005		2.51	35
85	Shale	0.0093	15.9000	0.20	0.093			0.0090	0.190		0.430	0.114	1.910	1.050	0.285		0.87	30
78.8	Shale	0.0097	15.5200	0.23	0.122	0.0001	1.57	0.0156	0.220	0.260	0.580	0.004	1.780	0.950	0.014	0.39	1.38	30
75	Shale	0.0057	18.3200	0.13	0.147		32.73	0.0183	0.260		0.330	0.009	2.130	1.060	0.053		0.86	30
67.65	Shale	0.0077	14.4200	0.15				0.0189	0.200		0.390	0.012	2.200	1.020	0.130	0.25	0.96	30

Appendix VI: PXRF elemental concentration data (ppm)

Sample name	P		S		Cl		K		Ca		Ti		V		Cr		Mn		Fe		Co		Ni		Cu		Zn		
	P	+/-	S	+/-	Cl	+/-	K	+/-	Ca	+/-	Ti	+/-	V	+/-	Cr	+/-	Mn	+/-	Fe	+/-	Co	+/-	Ni	+/-	Cu	+/-	Zn	+/-	
914.8	4544		50352	774	940	75		105	6983	77	296	13		4	7		68	3	25149	181		110		10	16	3	40	3	
804.1	7924		101453	1456	2419	144		192	3865	84	368	23	9	6	13		101	5	73436	572		222		13	13	6	52	3	
635	6641		114537	1608	1681	142	2176	101	791	66	534	26	21	3	24	11	117	6	82714	660		242		15	40	5	17	3	
547.2	5921		72863	1040	2581	115		138	6514	84	237	15		5	9		115	4	40559	293		147		10		9	41	3	
390.65	3439		32967	561	1413	68	2299	53	4711	57	396	11	17	1	14	2	85	3	13369	99		73		9		8	47	2	
66.8	7137		83083	1236	1041	110	4237	104	12507	132	932	24	72	3	36	4	182	6	46797	363		172	35	5	48	5	809	12	
871.8	14937		141314	2235	1032	192	2531	148	264999	1963	558	30	41	4	33	6	1102	16	67587	667		264	39	7	28	6	2917	37	
820	7554		72791	1310	607	127	12463	195	3490	93	2776	43	95	5	48	6	188	7	69369	600		240	33	6	59	6	38	4	
632.85	7617		82832	1361	1182	131	9871	168	1534	74	1597	33	66	4	40	5	153	6	65009	539		220	25	9	20	4	62	4	
626.85	6660		34120	710	2254	104	722	55	63496	372	167	12	8	2	7		676	8	20634	169		108		11	10	8	479	9	
447.5	6142		57992	1071	1339	120	16214	204	2213	75	1841	31	86	4	58	5	146	5	42876	349		171	26	5	32	4	119	5	
390.5	8253		103832	1526	1425	136	4285	120	4350	93	892	28	60	4	37	5	229	7	74420	604		233	20	8	29	5	79	4	
178.8	4607		241781	2956	1525	197		327	3672	111	309	33	18	9		20	196	9	163908	1597		426		21	35	6	25	4	
73	10389		80988	1496	1248	156	21572	282	46268	394	2855	46	109	5	76	6	412	9	64072	588		239	38	7	55	6	84	5	
915.2	14573		9247	707		421	25736	327	200836	1467	4718	60	80	5	65	6	1376	17	31464	322		176	47	7	31	5	846	16	
872.3	31781		8358	1135	843	222	4555	207	897569	6935	302	19	13	2		11	2591	29	8944	134		109	31	7		16	665	16	
820.25	19211		18149	973	645	173	27482	367	317244	2407	2535	46	59	5	60	6	3131	32	36180	389		199	45	7	32	6	420	11	
547.55	13570		16777	819	519	242	32938	383	160173	1197	3202	49	96	5	77	6	829	13	38427	382		194	49	7	28	5	59	4	
547.25	15190		50181	1552	1059	216	9732	242	622996	4852	753	28	26	3	18	5	2503	28	23304	278		168	33	11	22	13		10	
189	33283		22987	1365		675	825	293	964248	7553	91	14	14	2		12	2038	24	6158	102		90	28	6		16		11	
179.75	32803		96372	2205		734	3773	213	816828	6666	243	26	28	4		17	1572	22	34540	414		218	37	12	24	6		10	
74	22410		35031	1258		527	21787	325	461867	3481	1846	38	50	4		34	5	1369	18	21468	251		158	41	7	21	9	20	4

73.8	25576	77455	1837	1259	223	19644	328	516659	4058	1603	41	79	5	25	6	1491	20	43548	490	234	33	7	27	6	252	9
67.05	20619	80091	1821	592	31151	422	292541	2363	2160	48	58	5	51	7	1912	24	62005	670	276	49	12	23	6	116	7	
914.6	7865	36365	1076	428	38108	432	277	6377	77	123	7	131	8	321	10	75676	747	284	74	8	48	6	94	6		
871.4	6545	1121	366	36115	396	3403	111	6433	73	123	6	113	7	969	14	55949	528	229	56	7	29	5	78	5		
612.8	6147	16935	690	349	34152	362	222	5072	60	124	6	104	7	309	8	50969	464	209	34	6	13	98	5			
72.25	5998	2044	403	354	41276	428	336	145	6482	72	121	6	125	7	320	8	48122	450	208	54	7	26	5	145	6	
66.55	6245	15738	686	356	41357	423	1340	93	5491	64	112	6	116	7	287	8	44034	415	199	53	7	39	5	168	6	
915.85																										
872.8	7641	1205	380	42668	454	19053	228	5543	69	126	6	127	8	615	11	61024	582	243	61	7	27	5	89	5		
807.25	8436	1449	475	23462	336	6379	150	6025	79	111	7	86	9	3203	33	142230	1438	402	41	14	26	6	59	5		
801.5	6944	1235	396	37907	427	3621	122	5923	73	119	6	112	8	897	14	77354	750	281	64	8	31	6	97	5		
627.4	5424	1125	746	324	22389	274	2022	84	6017	65	90	5	90	6	732	11	36380	340	175	45	6	28	5	65	4	
580	5868	961	432	204	31843	352	940	85	6519	71	106	6	104	7	302	8	43893	412	199	55	7	32	5	80	5	
548.7	5715	944	315	26084	301	8533	133	5819	64	91	5	79	6	691	11	32900	310	166	43	6	29	5	78	4		
449.4	22572	103679	2111	1161	223	24146	370	344998	2799	1775	46	51	5	47	7	1924	24	68690	755	297	42	8	39	7	561	14
447	8204	47631	1197	420	37380	418	5024	128	4884	64	111	6	108	7	324	9	64138	628	258	63	8	54	6	75	5	
445	5053	1853	334	307	26040	294	1324	76	7017	70	101	5	90	6	346	8	28078	266	153	43	6	23	5	115	5	
390.45	6615	21440	798	369	38935	416	443	88	6306	72	127	6	126	7	432	10	48677	467	216	54	7	27	5	68	4	
188.9	6837	25130	859	380	38855	415	1361	97	5875	69	125	6	114	7	325	9	52750	500	222	44	7	38	6	112	6	
180.7	5771	2077	385	344	28185	327	2333	94	6381	70	103	6	100	6	679	11	42429	400	194	47	7	33	5	85	5	
180.3	15747	36391	1169	639	276	33445	408	194049	1500	3557	55	73	5	80	7	997	15	48936	509	231	53	7	30	6	65	5
85	5991	1077	359	44675	452	1521	99	6174	70	122	6	116	7	433	9	48218	455	210	64	7	43	6	91	5		
78.8	10694	35787	1067	450	344	40669	443	63330	537	4330	60	104	6	109	7	874	14	56096	546	235	58	7	39	6	74	5
75	6480	1223	366	337	32447	355	13878	176	6150	68	107	6	100	6	733	11	40041	378	189	50	6	31	5	84	5	
67.65	7643	1344	411	35004	407	11597	179	6217	76	101	6	100	8	1513	19	80098	779	286	46	7	30	6	79	5		

Color fields are lithology indicators:

Dark grey = coal

Light grey = coaly mudstone

Light blue = limestone

Light yellow = shale

Light green = paleosol

pXRF elemental concentration data (cont.)

Sample name	As +/-	Se +/-	Rb +/-	Sr +/-	Y +/-	Zr +/-	Nb +/-	Mo +/-	Ag +/-	Cd +/-	Sn +/-	Sb +/-	Ba +/-	La +/-
914.8	178 4	2	7 1	110 2	32 1	17 1	2	25 1	10	5	10	10	56 11	48
804.1	294 6	3	8 1	63 2	11 1	16 1	2	33 1	11	6	10	10	47 20	53
635	113 6	3	22 1	73 2	33 2	17 1	3 1	31 1	11	6	10	18 3	68 12	55
547.2	47 3	2	8 1	97 2	3 2	11 1	2 1	22 1	10	5	10	10	44 11	49
390.65	12 1	2	23 1	128 2	29 1	19 1	3 1	19 1	9	5	10	9	61 11	55 36
66.8	141 5	3	34 2	90 2	54 2	37 1	4 1	27 1	10	13 2	10	10	81 12	51
871.8	123 5	4	11 1	440 5	88 3	18 2	4 2	15 1	42 4	9 2	11	14 4	182 14	61
820	940 12	3	85 2	68 2	19 2	59 1	8 1	44 1	11	5	10	10	175 13	55
632.85	205 6	3	57 2	108 2	28 2	48 1	6 1	39 1	11	6	10	13 8	140 13	55
626.85	315 5	2	7 1	122 2	8 1	11 1	2	30 1	10	5	10	10	37 27	51
447.5	17 2	2	88 2	102 2	31 2	49 1	7 1	24 1	10	5	10	10	174 12	52
390.5	152 5	3	29 1	109 2	71 2	28 1	5 1	28 1	11	6	10	10	89 12	55
178.8	183 7	3	10 1	52 2	24 2	12 1	3 2	54 2	40 4	6	12	12	47 24	66
73	54 5	3	92 2	179 3	50 2	78 2	13 1	11 1	19 4	6	11	10	269 13	57
915.2	20 3	3	92 3	263 4	29 2	115 2	14 1	4 2	39 4	9 2	10	10	314 14	57
872.3	14 3	4	5 1	684 8	13 2	20 2	3 1	6 1	66 4	6	11	11	215 15	64
820.25	28 3	3	81 3	391 5	41 2	56 2	9 1	8 1	59 4	6	12 9	10	352 15	62
547.55	17 3	3	143 3	199 3	34 2	75 2	11 1	4 1	38 4	5	10	10	554 14	57
547.25	32 4	4	21 2	527 6	11 2	22 2	4 1	5 1	65 4	6	12 6	11	251 15	63
189	11 2	3	4	594 7	35 2	9 2	3 2	5 2	74 4	6	11	11	247 15	65
179.75	50 5	4	4	517 7	21 2	12 2	3 2	10 1	91 5	6	18 9	11	412 16	67
74	13 3	3	44 2	517 6	47 2	51 2	9 1	4 3	55 4	6	11	11	373 15	62
73.8	46 4	4	39 2	517 6	11 2	36 2	7 1	6 1	80 4	6	16 9	11	1282 20	63
67.05	32 4	4 3	86 3	343 5	15 2	48 2	9 1	6 1	62 4	6	15 9	11	326 15	64
914.6	57 4	3	185 4	145 3	36 2	115 2	20 1	6 1	46 4	5	14 9	10	476 15	60
871.4	18 2	3	177 3	149 3	48 2	126 2	21 1	5 3	33 4	5	10	10	500 14	56
612.8	42 4	3	176 3	162 3	33 2	112 2	18 1	8 1	18 9	5	10	10	413 13	55
72.25	16 2	3	183 3	135 3	47 2	137 2	26 1	4	33 4	5	12 8	10	441 14	69 31

66.55	33	3	3	195	4	164	3	45	2	129	2	21	1	5	1	28	4	5	11	8	10	395	14	76	32
915.85																									
872.8	14	3	3	204	4	139	3	32	2	105	2	19	1	4	3	40	4	5		10	10	575	14		57
807.25	26	3	3	117	3	113	3	43	2	159	3	20	1		4	52	4	6		11	11	416	15		63
801.5	14	2	3	187	4	128	3	45	2	116	2	20	1	4	3	38	4	6	11	9	10	491	14	75	33
627.4	11	2	3	113	3	86	2	52	2	205	3	23	1		4	25	6	5	10	8	9	345	13	59	42
580	10	2	3	165	3	121	2	46	2	178	2	23	1		4	29	4	5		10	10	404	13		55
548.7	9	5	3	119	3	107	2	48	2	230	3	21	1	5	3	22	4	5	11	8	10	380	13	58	42
449.4	59	5	4	68	3	379	5	33	2	46	2	7	1	8	1	68	4	6	15	6	11	346	15		65
447	21	3	3	173	4	117	2	28	2	98	2	15	1	8	1	45	4	5		11	10	499	15	74	46
445	8	2	3	131	3	115	2	64	2	203	3	27	1		4	20	4	5		10	9	376	13		54
390.45	24	3	3	187	4	150	3	37	2	118	2	23	1		3	32	4	5	11	8	10	518	14	62	45
188.9	27	3	3	190	4	171	3	34	2	120	2	21	1	5	1	27	4	5		10	10	453	14	59	44
180.7	12	2	3	133	3	109	2	46	2	206	3	23	1	4	1	28	4	5		10	10	417	14	72	44
180.3	16	3	3	106	3	266	4	43	2	79	2	14	1	5	3	50	4	6	14	6	10	335	14		61
85	15	2	3	199	4	173	3	52	2	139	2	25	1		4	24	4	5	10	8	10	405	13	61	43
78.8	52	4	3	163	3	225	3	55	2	89	2	16	1	5	3	41	4	5		10	10	386	14		58
75	12	2	3	141	3	121	2	48	2	173	2	27	1		4	33	4	5		10	10	372	13	65	19
67.65	12	2	3	148	3	142	3	46	2	149	2	23	1		4	49	4	5		11	10	362	14	64	46

pXRF elemental concentration data (cont.)

Field Label 1	Ce +/-	Pr +/-	Nd +/-	Sm +/-	W +/-	Hg +/-	Pb +/-	Bi +/-	Th +/-	U +/-	Si +/-	Hf +/-	LE +/-
914.8	62	64	94		29 6	15 3	90 3	20	6	8	234518 0		
804.1	69	71	106		17	8 6	203 5	24	6	8	164390 0		
635	71	73	108		84 10	40 4	291 6	25	7	9	14724 0		
547.2	64	67	98		15	7 5	61 3	21	6	8	222606 0		
390.65	59	61	91		13	5	15 2	19	6	12 3	20451 0		
66.8	67	69	102		30	12 5	166 5	24	8	82 5	21596 0		
871.8	81	82	123		99 38	47 6	45 4	31	12 5	13	241334 0		
820	73	74	110		30 13	12 6	181 6	27	8 6	9	133333 0		
632.85	72	73	109		20	8	284 7	26	7	12 8	90154 0		
626.85	66	68	100		24	8	63 3	22	6	9	219972 0		
447.5	68	70	103		19	7	11 2	24	13 6	20 8	16015 0		
390.5	72	73	109		22	14 3	122 4	26	7	19 4	228394 0		
178.8	88	89	133		27	16 4	182 7	32	8	12	33023 0		
73	88 42	77	115		23	12 7	145 5	29	10 3	11	82466 0		
915.2	76	91 26	198 39		38	13 8	43 3	31	12 3	11	281332 0		
872.3	85	269 29	517 43		41	12	20 3	37	18 4	15	10094 0		
820.25	82	136 28	265 41		32	11	15 3	33	14 3	13	208301 0		
547.55	76	77	117 89		23	13 7	17 3	30	11 3	11	258736 0		
547.25	84	225 28	418 43		26	13 9	62 4	35	13 3	14	272624 0		
189	87	341 30	646 44		25	10	7	34	13 4	14	168547 0		
179.75	90	253 30	518 46		25	19 6	103 6	36	13 6	14	50442 0		
74	83	162 28	341 42		25	13 8	19 3	34	19 6	14	11614 0		
73.8	84	125 29	291 43		32	15 9	49 4	35	16 6	14	103913 0		
67.05	85	104 67	201 72		29	18 9	83 5	35	18 3	13	104305 0		
914.6	90 44	80	120		25	11 8	58 4	33	18 3	11	217491 0		
871.4	109 42	76	113		23	9	11 3	30	18 3	11	279405 0		
612.8	85 57	74	110		23	12 7	114 5	29	14 3	11	23235 0		
72.25	99 25	75	112		23	9	9 6	30	19 3	11	35746 0		

66.55	107	25	75	112		24	9	55	4	30	21	3	12	233908	0
915.85														4860	0
872.8	93	25	76	114		24	9	17	3	31	17	3	10	210995	0
807.25	108	47	84	127		26	10		11	35	14	3	11	265633	0
801.5	93	44	79	119		24	10		8	32	17	3	11	162785	0
627.4	118	56	73	109		21	8	19	3	29	14	3	9	22721	0
580	126	24	74	111		23	9		7	30	20	3	10	21943	0
548.7	83	56	73	109		21	8	14	3	29	15	3	10	224327	0
449.4	101	67	123	49	202	44	39	16	4	90	5		13	178753	0
447	98	26	79	118		23	12	5	42	4	32	14	3	253720	0
445	91	56	72	108		22	9	6		6	28	16	3	94103	0
390.45	103	42	76	114		22	9	49	4	31	17	3	11	76156	0
188.9	111	42	75	113		24	9	37	3	31	16	3	11	120310	0
180.7	109	41	75	112		23	9		7	30	17	3	10	232287	0
180.3		81	86	63	183	68	25	15	8	20	3		12	229832	0
85	94	24	75	111		23	9	14	6	31	19	3	11	111720	0
78.8	100	26	77	116		24	10	7	62	4	31	15	3	50289	0
75	105	25	74	111		22	8		7	29	17	3	11	219207	0
67.65	112	61	79	119		23	10		8	32	15	3	11	234518	0